Thesis for the Degree of Doctor of Wave Propagation Engineering

New Address and Sustain Waveforms
for AC Plasma Display Panel

Ki-Duck Cho

Department of Electronics, Major in Wave Propagation Engineering
The Graduate School

June 2004

The Graduate School
Kyungpook National University

New Address and Sustain Waveforms
for AC Plasma Display Panel

Ki-Duck Cho

Department of Electronics, Major in Wave Propagation Engineering
The Graduate School

Supervised by Professor Heung-Sik Tae

Approved as a qualified thesis of Ki-Duck Cho
for the degree of Doctor of Wave Propagation Engineering
by the Evaluation Committee

June 2004

Chairman _____

_____

_____

_____

_____

The Graduate School Council, Kyungpook National University

ABSTRACT

Although Plasma Display Panels (PDPs) would seem to be a promising candidate to replace the conventional Cathode Ray Tube (CRT), they still suffer from several serious problems related to their driving characteristics. Accordingly, this paper suggests some new driving methods to improve the driving characteristics of a three-electrode-type AC-PDP, including the luminance, luminous efficiency, color temperature, gray-level expression, and addressing speed. The proposed driving methods are evaluated using a 4-inch AC-PDP test panel, and the results summarized and discussed. In addition, a Vt closed curve, a powerful analysis method for driving waveforms, is also used to validate the proposed driving methods.

A new ramped-square sustain waveform is proposed to improve both the luminance and luminous efficiency of an AC-PDP. It was observed that the luminance and luminous efficiency strongly depend on the characteristics of the discharge relation between the main discharge at the rising edge and the self-erasing discharge at the falling edge of a ramped-square sustain waveform. Thus, when compared with the conventional square sustain waveform, a 22 % improvement in the luminance and 36 % improvement in the luminous efficiency were simultaneously obtained based on a properly adjusted square-voltage and ramp-voltage for a ramped-square sustain waveform in a 4-inch AC-PDP test panel at a frequency of 62 KHz.

A new driving scheme is proposed to improve and increase the flexibility of the color temperature without sacrificing the peak white luminance based on independent control of the red (R), green (G), and blue (B) luminance in an AC-PDP. As such, when various auxiliary pulses were applied, facilitating the simultaneous control of each color's luminance, the new driving scheme was found to improve the color temperature from 5,396 K to 10,980 K in a 4-in. test panel with almost the same peak white luminance as that of the conventional driving scheme.

A new multi-luminance-level subfield method is proposed to reduce the low gray-level contour of an AC-PDP. The luminance levels in the 1- and 2-sustain-cycle subfields are fine-tuned into 5 luminance-steps by applying various auxiliary short pulses to the address electrodes in the same sustain-cycle subfields. As a result, the 28 luminance levels produced in the low gray level up to 6 by the new multi-luminance-level subfield method were confirmed to help suppress the low gray-level contour of an AC-PDP.

A new bipolar scan waveform is proposed to considerably reduce the addressing time during an address period. The new bipolar scan waveform consists of a two-step scan pulse that can separate the conventional addressing discharge mode into two different discharges modes: a space-charge generation mode and wall-charge accumulation mode. When compared with the conventional address-driving waveform in the single scan ADS driving scheme, the proposed bipolar scan waveform can reduce the addressing time by about 50 %, thereby achieving an almost two-fold improvement in the light-emission time for one TV field.

CONTENTS

LIST OF FIGURES

LIST OF TABLES

1. Introduction

The recent focus on the development of information technology has led to remarkable improvements in display devices. Plus, to overcome the space restriction of the conventional cathode ray tube (CRT), various studies are currently concentrating on flat panel display (FPD) devices, such as liquid crystal displays (LCDs), plasma display panels (PDPs), field emission displays (FEDs), and electroluminescence displays (ELDs). Among these FPDs, PDPs are regarded to be the most suitable for large area full color wall hanging flat panel display devices [1],[2], while in the commercial display market, PDPs are also considered as a promising candidate for large area digital high definition televisions (HD-TVs).

However, before completely replacing the conventional CRT, PDPs still need to overcome several serious problems, including a low luminance [3]-[5], low luminous efficiency [6]-[10], low color temperature [11],[12], low contrast ratio [13], dynamic false contour [14]-[17], and low gray-level contour [18],[19]. Accordingly, this paper proposes various new driving methods to improve the driving characteristics of a three-electrode-type AC-PDP, including the luminance, luminous efficiency, color temperature, gray-level expression, and addressing speed.

In the remainder of this paper, Chapter 2 explains the structure of a typical three-electrode-type AC-PDP and the basic driving technique, while Chapter 3 introduces the Vt closed curve as a powerful method for analyzing a driving waveform. To demonstrate the application of a Vt closed curve, it is used to analyze the changes in the wall and cell voltages during the reset and sustain periods, and verify the operation of the new driving methods proposed in the following chapters.

Chapter 4 presents a new ramped-square sustain waveform to improve the luminous efficiency of an AC-PDP. The proposed sustain waveform is a superimposed waveform that adds a ramp-waveform to a square-waveform

and has an increasing voltage slope between the rising and falling edge. This waveform induces a longer-sustained discharge at the rising edge and self-erasing discharge at the falling edge, thereby improving the luminous efficiency. When measuring the luminous characteristics, such as the luminance and luminous efficiency, based on the square-voltage and ramp-voltage (or voltage slope) of the proposed sustain pulse, it was found that the luminance and luminous efficiency strongly depend on the characteristics of the discharge relation between the main discharge at the rising edge and the self-erasing discharge at the falling edge of the ramped-square sustain waveform. With an increase in the square-voltage of the ramped-square sustain waveform, the luminance increases, yet the luminous efficiency decreases. Conversely, with an increase in the ramp-voltage of the ramped-square sustain waveform, both the luminance and the luminous efficiency increase.

Chapter 5 introduces two auxiliary address pulse applications. The first is a new driving scheme to improve and increase the flexibility of the color temperature in an ac-PDP without decreasing the gain of the G and R signals or employing asymmetric cell structures. As such, independent control of the R, G, and B emissions is achieved by the selective application of various narrow auxiliary pulses to the R, G, and B address electrodes during a sustain-period, where the auxiliary pulses control the luminance levels independently from the R, G, and B cells based on the fast and efficient formation of plasma or slightly disturbing the wall-charge accumulation. The second auxiliary address pulse application is a new multi-luminance-level subfield method to improve the low gray-level color reproducibility based on reducing the low gray-level contour of an AC-PDP. The luminance levels in 1-pulse and 2-pulse subfields are fine-tuned into 5 luminance-steps by applying various auxiliary pulses to the address electrode in the same sustain-pulse subfields.

Chapter 6 outlines a new bipolar scan waveform to considerably reduce the addressing time during an address period in an AC-PDP. The new bipolar

scan waveform reduces the scanning time per single scan line from 1.5 µs to 0.6 µs by separating the address discharge mode into two different discharge modes: a space-charge generation mode and wall-charge accumulation mode.

The final chapter provides a summary of all the driving methods proposed to improve the driving characteristics of an AC-PDP.

2. FUNDAMENTALS OF AN AC-PDP

2.1 STRUCTURE OF AN AC-PDP

Figure 2-1 shows the single pixel structure of a typical three-electrode AC-PDP. A single pixel is the minimum unit for displaying a full color image, and consists of three cells that emit red, green, and blue lights based on the stimulation of R, G, and B phosphor layers by vacuum ultraviolet (VUV: 147nm) produced from a He-Ne-Xe plasma discharge, respectively. Figure 1-2 shows a 3-dimensional structure of typical three-electrode AC-PDP with separated figures into the front glass part and the rear glass part. There are three electrodes for supply electric power into a discharge space in a single cell. Two sustain electrodes (X and Y) are on the front glass plate, and one address electrode (A) are on the rear glass plate. One of two sustain electrodes (Y scan-sustain electrode) is used for scan and sustain procedure, and the other of those (X common-sustain electrode) is used for sustain procedure. Generally, the scan-sustain electrodes (Y) and the address electrodes (A) of all cells are separated horizontally and vertically, respectively. The common-sustain electrodes of all cells (X) are joined together. Two sustain electrodes consist of bus electrode and ITO electrode. The transparent ITO electrode which supplies electric power into a discharge space has low conductivity, thus this is not adoptable to a large area display device. To compensate this property, the opaque bus electrode is used together with the ITO electrode. A dielectric layer which covers the sustain electrodes plays role of restriction of electric current flow into the discharge space. Below the dielectric layer, there is a protection layer (MgO layer) which protects the sustain electrodes and helps to activate the production of plasma discharge by secondary electron emission. The address electrodes and the barrier rib are on the rear glass plate. The barrier rib separates the discharge space of each cells filled with He-Ne-Xe mixture gas. On the

4

surface of rear glass plate and the barrier rib, the phosphor layers of red, green, and blue colors exist.

A He-Ne-Xe plasma discharge produced in the discharge space by supplied
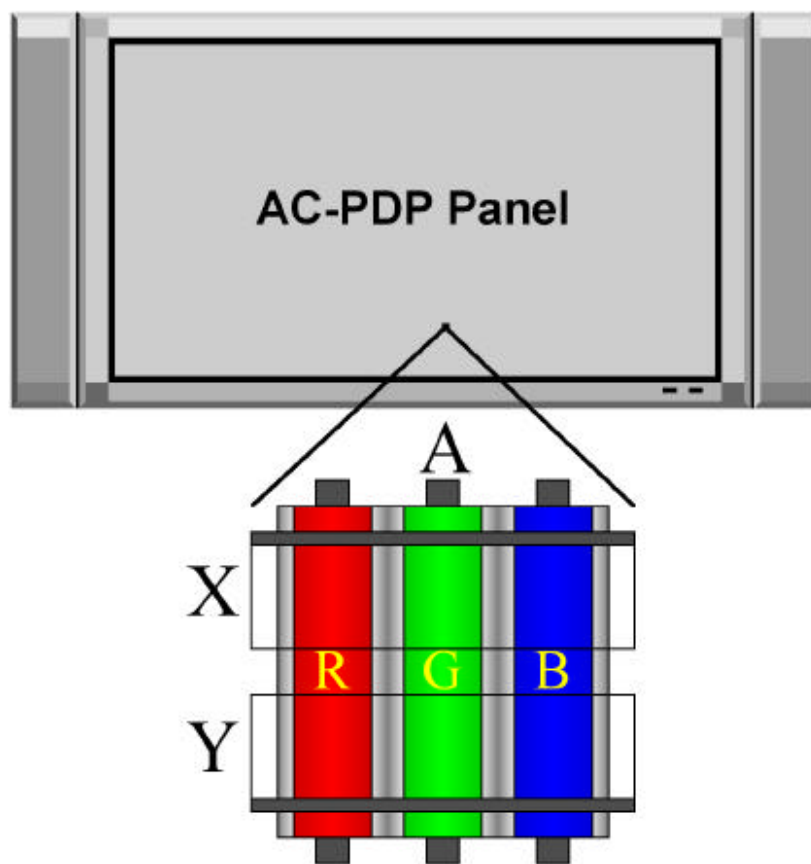
Figure 2-1: Cell structure and three electrodes of single pixel composed of red, green, and blue cells in AC-PDP.

(a)

(b)

(c)
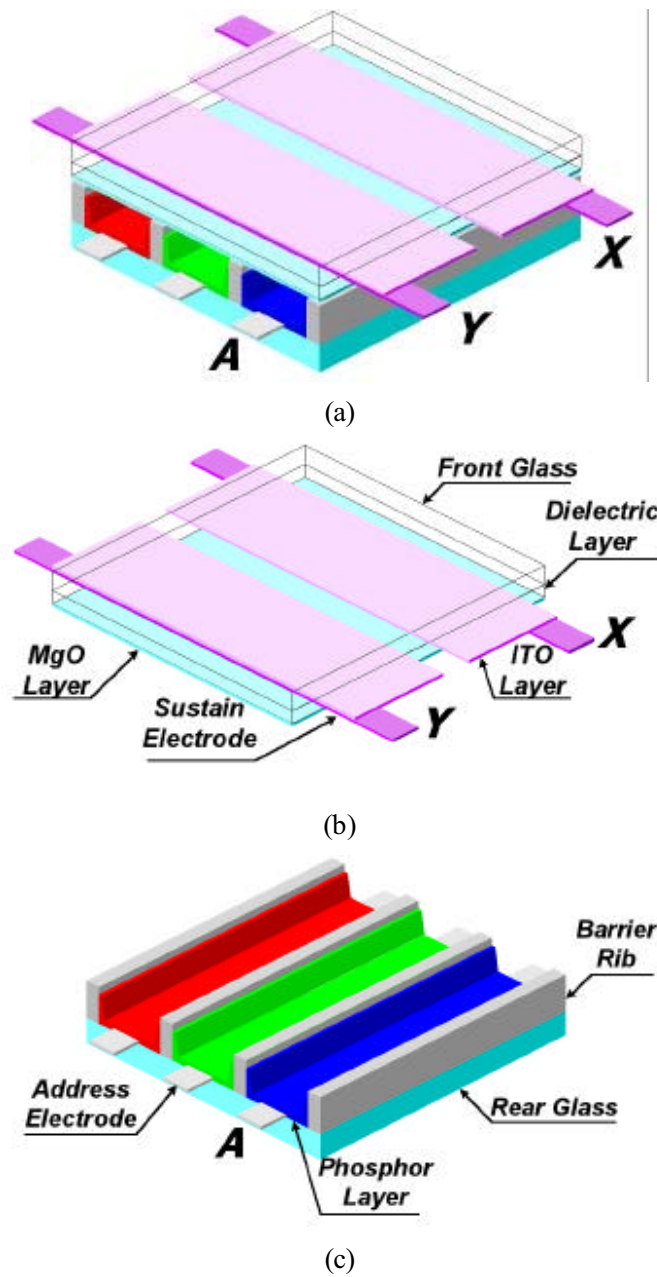
Figure 2-2: 3-dimensional structure of typical three-electrode AC-PDP (a), with separated figures into front glass part (b) and rear glass part (c).

electric power generates vacuum ultraviolet (VUV: 147 nm) to the phosphor layer. The phosphor layer is excited by the VUV, and emits visible light when the phosphor returns to stable state.

2.2 DRIVING TECHNIQUE OF AN AC-PDP

Figure 2-3 shows the video signal processing procedure from input analog video signal to visible light emission in a typical PDP module. An analog video signal inputted to the PDP module is separated into red, green, and blue signal, and then each separated analog signal is converted into digital signal by A/D converter. 8 bits digital signal conversion is used in the typical PDP module, however 10 bits conversion is also used for the improvement of image quality. Converted digital video signal is sent to driving circuits in 8 bits binary code form for displaying image on PDP panel. The driving circuits apply voltage waveforms to electrodes (X, Y, and A electrodes) of PDP panel using 8 bit binary code based on the subfield method.

The subfield method uses a number of subfields divided from 1 TV-field (16.67 msec) for displaying image, as shown in Figure 2-4 (a). All subfields have assigned luminance level based on binary code $1(2^0)$, $2(2^1)$, $4(2^2)$, $8(2^3)$, $16(2^4)$, $32(2^5)$, $64(2^6)$, and $128(2^7)$. This luminance level set based on binary code can be modified variously for the improvement of image quality. The desired luminance level is realized by a combination of several subfields among the subfields composing 1 TV-field. Each subfield consists of reset, address, and sustain period, as shown in Fig. 2-4 (2). In the reset period, states of all cells are initialized to OFF state by applying reset waveform to all electrodes in same time. If corresponding subfield is a selected subfield, there is an action for changing cell state to ON state during the address period by applying scan and address waveform to electrodes concerned with selected cell. On the other hand, if corresponding subfield is not a selected

subfield, the cell state is reserved in OFF state during the address period. In sustain period, a number of light pulses are emitted in only selected cells which are ON state by applying a number of square sustain pulses alternately to two sustain electrodes (X and Y). The number of sustain pulses of each subfield is determined by the assigned luminance level. In the case of typical WVGA (Wide VGA) grade PDP panel, the assigned times of each period in 1 subfield are 0.3 msec for the reset period, 0.96 msec for the address period, and 0.005 ~ 0.64 msec for the sustain period, respectively, as shown in Fig. 2-4 (2).

Figure 2-5 shows the electrodes layout of WVGA grade PDP panel which has the resolution of 852×480. This panel consists of 480 pairs of sustain electrode (X and Y) and 2556 lines of address electrode (A; 852×3 colors). Generally, the common and sustain electrodes (X) are connected commonly, while the scan and sustain electrodes (Y) and the address electrodes (A) are separated mutually. Figure 2-6 shows the applied voltage waveforms to each electrode shown in Fig. 2-5 during 1 subfield according to the conventional driving method. In reset period, ramp reset waveform applied to the scan and sustain electrode (Y) and square waveform applied to the common sustain electrode (X) initialize the state of all cells to OFF state. Then, in address period, scan pulses are applied to $Y_1 \sim Y_{480}$ electrodes sequentially to select a horizontal line, as shown in Fig. 2-6. When a horizontal line is selected by applying scan pulse to a scan and sustain electrode (Y_{xxx}), the address pulses are applied to address electrodes of the cells which are located on selected horizontal line, and which must be turn-on in corresponding subfield. This method is called as 'Matrix Driving Method'. If the scan pulse and address pulse are applied to a single cell at same time, an address discharge is produced, thereby resulting to changing the state from OFF state to ON state. A thing determining the cell state is the 'wall charges' which are produced by the address discharge. In sustain period, sustain discharges are produced in only selected cells which are ON state by applying sustain pulses, while there is no discharge in cells which

are OFF state.

Figure 2-7 (a) shows the wall charge schematic model in ON and OFF cell according to the applied waveform shown in Fig. 2-7 (b). All electrodes of a PDP panel are covered with dielectric layer, thus it can be assumed that a PDP panel is a capacitor. The charges produced by a gas discharge can not flow through the electrodes, and accumulated on the dielectric layer covering the electrodes. At the end of the reset period, the charges produced during the reset period are accumulated below each electrode, as shown in Fig. 2-7 (b) (1). This charges are called as the 'wall charges', and a voltage induced by the wall charges is called as the 'wall voltage'. When a horizontal line is selected by applying a scan pulse to the Y electrode with voltage of V_Y, an address pulse with voltage of V_A produce an address discharge in only an ON cell, as shown in Fig. 2-7 (b) (2). After the address discharge, the wall charge distribution is changed as shown in Fig. 2-7 (b) (3). At the end of the address period, the wall voltages between two sustain electrodes induced by the wall charges are greatly different between ON and OFF cells. The sustain pulse with voltage of V_{sus} produces sustain discharges in only an ON cell with help of the wall voltage, as shown in Fig. 2-7 (b) (4).

2.3 EXPERIMENTAL SETUP

Figure 2-8 shows the experimental setup for the measurement employed in this research. The PR-704 spectrometer was used to measure the luminance of PDP test panel. Table 2-1 shows the panel design specifications of the 4-inch AC-PDP test panel utilized in this experiment. The power consumption dissipated in the 4-inch PDP test panel was measured in the input line between the driving circuits and the test panel using the PM3000A power analyzer. The voltage and current waveforms were measured by the voltage and current probes, respectively. The infrared (IR: 828 nm) signals were measured by the digital oscilloscope after being converted into electrical

signals by the PMT tube.
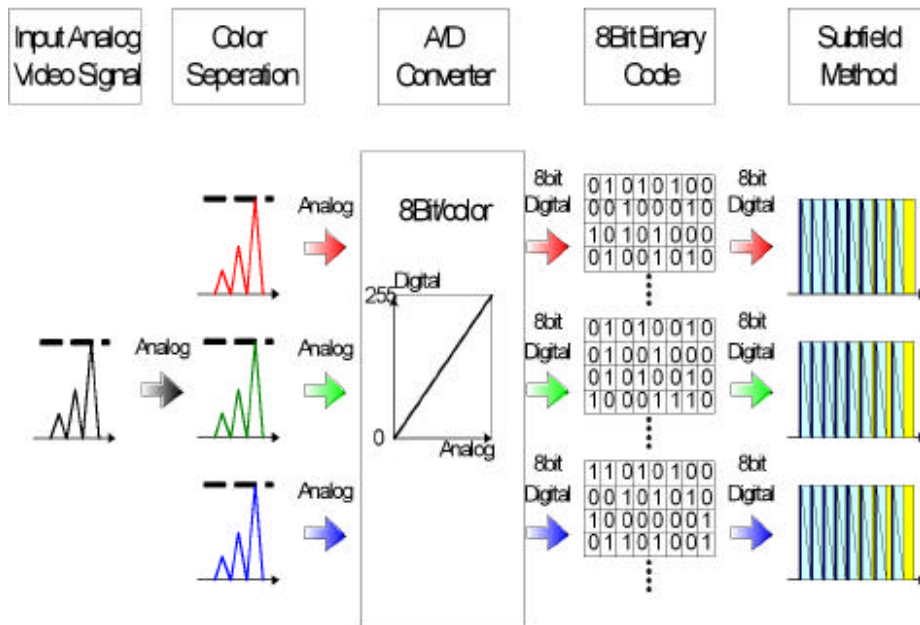
Figure 2-3: Video signal processing procedure in typical PDP module.
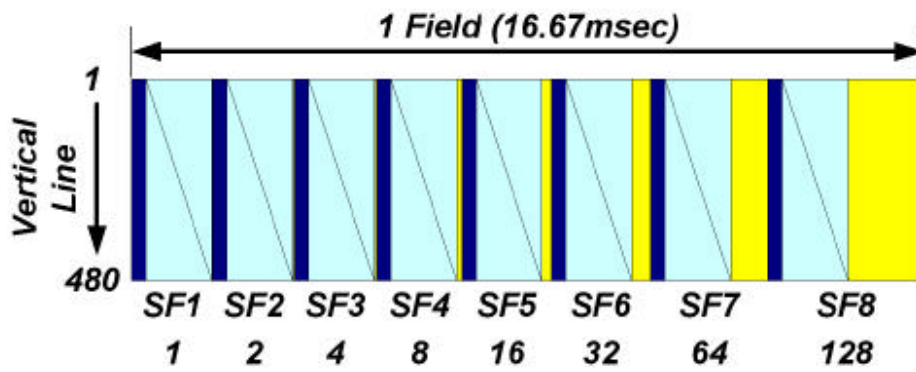
(a)
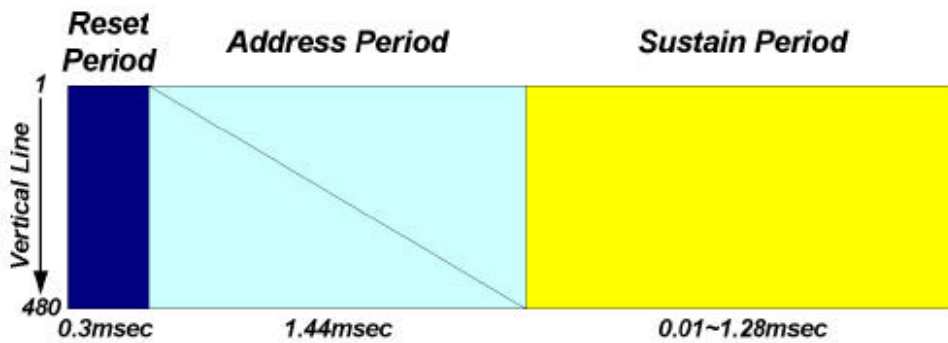
(b)

Figure 2-4: Subfield method using 8 subfields during 1 TV-field (a), and structure of 1 subfield composed of reset, address, and sustain period (b).
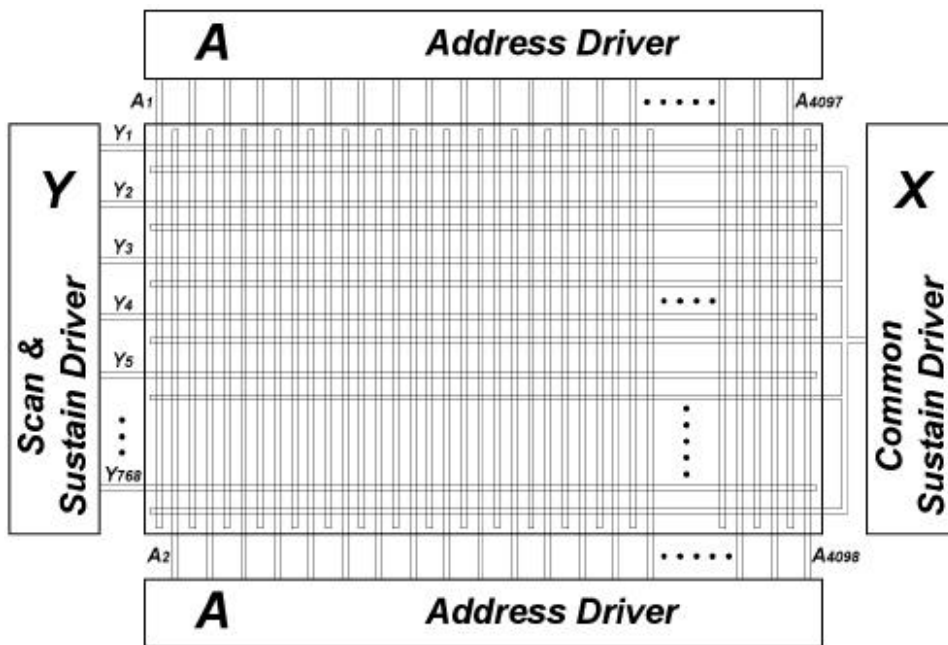
Figure 2-5: Electrodes layout of WVGA grade (852×480) PDP panel.
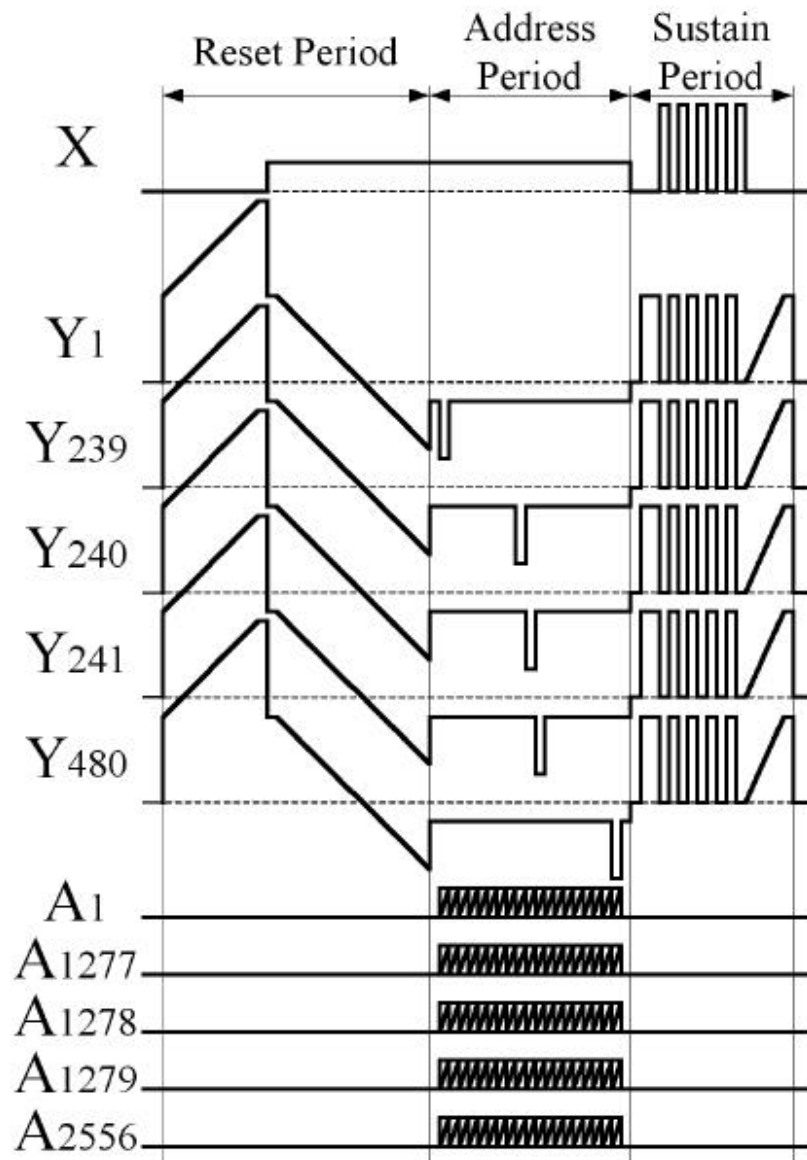
Figure 2-6: Applied voltage waveform to each electrode shown in Fig. 2-5 according to conventional driving method.
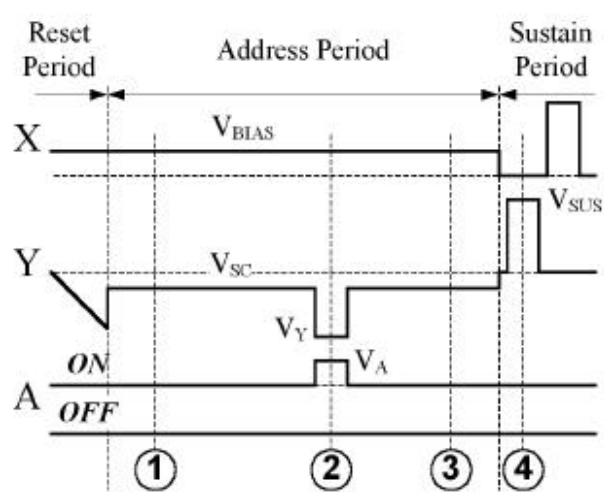
(a)
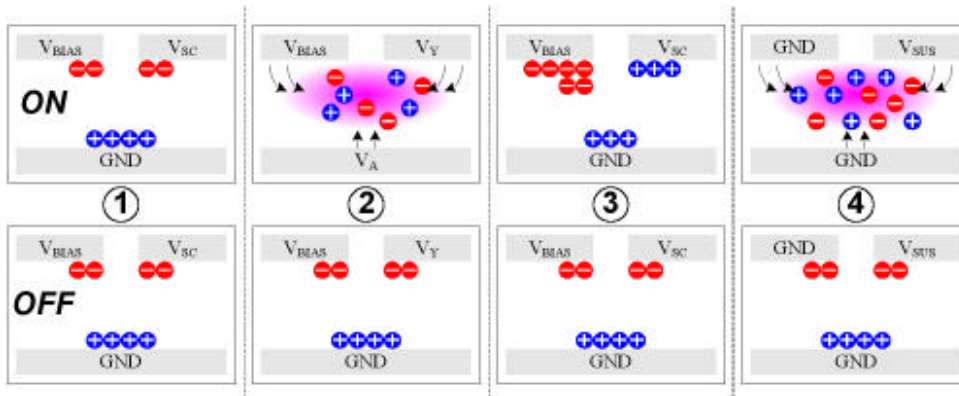
(b)

Figure 2-7: Applied voltage waveform during address period to each electrode (a), and wall charge schematic model of ON and OFF cells during address period.
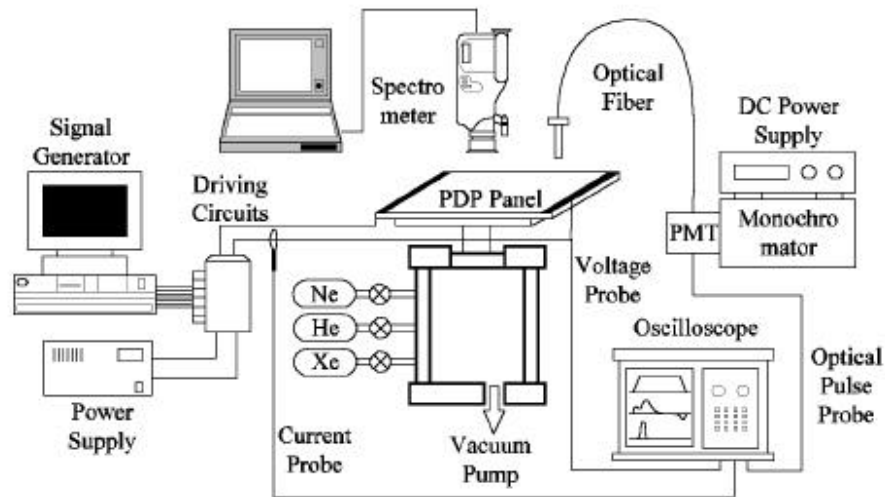
Figure 2-8: Experimental setup for measurements.

Table 2-1: Panel design specifications of 4-inch AC-PDP test panel employed in this experiment.

ITO Width	$310\,\mu$m
ITO Gap	$80\,\mu$m
Bus Electrode Width	$100\,\mu$m
Address Electrode Width	$100\,\mu$m
Barrier Rib Width	$70\,\mu$m
Barrier Rib Height	$150\,\mu$m
Cell Pitch	$360\,\mu$m
Gas Composition	Ne (96%) + Xe (4%)
Gas Pressure	400 Torr

3. Vt CLOSED CURVE

3.1 INTRODUCTION TO Vt CLOSED CURVE

For the analysis of discharge characteristics of AC-PDP, the wall voltage transfer curve and the simulation methods are used. However, these methods can not estimate the full operation of three-electrode AC-PDP. K. Sakita *et al.* proposed the Vt closed curve as an powerful analytic method of an AC-PDP [20]-[22]. Although the Vt closed curve can not provide the information about luminance or luminous efficiency, this method can represent exact wall and cell voltage state during all operation period of an AC-PDP.

Generally, it is assumed that there are just two kinds of discharges: a discharge produced between two sustain electrodes (X and Y), and a discharge produced between an address electrode (A) and one of two sustain electrodes (X or Y). Thus, only two threshold voltages (firing voltage) are measured to investigate the static characteristics of the three-electrode AC-PDP. However, the threshold voltage of AY-discharge is different from that of YA-discharge, due to the difference of secondary electron emission coefficients of the phosphor and the MgO layer. The AY-discharge represents the discharge which is produced when an address electrode (A) acts as anode and an sustain electrode (Y) acts as cathode. Thus, there are six kinds of discharges and six corresponding threshold voltages in the three-electrode AC-PDP. The six threshold voltages are the threshold voltage of AY-, YA-, AX-, XA-, XY-, and YX-discharge and these are called as Vt_{AY}, Vt_{YA}, Vt_{AX}, Vt_{XA}, Vt_{XY}, and Vt_{YX}, respectively. Figure 3-1 shows the 6 threshold voltages on the cell voltage plane. In the cell voltage plane, horizontal axis represents the gap voltage between two sustain electrodes (X and Y), and vertical axis represents the gap voltage between an address electrode (A) and an scan-sustain electrode (Y). If the six threshold voltage are marked on cell voltage plane, an hexagon is obtained, as shown in Figure 3-2. This hexagon

18

is call as "Vt closed curve," and divide the cell voltage plane into non-discharge region and discharge region. A cell voltage state marked in the discharge region represents that any kind of discharge is produced in appropriate cell.

Figure 3-3 shows the concept of cell voltage and changes of cell voltage by applied voltage. The cell voltage is vector sum of the wall voltage and applied voltage, and can be expressed as following equation.

$$\overrightarrow{V_C} = \overrightarrow{V_W} + \overrightarrow{V_A} \qquad [1]$$

In case the applied voltage is zero, the positions of cell voltage and wall voltage are same. The operation of an AC-PDP is determined by the cell voltage, thus it is important to track the changes of cell voltage. For example, positive voltage applied to common-sustain electrode (X) of a cell change the cell voltage position to right direction.

Figure 3-4 shows the measured Vt closed curve of the 4-inch PDP test panel employed for experiments. The threshold voltages of AY- and AX-discharge are about 180 V, those of XY- and YX-discharge are about 210 V, and those of YA- and XA-discharge are about 250 V. The difference of secondary electron emission coefficients between the phosphor layer and the MgO layer causes the voltage differece of about 70 V.

3.2 ANALYSIS OF RESET WAVEFORM USING Vt CLOSED CURVE

There are two distinguishable discharge types in typical AC-PDP operation, namely weak discharge and strong discharge. The weak discharge is produced during the reset period by gradual change of the cell voltage, and the strong discharge is produced during the address and the sustain periods by abrupt change of the cell voltage. Figure 3-5 illustrate the operation of weak discharge on the cell voltage plane. Gradually changing applied voltage to negative Y direction leads the cell voltage to discharge region, and produces
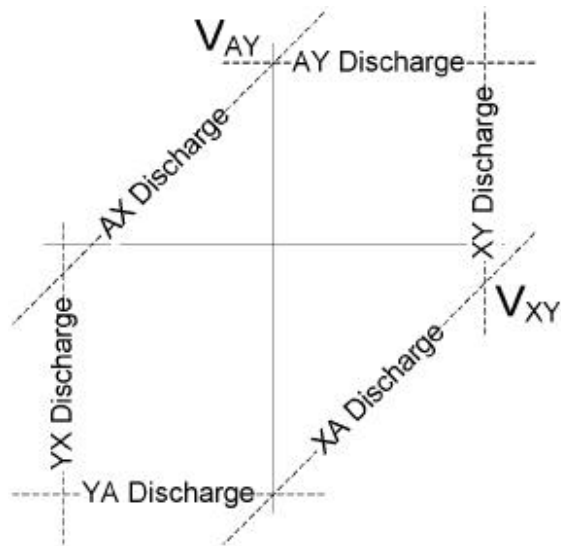
Figure 3-1: 6 threshold voltages in three-electrode type AC-PDP.
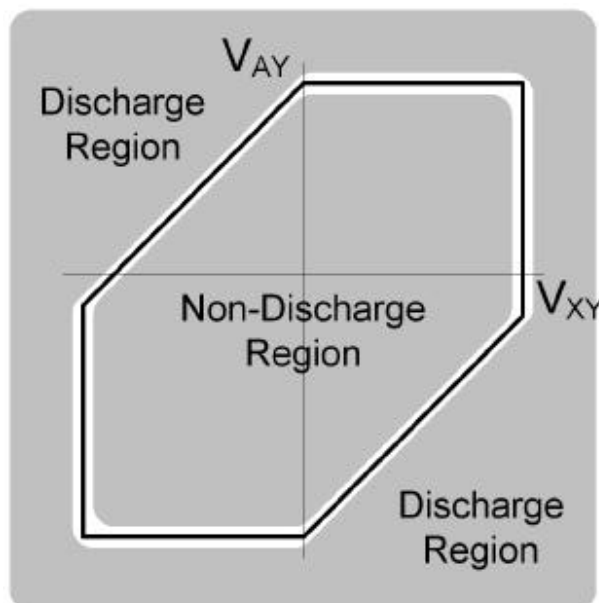
Figure 3-2: Non-discharge region and discharge region which are divided by Vt closed curve.
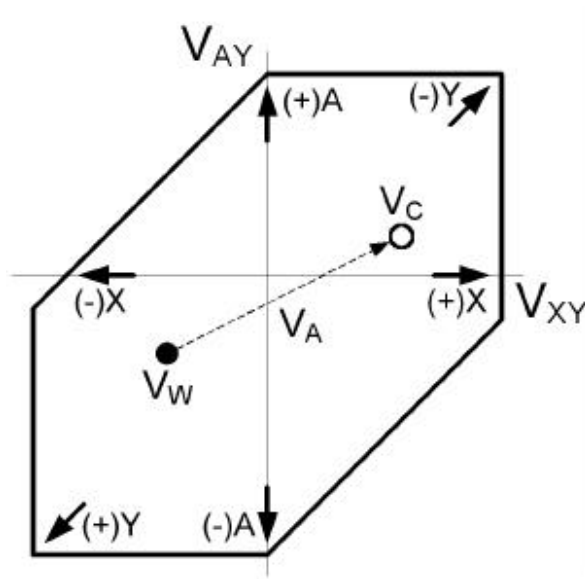
Figure 3-3: Concept of cell voltage and Vt closed curve.
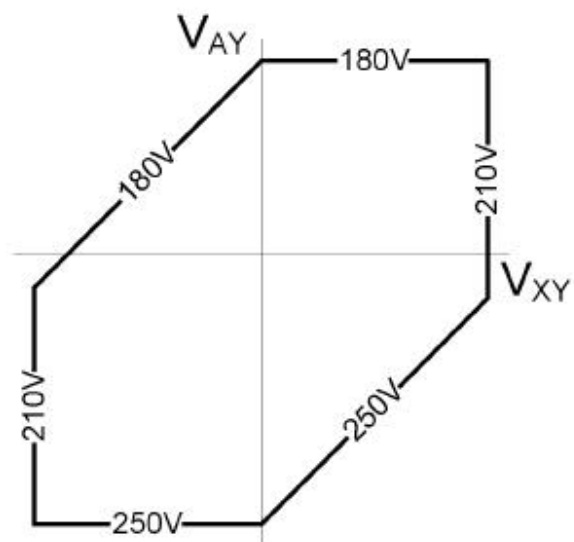
Figure 3-4: Vt closed curve of 4-inch test panel employed in experiments.

a discharge between two sustain electrodes (X and Y). After the occurrence of the discharge, space charges produced by the discharge move toward opposite polarity electrodes, and the cell voltage moves into non-discharge region. Although the decrease of the cell voltage extinguishes the discharge, the applied voltage changing gradually leads the cell voltage to discharge region again. The weak discharge is produced by the repetition of this process. As previously mentioned, the cell voltage can be calculated by vector sum of the wall and the applied voltage, thus total changes of cell voltage during the weak discharge is summarized as right figure of Fig. 3-5.

Figure 3-6 shows the changing direction of wall voltage with incident point of cell voltage from non-discharge region into discharge region. Gradually charging applied voltage to positive X direction charges the wall voltage position in horizontally right direction. Each slope matches well in case the capacitance between an address electrode (A) and one of two sustain electrodes (X or Y) is same with that between two sustain electrodes (X and Y).

The Vt closed curve method is powerful tools for not only analysis of static characteristics of PDP panel, but also driving waveform design. Figure 3-7 shows the typical driving waveform using ramp reset method and the trajectories of wall and cell voltage during reset period. Initial positions of wall voltage of ON and OFF cells are as shown in Fig. 3-7 (1). By the ramp setup waveform, the weak discharge is produced between two sustain electrodes, and the cell voltages move downward following YX-discharge line. At the peak point of setup waveform, the wall voltages are at discharge region, however there is no discharge because the cell voltages are at non-discharge region. At the point of Fig. 3-7 (2), the abrupt changes of cell voltage do not cause any discharge, thus there is no change of the wall voltage. During the set-down period, the weak discharge is produced between two sustain electrodes, and the cell voltages move upward following XY-discharge line. At the end of set-down waveform, the cell voltages arrive at a vertex called as "simultaneous discharge point" where the XY- and AY-
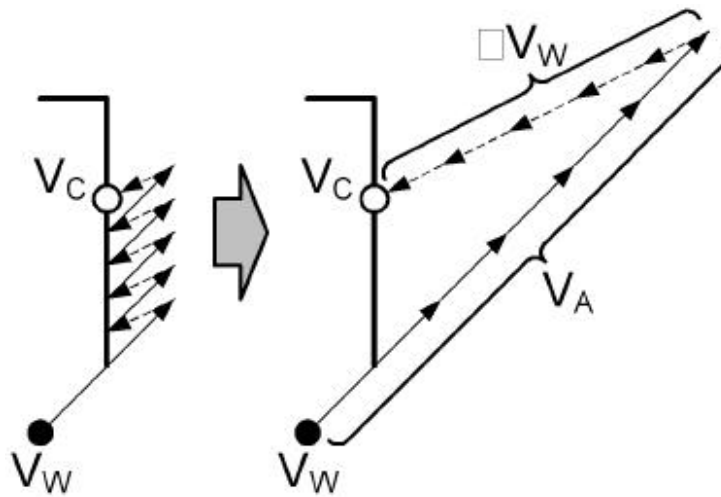
Figure 3-5: Changes in wall and cell voltages during weak discharge.
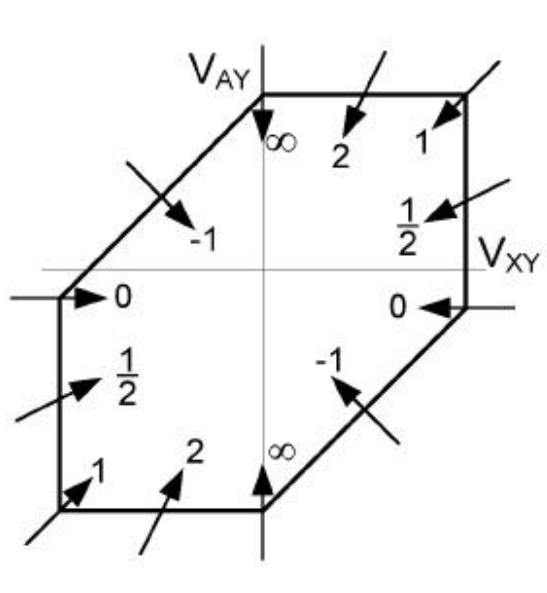
Figure 3-6: Direction of wall voltage vector at 6 lines and 6 vertices of Vt closed curve during weak discharge.

(a)

(b)
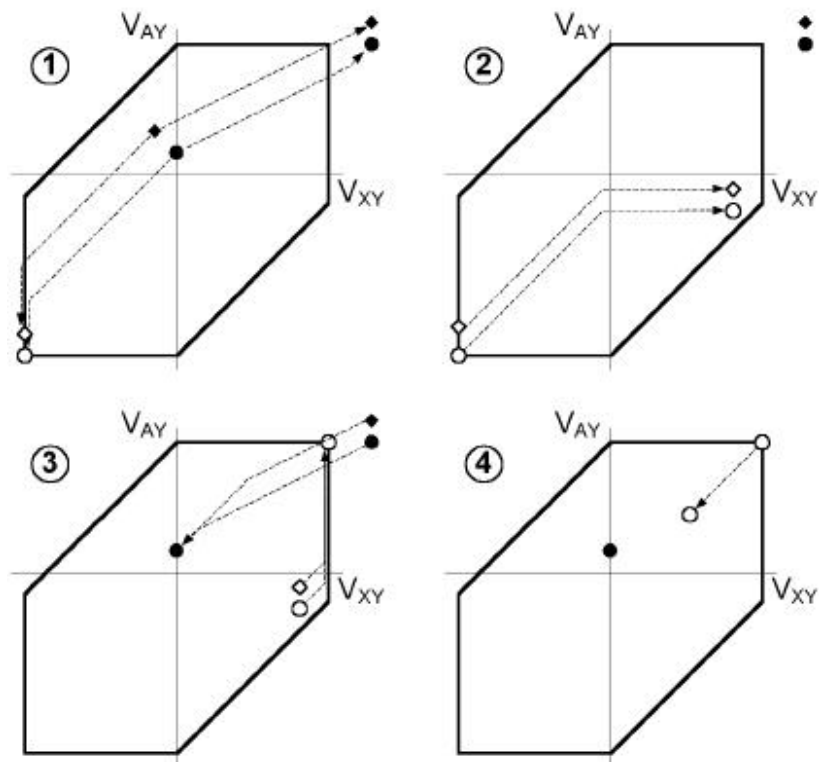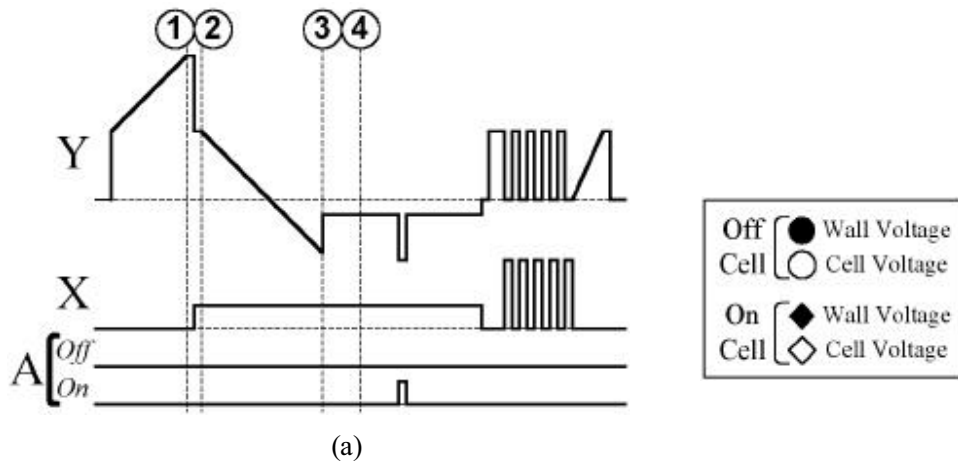
Figure 3-7: Typical driving waveform using ramp reset method (a), and trajectories of wall and cell voltage during reset period (b).
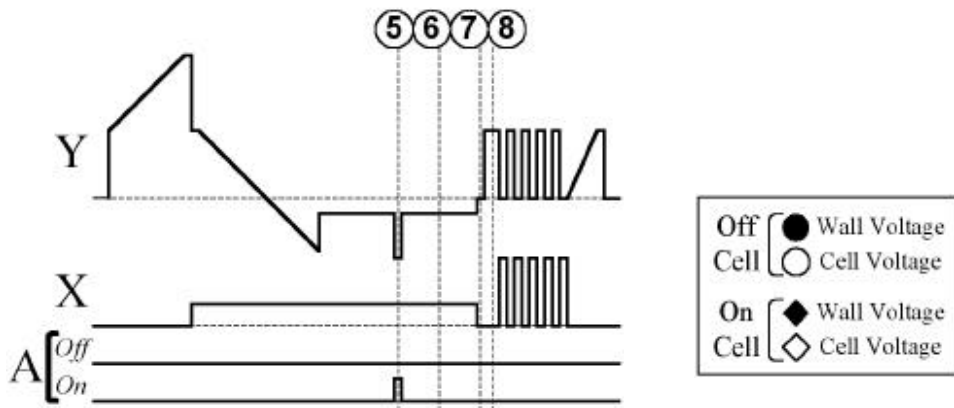
(a)
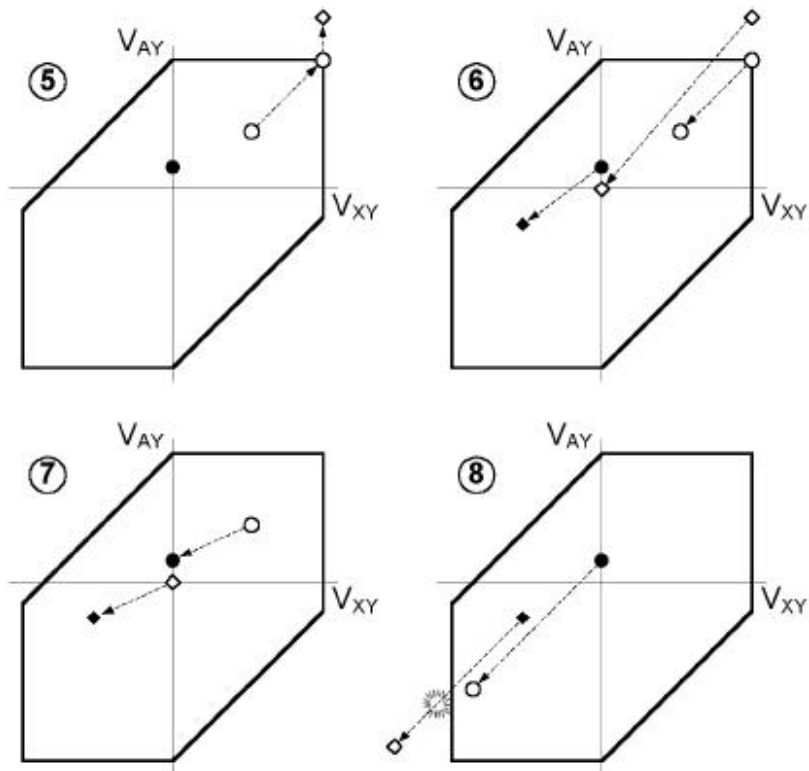
(b)

Figure 3-8: Typical driving waveform using ramp reset method (a), and trajectories of wall and cell voltage during scan and sustain period (b).

discharge are produced at the same time. For the perfect reset of the cell voltage of all cells, the XY- and AY-discharge conditions must be initialized at the same time, thus this vertex must be used during the reset period. At this vertex, the cell voltages of all cells are at same position, and the wall voltages of all cells are also at same position automatically, as shown in Fig. 3-7 (3). Abruptly increased Y voltage moves the cell voltages of all cells to inside of the Vt closed curve, and prevents the undesired addressing discharge by applying only the address pulse without the scan pulse, as shown in Fig. 3-7 (4).

Figure 3-8 shows the typical driving waveform using ramp reset method and the trajectories of wall and cell voltage during scan and sustain period. The cell voltages of the cells which lie on the selected horizontal line by applying negative scan pulse at scan-sustain electrode (Y) move to the simultaneous discharge point to ready for the address discharge. If an address pulse is applied to the address electrode (A) of any cell, the cell voltage move upward into the discharge region leading the addressing discharge, as shown in Fig. 3-8 (5). The address discharge causes the movement of the wall voltage right and slightly downward, as shown in Fig. 3-8 (6). At the end of the scan period, the wall voltage conditions of the ON and OFF cells are distinguishable, as shown in Fig. 3-8 (7). The first sustain pulse moves the cell voltages of the ON cells into the discharge region, and causes the strong discharge in only the ON cells, as shown in Fig. 3-8 (8).

3.3 ANALYSIS OF SUSTAIN WAVEFORM USING Vt CLOSED CURVE

During the sustain period, there are only the strong discharges by the square pulses applied to two sustain electrodes (X and Y). The principle of changes of the wall voltage by the strong discharges is that the wall voltage positions are changed in opposite direction with the applied voltage during

the strong discharges. Figure 3-9 shows the change of wall voltage during the sustain period with various sustain pulses: positive sustain pulse, the TERES (Technology of Reciprocal Sustainer) sustain waveform and negative sustain pulse. After the strong discharge by a positive sustain pulse of common-sustain electrode (X), the wall voltage is positioned at opposite side (-X direction) with the applied voltage. The distance between the origin of the Vt closed curve and the wall voltage position is almost same with the applied voltage, as shown in Fig. 3-9 (a)-(1). A positive sustain pulse of scan-sustain electrode (Y) move the wall voltage to the position of Fig. 3-9 (a)-(2). In the case of the TERES [23] and negative sustain pulse, the wall voltage is changed in same manner with the case of the positive sustain pulse.

3.4 WALL VOLTAGE TRANSFER FUNCTION

Although changes of the wall voltage position by the strong discharge are determined by the applied voltages, the Vt closed curve is distorted after the strong discharge. This phenomenon is caused by the different changes of 6 threshold voltages due to the non-uniform wall charge distribution. The wall voltage transfer function shows the relation between the cell voltage position and the change of 6 threshold voltages [21],[24],[25]. From the wall voltage transfer function, we can estimate the changes of 6 threshold voltages and distorted shape of the Vt closed curve after the strong discharge, and strength of discharge according to arbitrary cell voltage position.
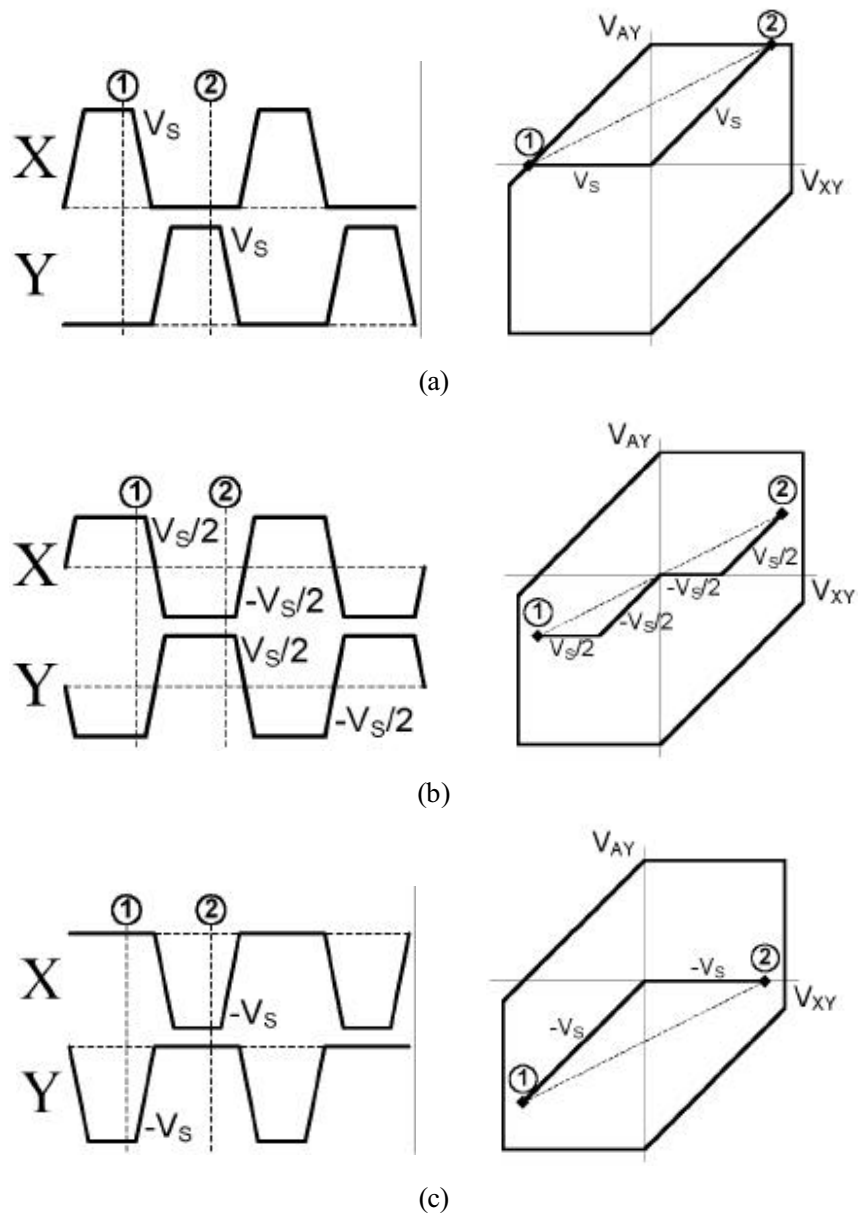
Figure 3-9: Change of wall voltage during sustain period with various sustain pulses: (a) positive sustain pulse, (b) TERES sustain waveform, and (c) negative sustain pulse.

4. RAMPED-SQUARE SUSTAIN PULSE

4.1 LUMINOUS EFFICIENCY IN AN AC-PDP

Most previous research related to improving luminous efficiency has focused on optimizing the PDP cell structure [26]-[30] including the emission of vacuum ultraviolet (VUV). Since luminous efficiency is determined based on the ratio of light emission intensity to input current amount, the development of a proper driving waveform for the sustain period, during which the red, green, and blue (R, G, B) visible light for displaying information is emitted, would contribute to the improvement of the luminous efficiency. It is well known that as the luminance tends to be saturated with an increase in the discharge current, the corresponding luminous efficiency decreases. It is well known that as the luminance tends to be saturated with an increase in the discharge current, the corresponding luminous efficiency decreases. Accordingly, the suggestion of an efficient method to lower the discharge current without sacrificing the luminance would contribute to the improvement of the luminous efficiency. In this sense, there have been some previous researches for improving the luminous efficiency using a sustain pulse waveform [31],[32]. The key idea of the previous researches was to enhance the luminous efficiency by producing a self-erasing discharge during a sustain-period in a high frequency region above 160 KHz, however, so far luminous efficiencies have not been improved without reducing the luminance. Therefore, it is necessary to develop a new sustain pulse waveform for improving the luminous efficiency without reducing the luminance. The luminous efficiency is calculated by following equation.

$$\text{Luminance Efficiency} = \frac{4\pi \times \text{Luminance} \times \text{Area}}{V \times A} \qquad [2]$$

29

4.2 PRINCIPLE OF RAMPED-SQUARE SUSTAIN PULSE

In this chapter, a new sustain waveform which adds a ramp-waveform to a square-waveform so as to improve the luminous efficiency is presented. The effects of this new sustain waveform on the cell discharge and the improvement of luminous efficiency in an AC-PDP operated below 100 KHz are then examined [33]-[35].

4.2.1 Cell Discharge Physics in Conventional Square Sustain Waveform

Figure 4-1 (a) shows the schematic waveforms of the voltage (1), current (2), and infrared (IR: 828 nm) (3) based on the actual waveforms measured from the 4-inch AC-PDP test panel in the case of a conventional square sustain waveform. The other driving conditions of Fig. 4-1 (a) were a frequency of 62 KHz, duty ratio of 40 %, and sustain voltage of 190 V. Figure 4-1 (b) shows a schematic model of the temporal behavior of the wall charge produced within the cell with a conventional square sustain waveform. In Fig. 4-1 (b), the upper two electrodes are the sustain electrodes, whereas the lower one is the address electrode. The wall charges are accumulated on the dielectric layer below the two sustain electrodes during the address period prior to applying the sustain pulse, as shown in (i) of Fig. 4-1 (b). As the sustain pulse of Fig. 4-1 (a)-(1) is initially applied to each sustain electrode, the displacement current, as shown by (i) in Fig. 4-1 (a), starts to flow. Then, when the electric field intensity generated within the cell by the sustain voltage plus the accumulating wall charges satisfies the discharge condition, the discharge current also begins to flow, thereby indicating the production of plasma within the cell, as shown in (ii) of Fig. 4-1 (b), and the simultaneous emission of IR light emitted, as shown in (i) in Fig. 4-1 (a)-(3). At this point, the space charges produced during the plasma discharge are

accumulated on the sustain electrodes with an opposite to the polarity to the space charges due to the electric field caused by the sustain voltage, as shown in (iii) of Fig. 4-1 (b) [36]. As illustrated in (2) and (3) of Fig. 4-1 (a), as soon as the discharge current flows, light is emitted and then abruptly disappears because the accumulation of wall charges from the space charges during the plasma discharge causes a reduction in the electric field intensity. However, as shown in (iii) of Fig. 4-1 (b), energetic space charges and metastable atoms still remain after the abrupt extinction of the discharge, although only for a very short time, and disappear as illustrated in (iv) of Fig. 4-1 (b) [37]. Accordingly, these energetic space charges and metastable atoms must be utilized to improve the luminous efficiency. The displacement current starts to flow again at the falling edge of the sustain pulse, as shown in (v) in Fig. 4-1 (a), and the cells shown in (vi) of Fig. 4-1 (b) exhibit the same condition as the previous state. When another sustain pulse is applied, the plasma is again produced within the cell, as shown in (viii) of Fig. 4-1 (b). This process for creating discharges and emitting light is repeated for the duration of the sustain period.

4.2.2 Effects due to Longer-Sustained Discharge

Figure 4-2 (a) shows the schematic waveforms of the voltage (1), current (2), and IR (3) based on the actual waveforms measured from the 4-inch AC-PDP test panel in the case of the proposed new sustain waveform. Figure 4-2 (b) shows a schematic model of the temporal behavior of the wall charges produced within a cell with a ramped-square sustain waveform. The voltage magnitudes at the rising and falling edge were 190 V and 250 V (constant slope: 9.3 V/μsec), respectively. The other driving conditions were the same as those in Fig. 4-1 (a). As shown in (i) of Fig. 4-2 (b), the wall charges are accumulated below the two sustain electrodes due to the write pulse during the address period. As the ramped-square sustain pulse is
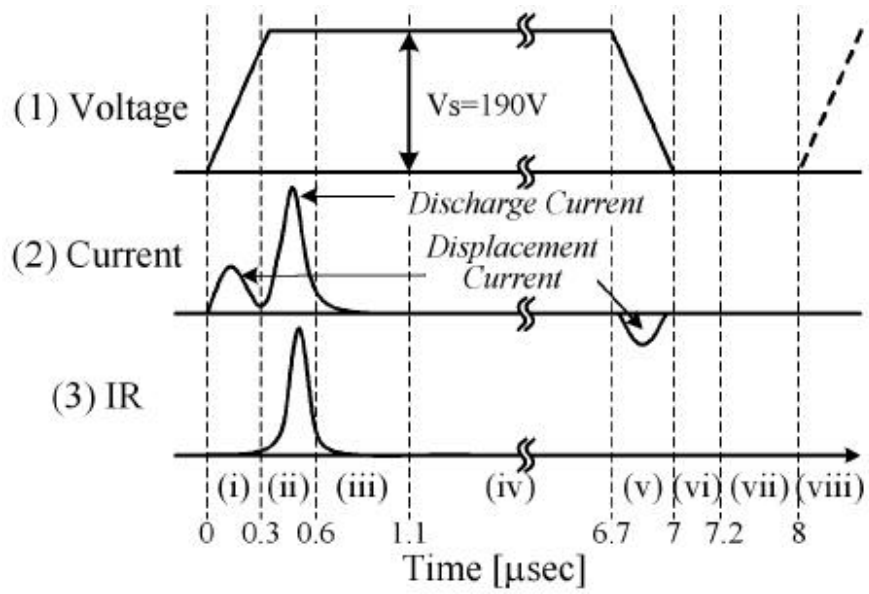
(a)
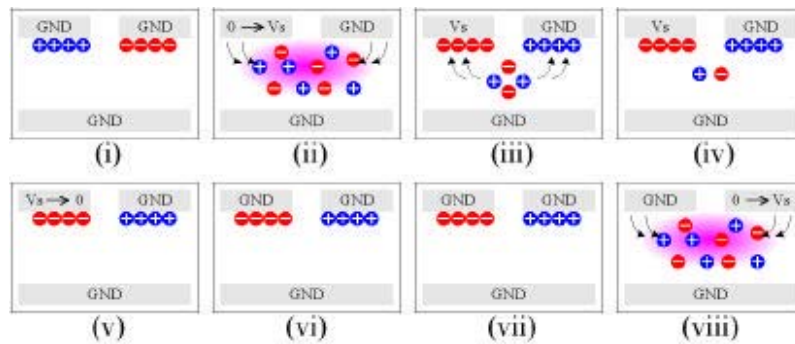
(b)

Figure 4-1: Current and IR (828 nm) waveforms and schematic model for temporal behavior of wall charges in 4-inch AC-PDP with conventional square sustain waveform (a) Conventional square sustain waveform (b) Temporal behavior of wall charges within cell.

applied to the sustain electrode, the displacement current begins to flow, as shown by (i) in Fig. 4-2 (a). Thereafter, the discharge current begins to flow and IR and visible light are simultaneously emitted, indicating the production of plasma within the cell, as shown by (ii) in Figs. 4-2 (a) and (b). As shown in (iii) of Fig. 4-2 (b), the space charges produced during the plasma discharge are accumulated on those the sustain electrodes with an opposite the polarity due to the electric field, thereby resulting in a reduced electric field strength and weak discharge. At this point, the ramped-sustain waveform with an increased voltage slope is able to prevent the abrupt extinction of the electric field caused by the accumulation of the wall charges, thereby resulting in a longer-sustained discharge due to the remaining space charges or metastable atoms, as shown in (iii) of Figs. 4-2 (a) and (b). Since this additional discharge after the first main discharge is due to the metastable atoms, it only requires a very small current, thereby enabling the proposed ramped-square sustain waveform to improve the luminous efficiency.

4.2.3 Effects due to Self-Erasing Discharge

At the falling edge in Fig. 4-2 (a)-(1), another discharge is produced without any additional discharge current consumption and the corresponding light is emitted, whereas, at the falling edge in Fig. 4-1 (a)-(1), there is only a displacement current flows with no light emission. Owing to the increased voltage slope in the ramped-square sustain waveform, as shown in (iv) of Fig. 4-2 (a), the electric field intensity in the discharge cell after the discharge-off at the rising edge remains almost constant such that additional wall charges are accumulated from the space charges, as shown in (iv) of Fig. 4-2 (b). This then causes a self-erasing discharge due to the excessively accumulated wall charges at the falling edge of the ramped-square sustain pulse, with the two sustain electrodes grounded, as shown in (vi) of Fig. 4-2
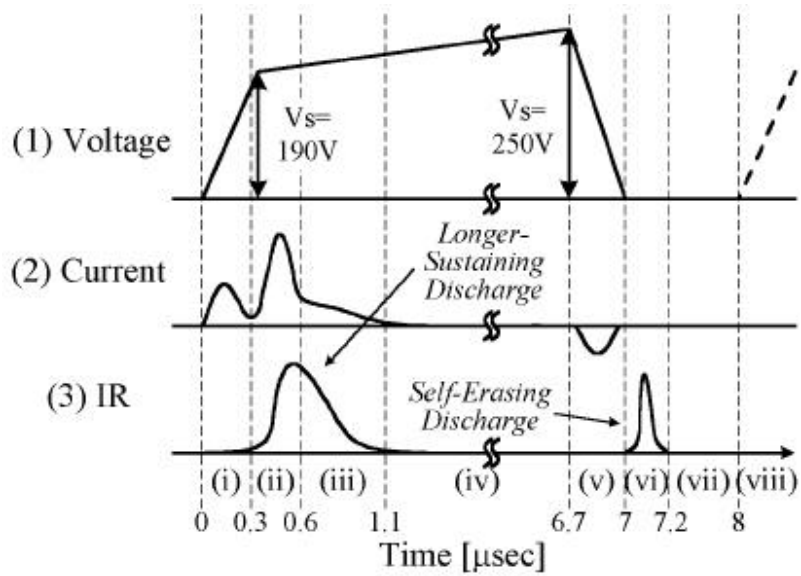
(a)
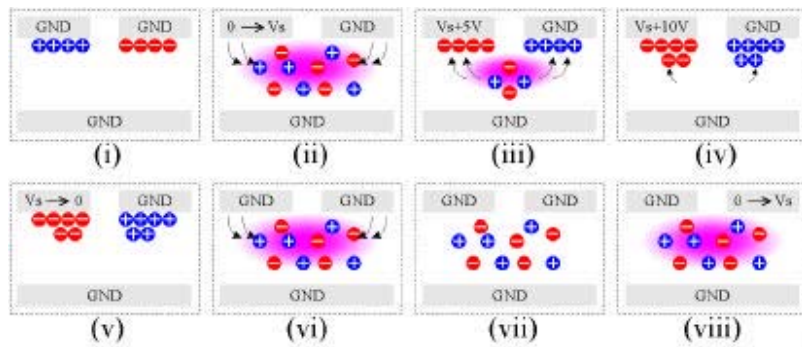
(b)

Figure 4-2: Current and IR (828 nm) waveforms and schematic model for temporal behavior of wall charges in 4-inch AC-PDP with new ramped-square sustain waveform (a) New ramped-square sustain waveform (b) Temporal behavior of wall charges within cell.

(b). Since this self-erasing discharge is produced only by those wall charges accumulated within the cell, the light emission is generated without any additional discharge current consumption, as shown in (vi) of Fig. 4-2 (a)-(2) and (3). Therefore, this self-erasing discharge can also improve the luminous efficiency. Furthermore, in addition to removing wall charges, this self-erasing discharge also produces the space charges, as shown in (vii) of Fig. 4-2 (b), which are necessary for the next sustain discharge. Accordingly, since the next sustain pulse is applied within the 0.8 μsec after the self-erasing discharge, the next sustain discharge is produced using only the space charges, as shown in (viii) of Fig. 4-2 (b) [37]. However, this result does not guarantee whether the wall charges during the self-erasing discharge is completely removed [38]. Through the further study, we will try to make it sure whether a non-negligible amount of wall charges still remains after the self-erasing discharge.

4.2.4 Analysis using Vt Closed Curve

Figure 4-3 shows the ramped-square sustain pulse and the trajectories of wall and cell voltage of ON cell during sustain period. The wall and cell voltage position of ON cell after the scan period may be at left side of Vt closed curve, as shown in Fig. 4-1 (1). Abrupt voltage change of Y electrode in +Y direction moves the cell voltage position into the discharge region through the Vt_{YX} side, and produces a strong discharge between two sustain electrodes (X and Y), as shown in Fig. 4-1 (1). Thereafter, the space charges produced by strong discharge are converted into wall charges by the applied voltages, thereby resulting that the cell voltage becomes zero, as shown in Fig. 4-3 (2). The increasing applied voltage of Y electrode according to the ramped-square sustain waveform maintains non-zero of the cell voltage, and convert more space charges into wall charges until the cell voltage becomes zero, as shown in Fig. 4-3 (3). This additional process can gather more wall

charges compared to the conventional square sustain waveform, and moves the wall voltage position to outside of the Vt closed curve. Excessively accumulated wall charges induces a self-erasing discharge at the falling edge of a sustain pulse using very high wall voltage, as shown in Fig. 4-3 (4). After the self-erasing discharge, the wall voltage position moves to inside of the Vt closed curve due to reduction of wall charges, as shown in Fig. 4-3 (4'). Subsequent ramped-square sustain pulse applied to Z electrode produce next sustain discharge using the wall voltage with help of space charges produced by the self-erasing discharge, as shown in Fig. 4-3 (5).

Figure 4-4 shows the trajectories of wall and cell voltage of OFF cell during sustain period. The wall and cell voltage position of OFF cell before the sustain period is determined by the reset waveform, exist on the vertical axis of Vt closed curve. The cell voltage position is moved to left side of Vt_{YX} side of Vt closed curve by the ramped-square sustain waveform applied to Y electrode, as shown in Fig. 4-4 (1). The increasing applied voltage according to the ramped-square sustain waveform moves the cell voltage position to near Vt_{XY} side of the Vt closed curve, as shown in Fig. 4-4 (2). If the cell voltage position is located in the discharge region by the exceeding applied voltage, an undesired sustain discharge can be occurred by the subsequent sustain pulses. Thus, the maximum voltage of ramped-square sustain waveform must be controlled to not occur the undesired sustain discharge at the OFF cell. The changes of cell voltage position by the ramped-square sustain waveform applied to X electrode shows same tendency with the case of applying pulse to Y electrode, as shown in Figs. 4-4 (5) and (6).
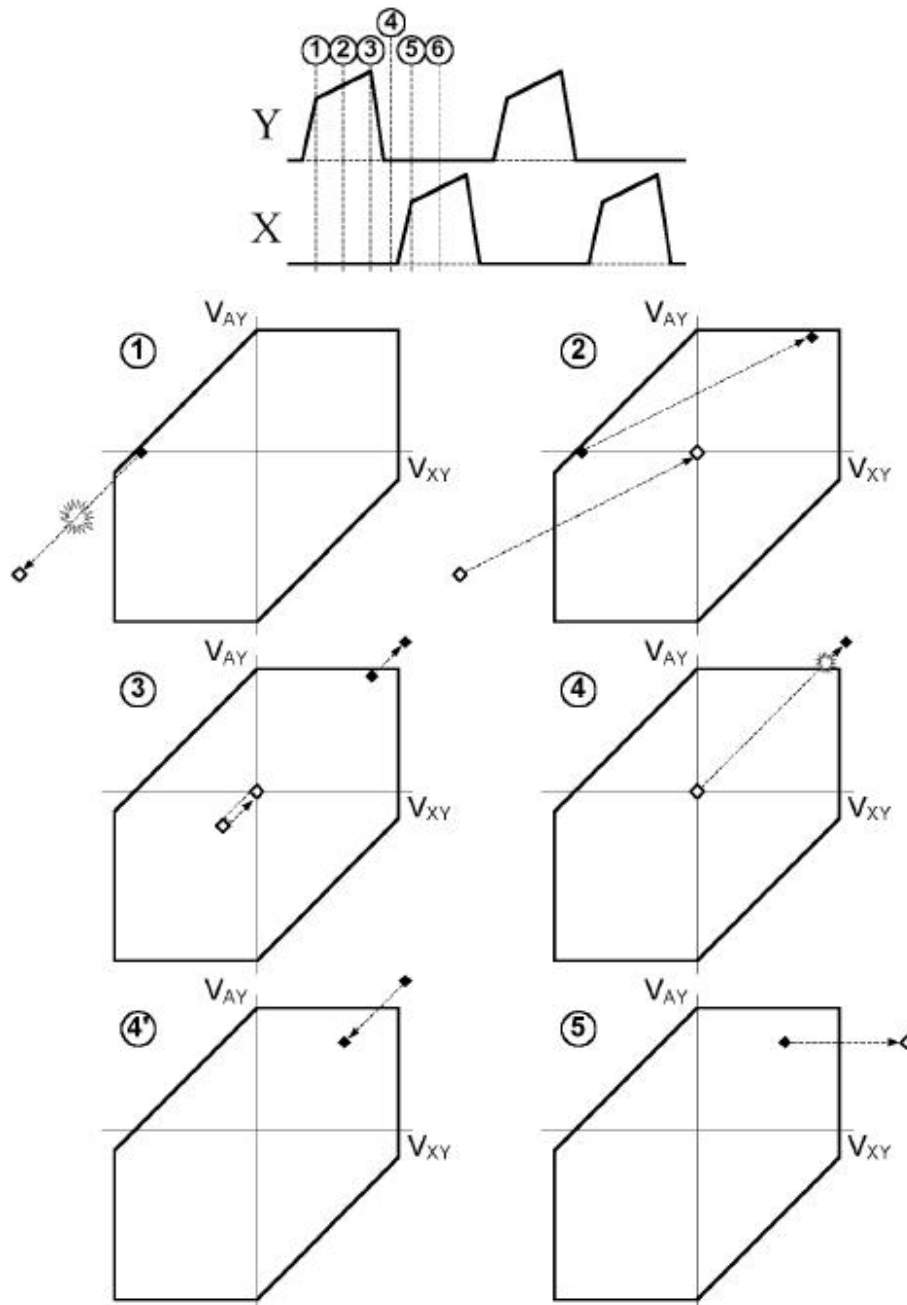
Figure 4-3: Ramped square sustain pulse and trajectories of wall and cell voltage of ON cell during sustain period.
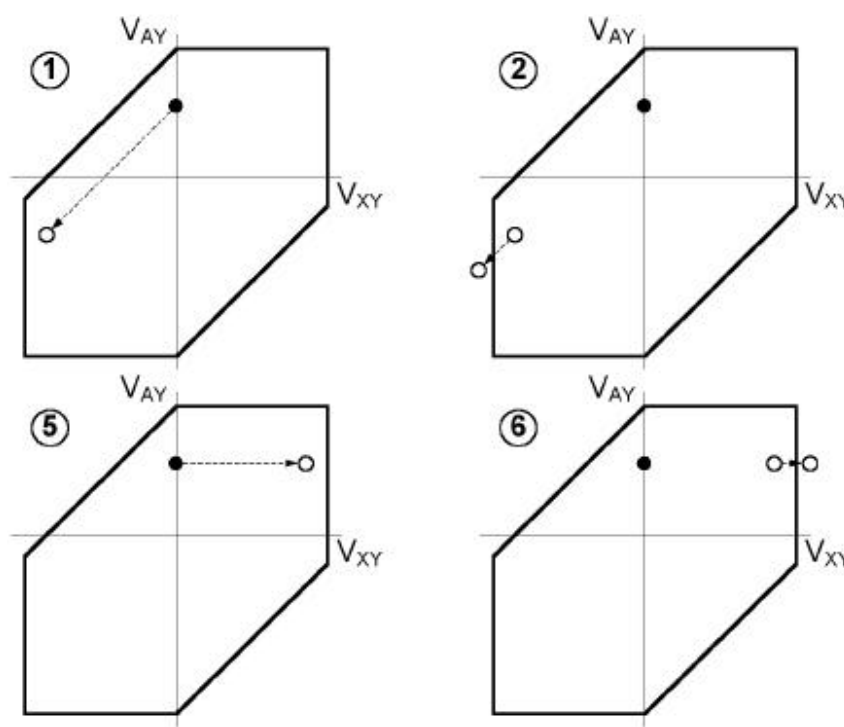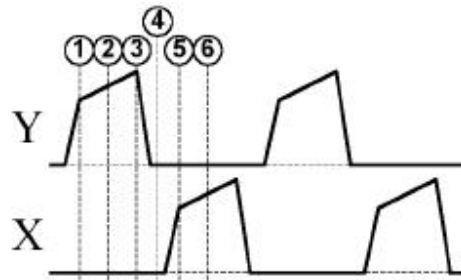
Figure 4-4: Ramped square sustain pulse and trajectories of wall and cell voltage of OFF cell during sustain period.

4.2.5 Improvement of Luminous Efficiency with Various Voltage Increase Rates

Figure 4-5 illustrates the changes in the luminance, discharge power consumption, and luminous efficiency measured from the 4-inch AC-PDP test panel employing the new ramped-square sustain pulses with increased voltage slopes from 0 V/μsec to 9.3 V/μsec. The power displayed on Fig. 4-5 includes only the consumed power by the test panel, except that by the driving circuits. The other driving conditions are similar to those in Figs. 4-1 and 4-2. As the voltage increase rates increased from 0 V/μsec to 9.3 V/μ sec, the consumption power decreased from 3.17 W to 1.47 W, and the luminance decreased from 711 cd/m^2 to 619 cd/m^2, except for the condition of 3.1 V/μsec. In contrast, the luminous efficiency improved 1.03 lm/W to 1.7 lm/W (65 % improvement), as the voltage increase rates increased from 0 V/μsec to 9.3 V/μsec.
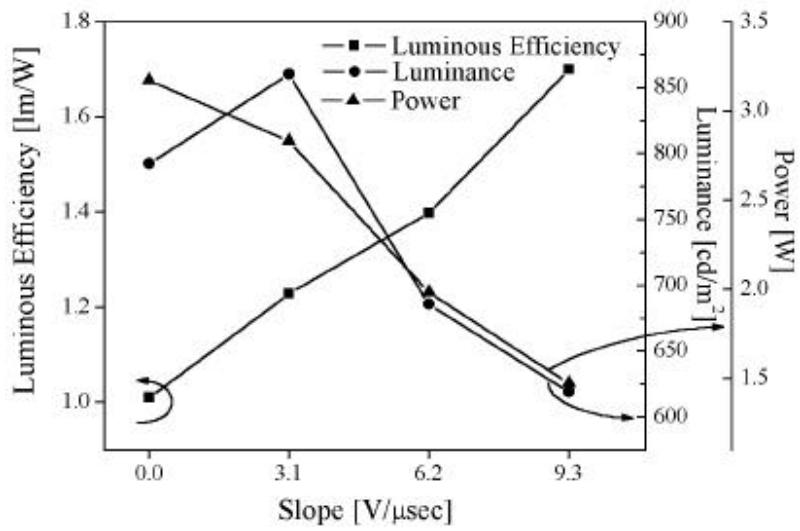
Figure 4-5: Change in luminance, consumption power, and luminous efficiency with increased voltage slope in new ramped-square sustain waveform.

4.3 CHARACTERISTICS OF RAMPED-SQUARE SUSTAIN PULSE

In previous chapter, the work has focused only on the improvement of luminous efficiency, and not on the improvement of luminance. Accordingly, in that work, we have not achieved the higher luminous efficiency without reducing the luminance. The luminance decreased to 22 %, and also misfiring problem was occurred, even though the higher luminous efficiency of 65 % was obtained at the high sustain voltage of 250 V. These side effects such as the reduction of the luminance and the misfiring problem are thought to be due to the too strong self-erasing discharge caused by the high sustain voltage.

In this chapter, a new ramped-square sustain waveform is presented for improving both the luminance and the luminous efficiency with a low square- and ramp-voltage. The effects of the square-voltage and ramp-voltage (voltage slope) in the ramped-square sustain waveform on the main and self-erasing discharges in a 4-inch AC-PDP test panel at a frequency of 62 KHz are then examined.

4.3.1 Discharge Characteristics of Ramped-Square Sustain Waveform

Figure 4-6 shows the schematic waveforms of the voltage (1), current (2) and infrared (IR: 828 nm) (3) based on the actual waveforms measured from the 4-inch AC-PDP test panel with the ramped-square sustain waveform. The ramped-square sustain waveform is a superimposed waveform, which adds a ramp-waveform to a conventional square sustain waveform with a same pulse width, and has an constantly increasing voltage slope between the rising and falling edge of the sustain pulse, as shown in Fig. 4-6 (1). The voltage of square-waveform in the ramped-square waveform, namely the voltage at the
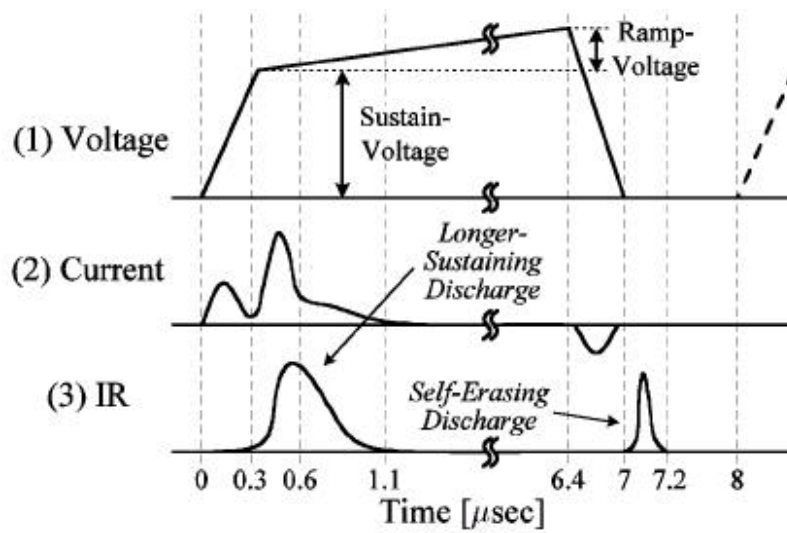
Figure 4-6: Voltage (1), current (2) and IR (3) waveform with ramped-square sustain pulse.

rising edge of the ramped-square sustain pulse (hereafter, this will be called `square-voltage'), has conditions of 150, 160, 170 and 180 V. The value of voltage difference between the rising and falling edge of the ramped-square sustain pulse (hereafter, this will be called `ramp-voltage'), has the conditions of 0, 10, 20, 30 and 40 V, indicating that the increasing voltage slopes are 0, 1.5, 3.1, 4.6, and 6.2 V/μsec, respectively. The other driving conditions are a frequency of 62 KHz, duty ratio of 40 %, rising time of 300 nsec, and falling time of 600 nsec.

In the case of a ramped-square sustain pulse, the constantly increasing voltage slope prevents the rapid reduction of an electric field caused by the accumulation of wall charges. Therefore, this new sustain waveform can prevent an immediate extinction of plasma discharge, thereby resulting in inducing a longer sustaining discharge. More energetic space charges and metastable atoms can be utilized in the case of a longer sustaining discharge, thereby contributing to the improvement of a luminous efficiency. However, it is important to note that all the ramped-square sustain waveforms cannot induce a longer sustaining discharge. To compensate the electric field intensity reduced due to the wall voltage, the increasing voltage slope in the ramped-square sustain waveform needs to be greater than the wall voltage with opposite polarity to applied sustain pulse. Thus only the ramped-square sustain waveforms with the ramp-voltage greater than the wall voltage produced by the accumulation of the wall charges can induce a longer sustaining discharge. In other words, a longer sustaining discharge depends on the magnitude of the ramp-voltage, namely increasing voltage slope. The ramp-voltages for inducing a longer sustaining discharge vary according to the wall voltages, which are determined by the amount of accumulation of wall charges. In this experiment, the ramped-square sustain waveforms with the ramp-voltages greater than 20 V began to produce a longer sustaining discharge.

After the longer sustaining discharge, the electric field intensity kept constant due to the constantly increasing voltage slope, transforming the space

charges into the additional wall charges. This excessively accumulated wall charges can produce a self-erasing discharge at the falling edge of the ramped-square sustain pulse, as shown in Fig. 4-6 (3). As the self-erasing discharge is produced only by the wall charges, it requires no additional power consumption, thereby improving the luminous efficiency. However, it is very difficult to separate whether the main contribution factor for improving the luminance and luminous efficiency is a longer sustaining discharge at the rising edge or a self-erasing discharge at the falling edge in this ramped-square sustain waveform. We will try to make this point clear through the further study on the discharge physics of the ramped-square sustain waveform.

4.3.2 Effects of Square-Voltage in Ramped-Square Sustain Waveform

Figure 4-7 shows the changes in the voltage (a) and IR (b) waveforms measured from the 4-inch AC-PDP test panel as a variation of square-voltage of the new ramped-square sustain pulses at a constant ramp-voltage of 30 V. The square-voltage conditions are 150, 160, 170 and 180 V, and the voltage slope is about 4.6 V/μsec in all square-voltages. The horizontal axes of Figs. 4-7 (a) and (b) are the same time scale. As shown in Figs. 4-7 (a) and (b), the main discharge and the self-erasing discharge are produced at the rising and falling edge of the proposed pulse, respectively, indicating that the ramped-square sustain waveform can induce two light pulses per one sustain pulse. Figure 4-8 (a) shows the changes in the IR intensity emitted from the self-erasing discharge during 6.8 ~ 7.3 μsec at the falling edge with an increase in the square-voltage of a ramped-square sustain pulse. As shown in Fig. 4-8 (a), the self-erasing discharge intensity becomes strong as the square-voltage increases. This strong self-erasing discharge is due to the larger amount of wall charges accumulated in the main discharge. Since the

44

Figure 4-7: Changes in IR intensity (b) of main discharge at rising edge and self-erasing discharge at falling edge with various square-voltages of ramped-square sustain waveforms (a).

Figure 4-8: Changes in intensities of IR waveforms produced from self-erasing discharge (a) and next main discharge (b) with various square-voltages of ramped-square sustain waveforms.

main discharge intensity before a self-erasing discharge becomes strong in proportion to the increase in the square-voltage, more space charges, which are converted into the wall charges, are generated in the cell. Therefore, as the square-voltage of a ramped-square sustain pulse increases, the self-erasing discharge intensity becomes stronger, as shown in Fig. 4-8 (a).

Figure 4-8 (b) shows the changes in the IR intensity emitted from the main discharge during 8.2 ~ 8.8 μsec at the rising edge after the self-erasing discharge with an increase in the square-voltage of a ramped-square sustain pulse. The vertical axes of Figs. 4-8 (a) and (b) are the same scale. As shown in Fig. 4-8 (b), the main discharge is produced more strongly with higher square-voltage, except for the square-voltage condition of 180 V. In a conventional self-erasing sustain discharge, if the sustain pulses applied have the same amplitudes, the IR intensity emitted from the main discharge tends to decrease as the self-erasing discharge intensity increases. In this experiment, however, the IR intensity from the main discharge does not decrease even though the self-erasing discharge intensity increases with an increase in the square-voltage of a ramped-square sustain pulse. In addition, at the square-voltage of 180 V, the intensity of the self-erasing discharge prior to the main discharge is produced so strongly, compared with that of the self-erasing discharge at the square-voltage of 170 V, that the emission of the IR from the main discharge is delayed and sustained slightly longer, as shown in Fig. 4-8 (b). This phenomenon is presumably due to the changes in the conversion rate of the wall charges into the space charges according to the intensity of the self-erasing discharge. We will make this point clear through the further study.

Figures 4-9 and 4-10 show the changes in the luminance and luminous efficiency with an increase in the square-voltages from 150 V to 180 V, in the cases of a ramped-square sustain waveform with a constant ramp-voltage of 30 V and a conventional square sustain waveform, respectively. As shown in Fig. 4-9, the luminance of a ramped-square sustain waveform at all square-voltage conditions is improved above 15 %, compared with that of a
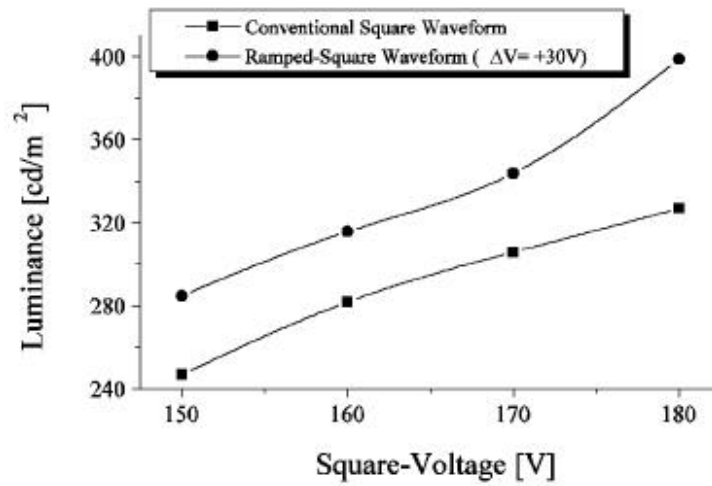
Figure 4-9: Changes in luminance of conventional square waveform and new ramped-square waveform with constant ramp-voltage of 30 V as variation of square-voltage.
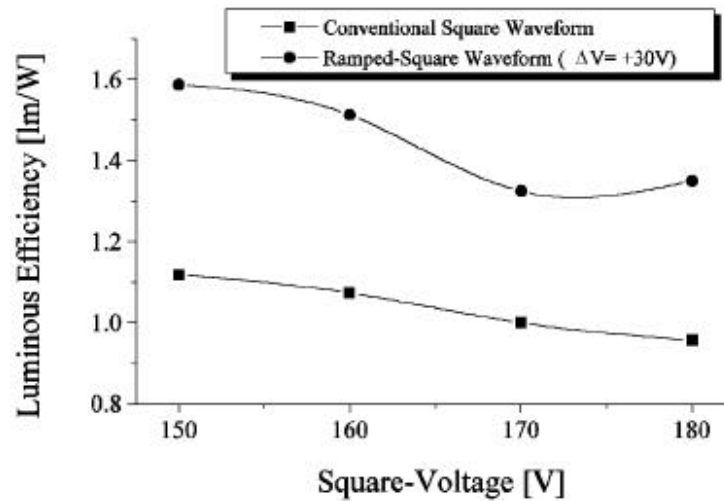
Figure 4-10: Changes in luminous efficiency of conventional square waveform and new ramped-square waveform with constant ramp-voltage of 30 V as variation of square-voltage.

conventional square sustain waveform. As the luminance is proportioned to the light intensity emitted from the main discharge plus the self-erasing discharge, the luminance of the ramped-square sustain waveform increases with an increase of the square-voltage. As shown in Fig. 4-10, the luminous efficiency of the ramped-square sustain waveform at all square-voltage conditions is also improved above 30 %, compared with that of a conventional square sustain waveform. The reason is that the ramped-square sustain waveform can induce two light pulses per one sustain pulse irrespective of the amplitude of the square-voltage.

4.3.3 Effects of Ramp-Voltage in Ramped-Square Sustain Waveform

Figure 4-11 shows the changes in the voltage (a) and IR (b) waveforms measured from the 4-inch AC-PDP test panel as a variation of the ramp-voltage of a new ramped-square sustain pulse at a constant square-voltage of 170 V. The ramp-voltage conditions are 0, 10, 20, 30 and 40 V, indicating that the voltage slopes are 0, 1.5, 3.1, 4.6 and 6.2 V/μsec, respectively. The horizontal axes of Figs. 4-11 (a) and (b) are the same time scale. Figure 4-12 (a) shows the changes in the IR intensity emitted from the self-erasing discharge during 6.8 ~ 7.3 μsec at the falling edge with an increase in the ramp-voltage of a ramped-square sustain pulse. As shown in Fig. 4-12 (a), the self-erasing discharge is produced at the ramp-voltage greater than 0 V, and the self-erasing discharge intensity becomes strong as the ramp-voltage increases. The increase in the ramp-voltage of a ramped-square sustain waveform means that the electric field intensity in the discharge cell after the discharge-off at the rising edge becomes stronger in proportion to the increasing ramp-voltage slope. The electric field is so strong that additional wall charges can be accumulated from the space charges. This then causes a strong self-erasing discharge due to the excessively accumulated

49
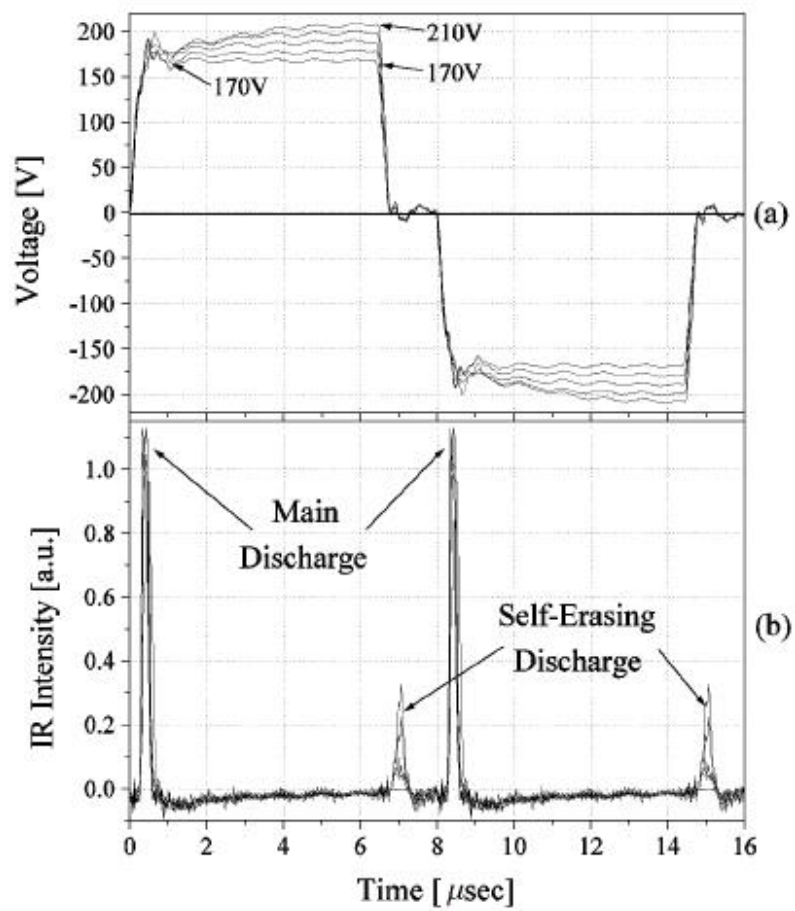
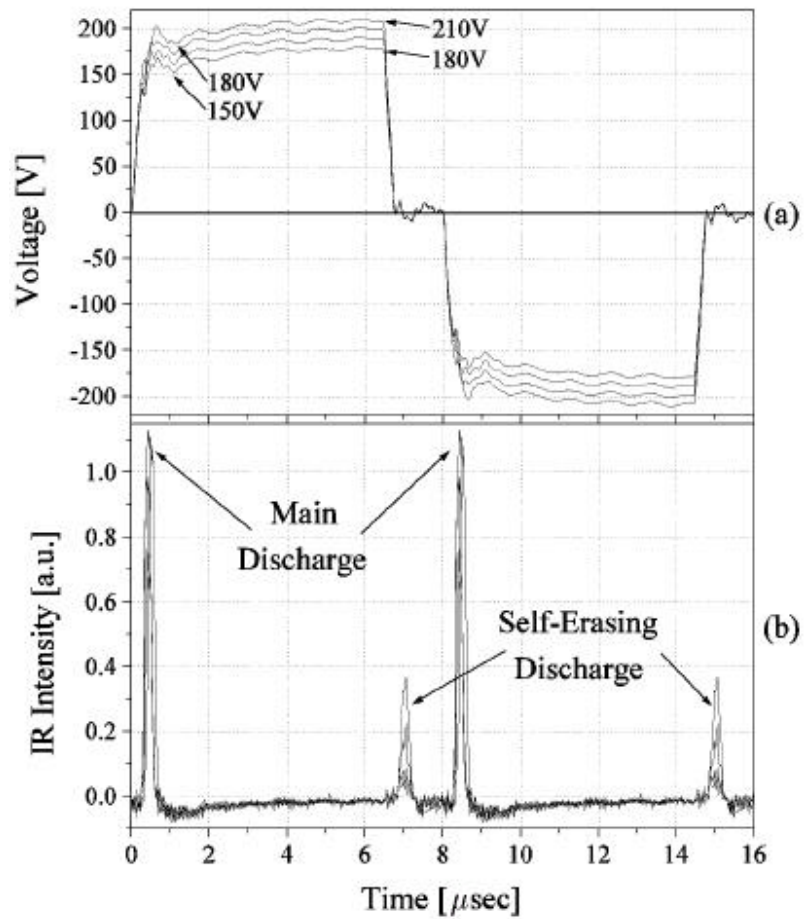**Figure 4-11:** Changes in IR intensity (b) of main discharge at rising edge and self-erasing discharge at fall edge with various ramp-voltages of ramped-square sustain waveform (a).
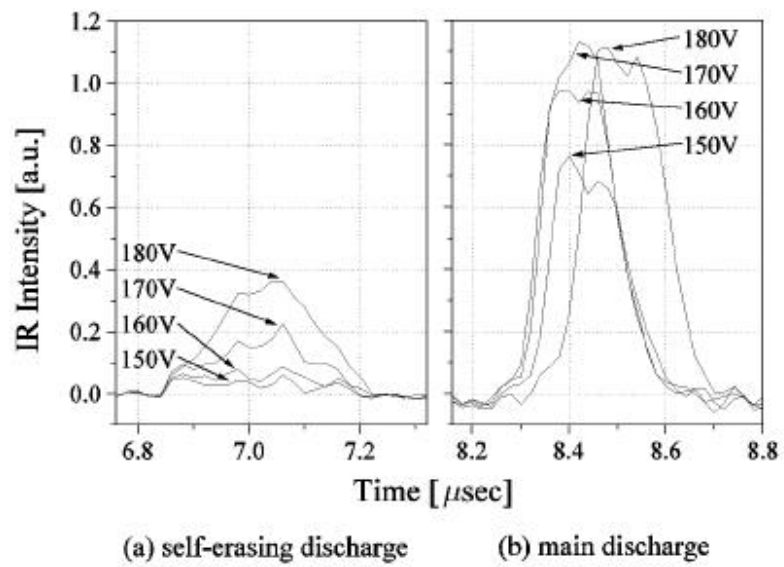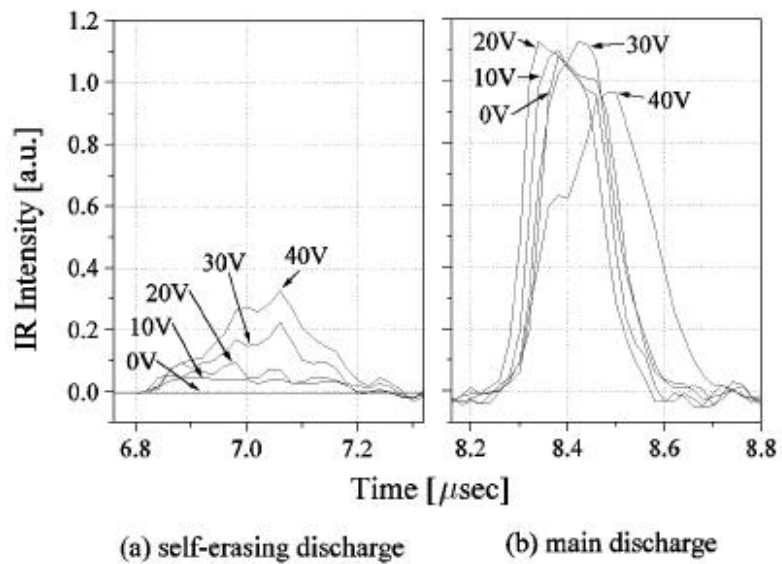
Figure 4-12: Changes in intensities of IR waveforms produced from self-erasing discharge (a) and next main discharge (b) with various ramp-voltages of ramped-square sustain waveforms.

wall charges at the falling edge of a ramped-square sustain pulse.

Figure 4-12 (b) shows the changes in the IR intensity emitted from the main discharge during 8.2 ~ 8.8 μsec at the rising edge after the self-erasing discharge with an increase in the ramp-voltage of a ramped-square sustain pulse. The vertical axes of Figs. 4-12 (a) and (b) are also the same scale. As shown in Fig. 4-12 (b), in the case of the increased ramp-voltage of a ramped-square sustain waveform, the IR intensity emitted from the main discharge rarely changes except for the ramp-voltage of 40 V, even though the self-erasing discharge prior to the main discharge becomes strong. The pulse widths of IR waveforms measured at the half point of peak value range from 229 to 231 nsec as the ramp voltages increase from 0 to 20 V at the constant square voltage of 170 V. At the ramp-voltage of 30 V, the IR pulse width is approximately 240 nsec, indicating that this magnitude of the ramp-voltage begins to induce a longer sustaining discharge. In particular, at the ramp-voltage of 40 V, the IR pulse width is approximately 320 nsec, indicating that the main discharge at the rising edge remains during much longer time. As a result, the longer sustaining main discharge at the rising edge can be induced if the ramped-square sustain waveform has the high ramp-voltage slope of 6.2 V/μsec. However, the self-erasing discharge intensity at the ramp-voltage of 40 V is so strong that the IR intensity emitted from the main discharge is slightly reduced, as shown in Fig. 4-12 (b).

Figures 4-13 and 4-14 show the changes in luminance and luminous efficiency with increased ramp-voltages from 0 V to 40 V in the case of a ramped-square sustain waveform at a constant square-voltage of 170 V. Since the luminance is determined based on the light emitted from a self-erasing discharge plus a main discharge, the luminance of the ramped-square sustain pulse is brighter than that of the conventional square sustain pulse, as shown in Fig. 4-13. The improvement rate of a luminance shows a maximum value of 20 % when the strongest self-erasing discharge is produced at 40 V ramp-voltage condition. As shown in Fig. 4-14, the luminous efficiency of
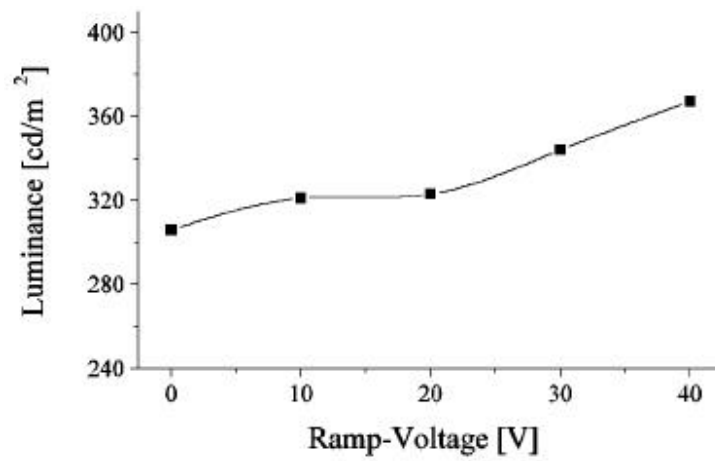
Figure 4-13: Changes in luminance of conventional square sustain waveform (ramp-voltage = 0 V) and new ramped-square sustain waveforms (ramp-voltage > 0 V) with constant square voltage of 170 V as variation of ramp-voltage.
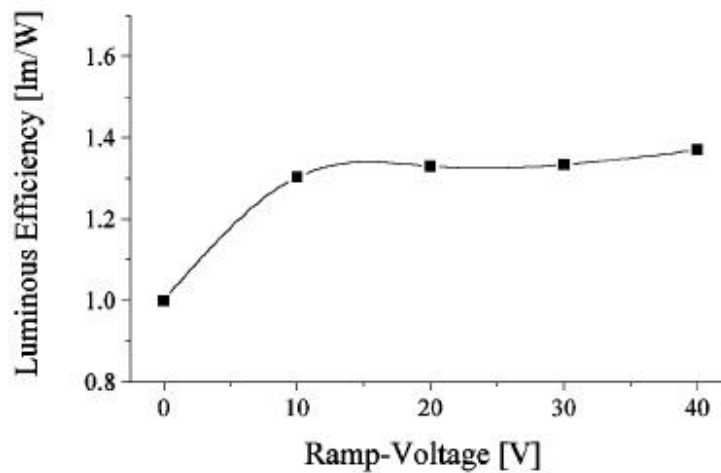
Figure 4-14: Changes in luminous efficiency of conventional square sustain waveform (ramp-voltage = 0 V) and new ramped-square sustain waveforms (ramp-voltage > 0 V) with constant square voltage of 170 V as variation of ramp-voltage.

53

the ramped-square sustain pulse is improved more than 30 %, compared with that of the conventional square sustain pulse. The improvement rate of a luminous efficiency shows a maximum value of 37 % when the strongest self-erasing discharge is produced at 40 V ramp-voltage condition. This improvement is due to both the longer-sustaining main discharge at the rising edge and the strong self-erasing discharge at the falling edge in the ramped-square sustain waveform with a high ramp-voltage slope of 6.2 V/μ sec.

5. AUXILIARY ADDRESS PULSE

5.1 PRINCIPLE OF AUXILIARY ADDRESS PULSE

Fig. 5-1 (a) shows the driving waveforms applied to the 4-in. test panel for the reset-, address-, and sustain-periods. Since the waveforms, particularly for the reset- and address-periods employed in this new driving scheme are typically used in the conventional address-display-separated (ADS) driving scheme, the corresponding reset and address discharge characteristics are observed to be almost the same as those in the conventional ADS driving method (not shown here). It was reported in that the proper control of the amplitudes and widths of the auxiliary address pulse during a sustain-period can improve both the luminance and the luminous efficiency in the PDP. The luminance variation is investigated according to the application conditions of the auxiliary pulses based on the discharge characteristics in the R, G, and B cells. In this work, as for the auxiliary pulses, the three parameters such as amplitude V_A, width T_W, and delay time T_D from a rising edge of the sustain pulse, are chosen to investigate the influence on the variation of the discharge characteristics, as shown in Fig. 5-1 (b). When the sustain pulses V_{SX} is applied to the sustain electrode X and no auxiliary pulse is applied to the address electrode, as shown in Case 1 of Fig. 5-2, the displacement current flows for about 0.3 μs through the dielectric layer prior to the flow of the discharge current. Thereafter, if the electric field intensity induced by the sustain voltage satisfies the discharge ignition condition, the discharge current begins to flow, implying that a plasma is produced within the cell. The IR of 828 nm is also emitted from the cell while the discharge current is flowing from 0.3 μs to 0.6 μs. During this time, the space charges such as electrons and ions, generated from the plasma, are attracted toward the sustain electrodes in an opposite direction to the electric field induced by the external sustain voltage V_{SX}. The conversion process from the space   charges
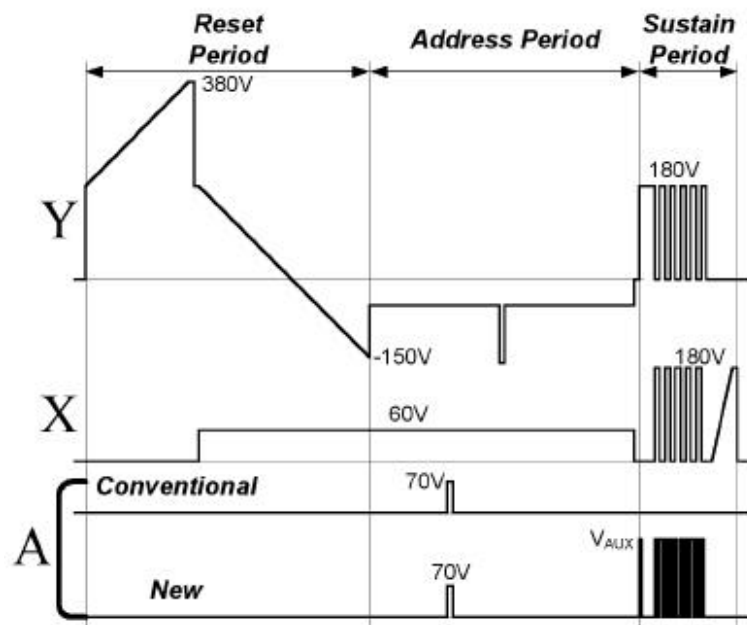
(a)
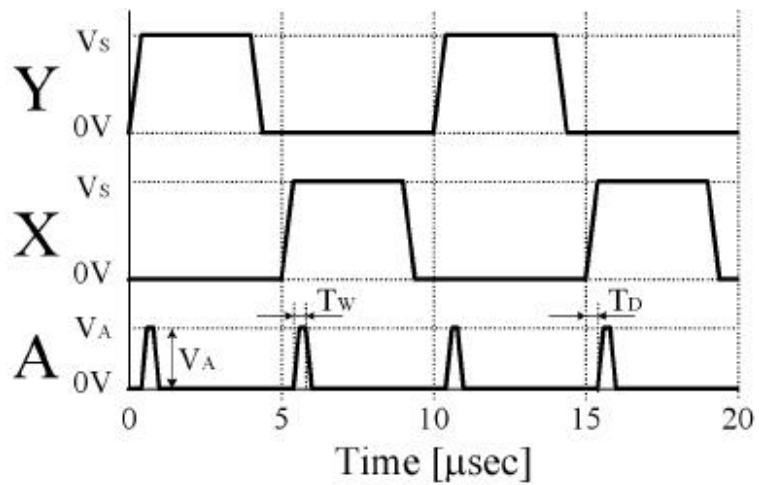
(b)

Figure 5-1: Driving waveforms (a) of 4-in. test panel and voltage waveforms (b) applied to three electrodes X, Y, and A for luminance control during sustain-period.
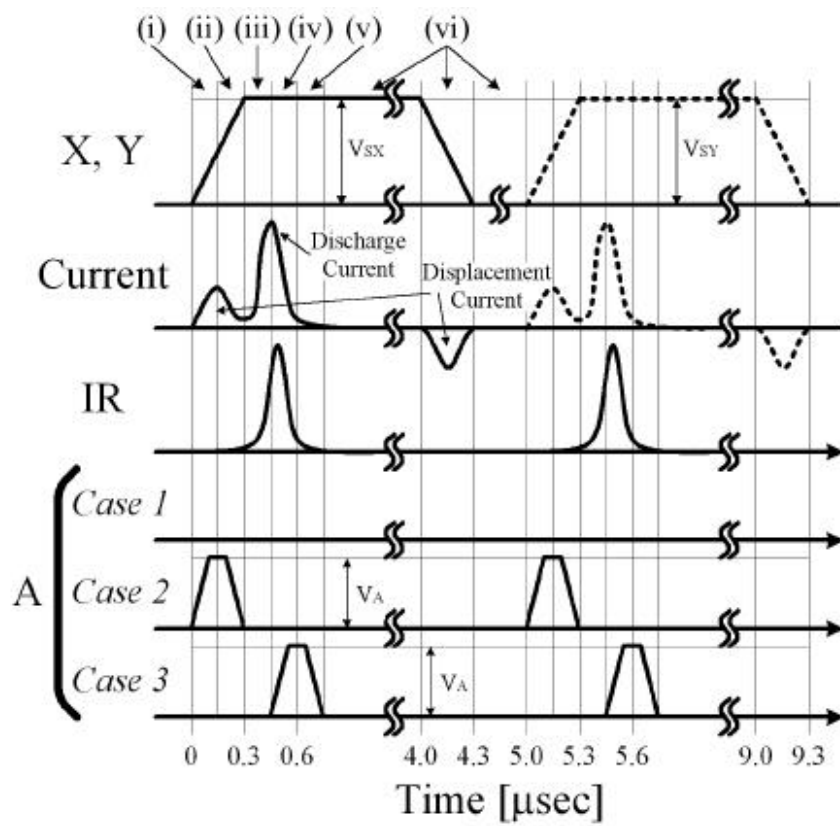
Figure 5-2: Displacement current, discharge current, and infrared (828 nm) waveforms when two sustain pulses are applied to sustain electrodes and no auxiliary is applied to address electrode (Case 1: conventional driving method). Two different types of new auxiliary pulses applied to address electrodes during sustain-period (Cases 2 and 3: new driving method).

into the wall charges during a discharge continues until the total electric field is too weak to maintain the discharge due to the opposite electric field induced by the accumulated wall charges.

Based on the experimental result for the discharge current flowing from 0.3 μs to 0.6 μs in the case of the conventional driving method (Case 1), the two different types of auxiliary pulses are chosen to be applied to the address electrode, as shown in Cases 2 and 3 of Fig. 5-2. The auxiliary short pulse in Case 2 is applied to the address electrode prior to the flow of the discharge current. It is expected that this additional short pulse prior to the main discharge can assist in producing the faster and more efficient plasma for the improvement of the luminance. Another case (Case 3) is that the auxiliary short pulse is applied to the address electrode with some delay time of about 0.45 μs. It appears that this additional short pulse would reduce the luminance slightly by disturbing the wall charge accumulation on the sustain electrodes. However, in Case 3, careful attention should be paid to the proper choice of the delay time for the slight disturbance of the wall charge accumulation.

Fig. 5-3 (a) shows the schematic model of the space charges/wall charges within the PDP cell when the auxiliary pulse shown in Case 2 of Fig. 5-2 is applied simultaneously to the address electrode. The pulse width of the auxiliary pulse is fixed as 200 ns, whereas the amplitudes of the auxiliary pulse vary from 0 V to 140 V. The driving condition for the sustain pulses are the same as that in Case 1 of Fig 5-2. The rising rate (rising time: 100 ns) of the auxiliary short pulse V_A is higher than that (rising time: 300 ns) of the sustain pulse V_{SX}. This positive auxiliary short pulse with a high rising rate attracts the electrons accumulated on the sustain electrode Y toward the address electrode A, as shown in (i) of Fig. 5-3 (a). The electrons detached by the auxiliary short pulse can work as the priming particles at the initiation of the discharge by the sustain pulse. Accordingly, this transition of these electrons from wall charges into space charges prior to an ignition of the sustain discharge can promote the activation of the plasma

(a)

(b)
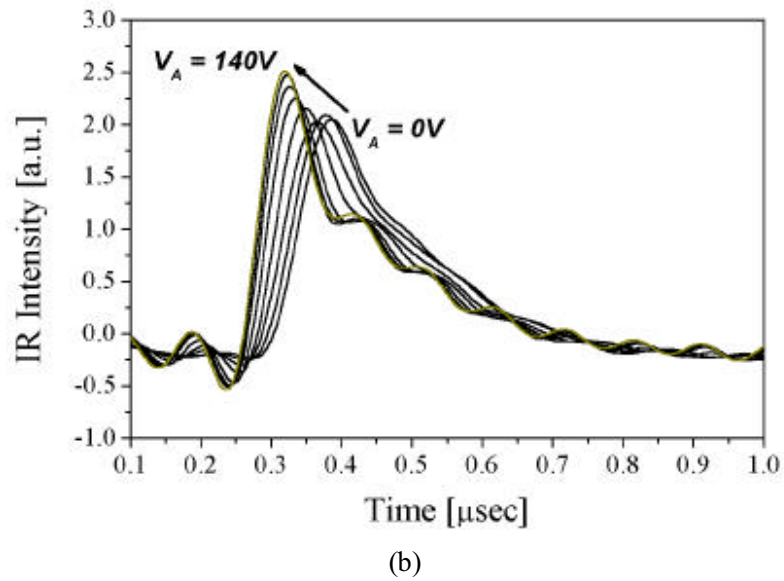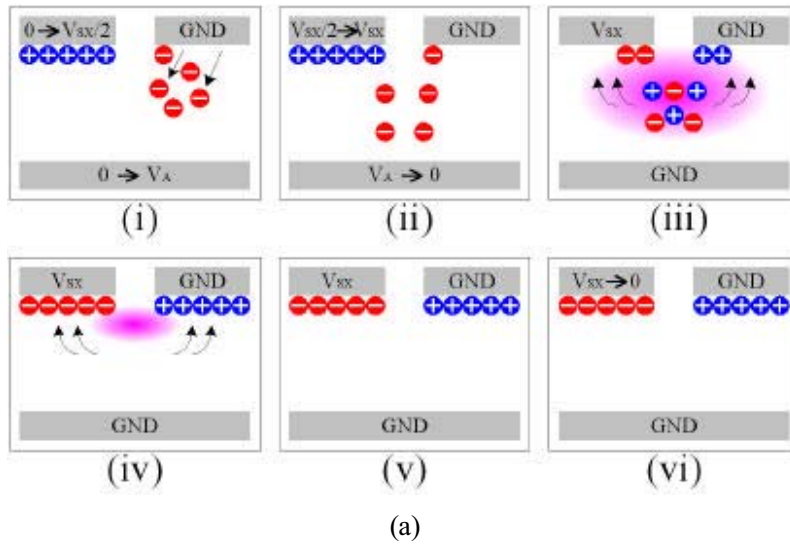
Figure 5-3: Schematic model (a) of space charges/wall charges within PDP cell and measured IR (828 nm) waveforms (b) in case of adopting auxiliary pulse shown in Case 2 of Fig. 5-2.

discharge, as shown in (ii, iii) of Fig. 5-3 (a). These priming particles, *i.e.*, electrons in this case, can play a role not only in improving the discharge efficiency but also in forming the faster discharge because they can produce the plasma efficiently even under the weak electric field condition. As illustrated in the measure IR (828 nm) waveforms of Fig. 5-3 (b), the peaks of the IR waveforms are observed to be shifted to the left and to get higher with an increase in the amplitude of the auxiliary pulse from 0 V to 140 V, confirming that the plasma is produced fast and efficiently under the weak electric field condition. It is also observed that as the pulse width is wider than 200 ns, the contribution to the fast and efficient plasma generation is reduced gradually (not shown here). This effect is thought to be presumably due to the disturbance of the wall charge accumulation during the sustaining discharge caused by the auxiliary pulse with the pulse width wider than 200 ns.

Fig. 5-4 (a) illustrates the schematic model of the space charges/wall charges within the PDP cell when the auxiliary pulse shown in Case 3 of Fig. 5-2 is applied simultaneously to the address electrode. The application time of the auxiliary pulse is delayed for about 450 ns from the rising edge of the sustain pulse. The pulse width of the auxiliary pulse is fixed as 200 ns, whereas the amplitudes of the auxiliary pulse vary from 0 V to 140 V. The driving condition for the sustain pulses are the same as that in Case 1 of Fig 5-2. When a plasma is produced within a cell by applying the sustain pulse, the wall charges begins to be accumulated below the sustain electrodes, as shown in (iii) of Fig. 5-4 (a). Most of wall charges are accumulated from 0.3 μs to 0.6 μs, as indicated in the IR data of Fig. 5-4 (b). If the auxiliary pulse is applied at about 0.45 μs to an address electrode, this positive pulse would attract the space charges such as the electrons toward the address electrode, thus resulting in disturbing the accumulations of the wall charges toward the sustain electrodes, as shown in (iv) of Fig. 5-4 (a). Accordingly, some electrons are accumulated on the address electrode, even though the other electrons are accumulated on the sustain electrode, as shown in (v) of

(a)

(b)
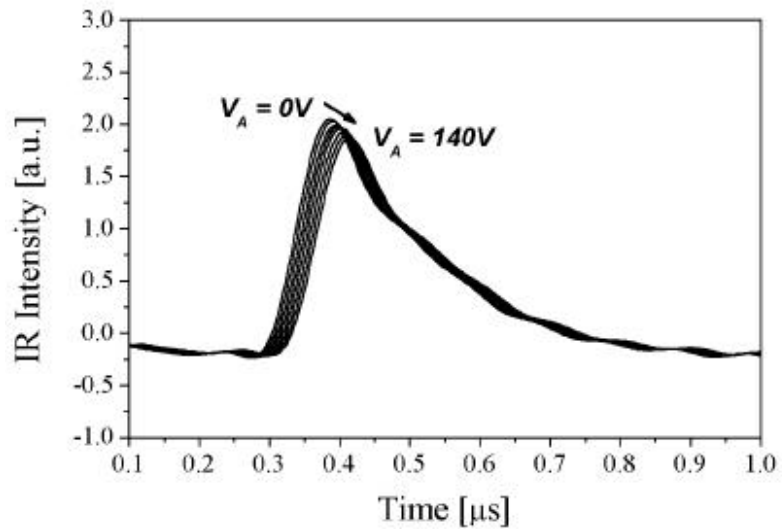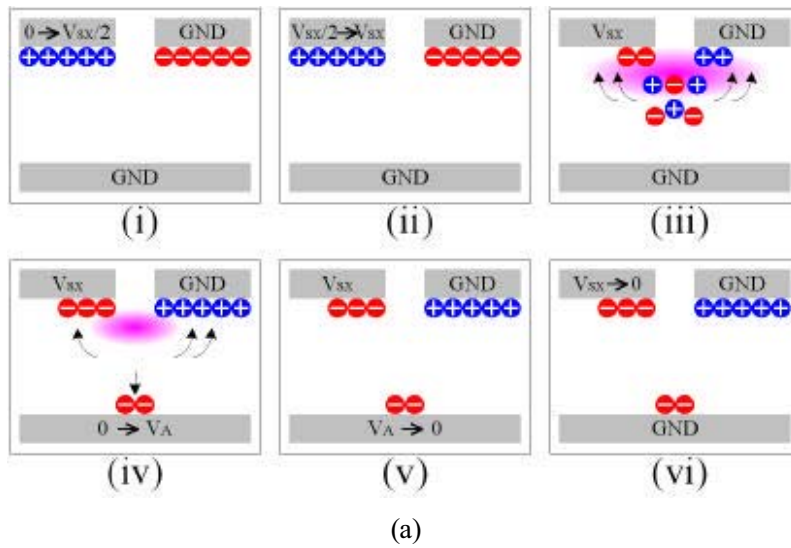
Figure 5-4: Schematic model (a) of space charges/wall charges within PDP cell and measured IR (828 nm) waveforms (b) in case of adopting auxiliary pulse shown in Case 3 of Fig. 5-2.

Fig. 5-4 (a). The wall charges on the address electrode scarcely participate in the next sustain discharge because the application of the auxiliary pulse is delayed for 0.45 µs. This also means that the wall charges on the address electrodes hardly contribute to producing the sustain discharge because the subsequent discharge is ignited only between the sustain electrodes X and Y by applying the sustain pulse to the sustain electrode. Therefore, the luminance decreases in inverse proportion to the increase in the amount of wall charges accumulated on the address electrode.

Unlike the IR waveform of Fig. 5-3 (b), the peaks of the IR (828 nm) waveforms of Fig. 5-4 (b) are observed to be slightly shifted to the right and to get lower as the amplitude of the auxiliary pulse increases from 0 V to 140 V, confirming that the delayed auxiliary pulse disturbs the accumulation of the wall charge toward the sustain electrodes. It is also observed that as the pulse width is wider than 200 ns, the IR peak is reduced to a greater extent and shifted farther to the right (not shown here). This phenomenon is presumably due to the fact that more wall charges tend to be accumulated on the address electrode rather than on the sustain electrode in proportion as the pulse width of the auxiliary pulse gets wider than 200 ns.

5.1.1 Analysis using Vt Closed Curve

Figure 5-5 shows the cell voltage vector of OFF cell during the sustain period according to the auxiliary address pulse method. To prevent an undesired sustain discharge in OFF cell, the cell voltages position of OFF cell must stay within the non-discharge region during the sustain period. Thus, the wall voltage position of OFF cell must keep the distance of V_{AUX} from the upper sides (Vt_{AY} and Vt_{AX}) of the Vt closed curve, as shown in Fig. 5-5 (a). The set-down voltage of Y electrode and bias voltage of X electrode which decide the wall voltage position of the OFF cell after the reset period are determined as 150 V and 60 V, respectively, as shown in

Fig. 5-5 (b). The reset waveform designed using the Vt closed curve is employed in the experiment, as shown in Fig. 5-1 (a).

Figure 5-6 shows the changes of the cell and wall voltage positions during the sustain period in case of adopting the auxiliary address pulse shown in Case 2 of Fig. 5-2. By the auxiliary address pulse applied together with a sustain pulse at same time, the cell voltage position moves to the discharge region, thereby resulting the occurrence of a strong discharge. Although the Vt_{YX} side of the Vt closed curve is straight line, the contour line of YX-discharge strength according to the wall charge transfer function is distorted as shown in Fig. 5-6 (1) [21],[24],[25]. Thus, the auxiliary address pulse induces a faster YX-discharge ignition, and produces stronger sustain discharge. An auxiliary address pulse with higher voltage can get more improvement of the luminance. After the sustain discharge, the cell voltage get zero by wall charges accumulation, as shown in Fig. 5-6 (2). At this time, the auxiliary address pulse with narrow pulse width (< 600 ns) don't be concerned in the accumulation of wall charges, thus the wall voltage position after the sustain discharge is same with the case of the conventional square sustain pulse. As the applied voltages of all electrodes are disappeared, the cell voltage position becomes same with the wall voltage position, as shown in Fig. 5-6 (3). The contour line of XY-discharge strength according to the wall charge transfer function is also distorted as shown in Fig. 5-6 (4). Therefore, the auxiliary address pulse contributes to the production of faster and stronger XY-discharge, thereby resulting the improvement of luminance. Figure 5-7 shows the effect of the changes of the auxiliary address pulse width in case of adopting auxiliary pulse shown in Case 2 of Fig. 5-2. An auxiliary address pulse with wider pulse width increases concern with the wall charge accumulation, and moves the wall voltage position after the sustain discharge from A to B, as shown in Fig. 5-7 (2). This transition of wall voltage position causes the different cell voltage positions (A' and B') at the rising edge of subsequent sustain pulse with the auxiliary address pulse. As the contour line of XY-discharge strength is also distorted, a discharge

produced at the cell voltage position of B' is weaker than that produced at the cell voltage position of A', as shown in Fig. 5-7 (4). From this reasons, it can be conclude that the auxiliary address pulse with wider pulse width leads lower luminance improvement.

Figure 5-8 shows the changes of the cell and wall voltage positions during the sustain period in case of adopting the auxiliary address pulse shown in Case 3 of Fig. 5-2. The auxiliary address pulse with delay time from a rising edge of a sustain pulse do not contribute to the production of a sustain discharge, however, affect the wall charge distribution. Consequently, the cell voltage position is moves from C (the cell position in the case of conventional square sustain pulse) to D by the auxiliary address pulse, as shown in Fig. 5-8 (2). As the applied voltages of all electrodes are disappeared, the cell voltage position becomes same with the wall voltage position, as shown in Fig. 5-8 (3). As a subsequent sustain discharge is produced by only a sustain pulse, the cell voltage is moves to the discharge region through the Vt_{XY} side of the Vt closed curve, as shown in Fig. 5-8 (4). The contour line of XY-discharge strength according to the wall charge transfer function is also distorted, thus the discharge get slower and weaker, thereby resulting the descent of luminance. Figure 5-9 shows the effect of the changes of the auxiliary address pulse width in case of adopting auxiliary pulse shown in Case 3 of Fig. 5-2. An auxiliary address pulse with wider pulse width increases concern with the wall charge accumulation, and moves the wall voltage position after the sustain discharge from E to F, as shown in Fig. 5-9 (2). This transition of wall voltage position causes the different cell voltage positions (E' and F') at the rising edge of subsequent sustain pulse. As the contour line of XY-discharge strength is also distorted, a discharge produced at the cell voltage position of F' is weaker than that produced at the cell voltage position of E', as shown in Fig. 5-9 (4). From this reasons, it can be conclude that the auxiliary address pulse with wider pulse width leads more luminance descent.
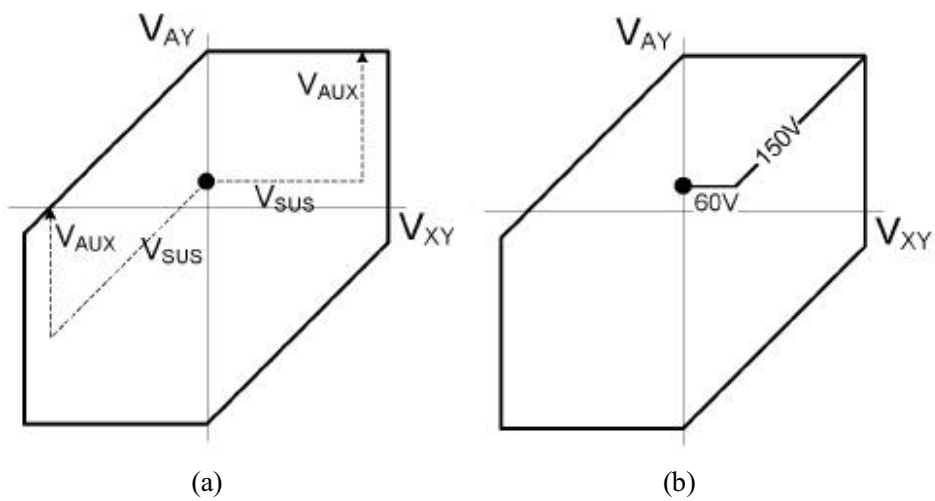
Figure 5-5: Applied voltage vector during sustain period (a), and OFF cell position to prevent occurrence of undesired sustain discharge in OFF cell during sustain period.
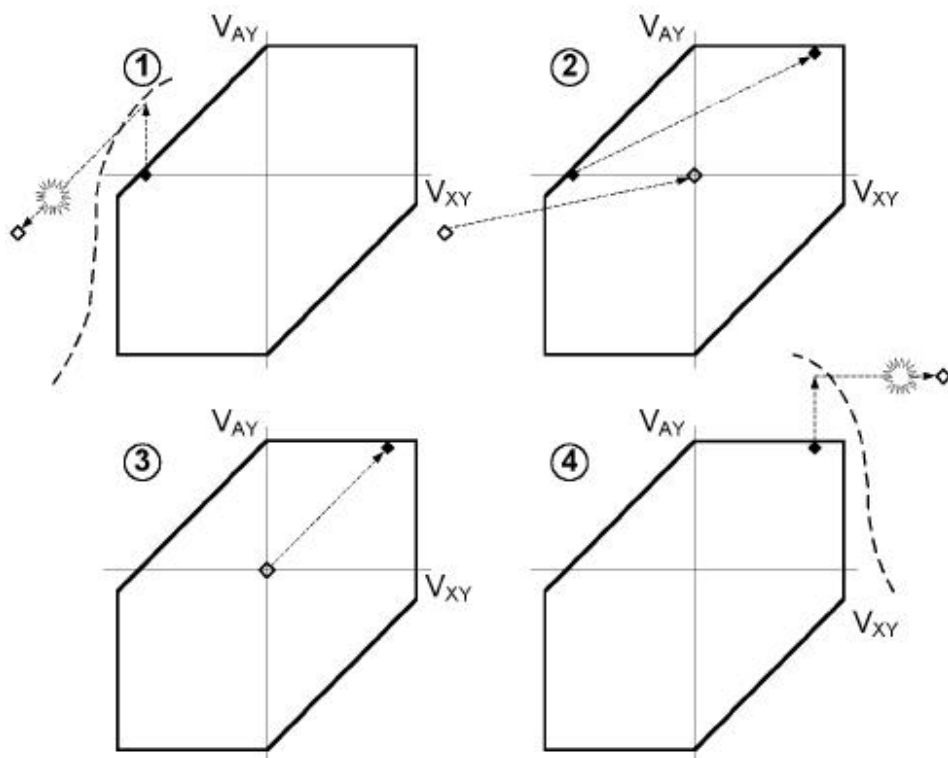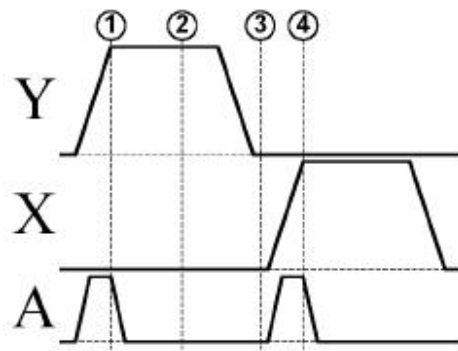
Figure 5-6: Changes of cell and wall voltages during sustain period in case of adopting auxiliary pulse shown in Case 2 of Fig. 5-2.
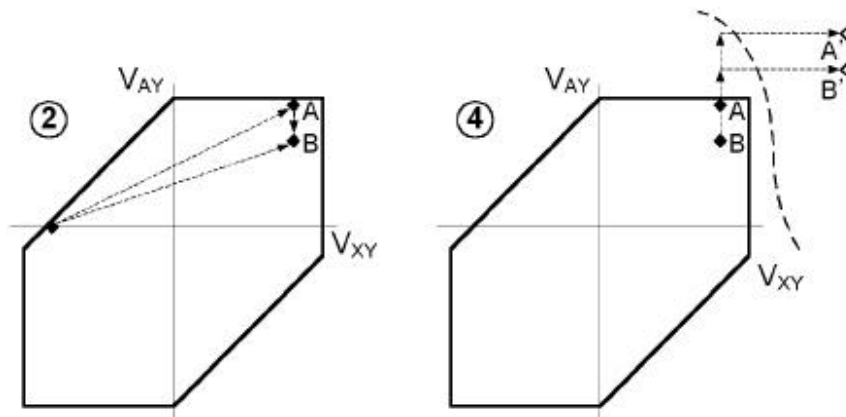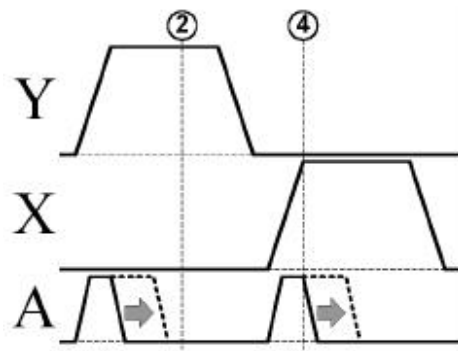
Figure 5-7: Effect of change of auxiliary pulse width in case of adopting auxiliary pulse shown in Case 2 of Fig. 5-2.
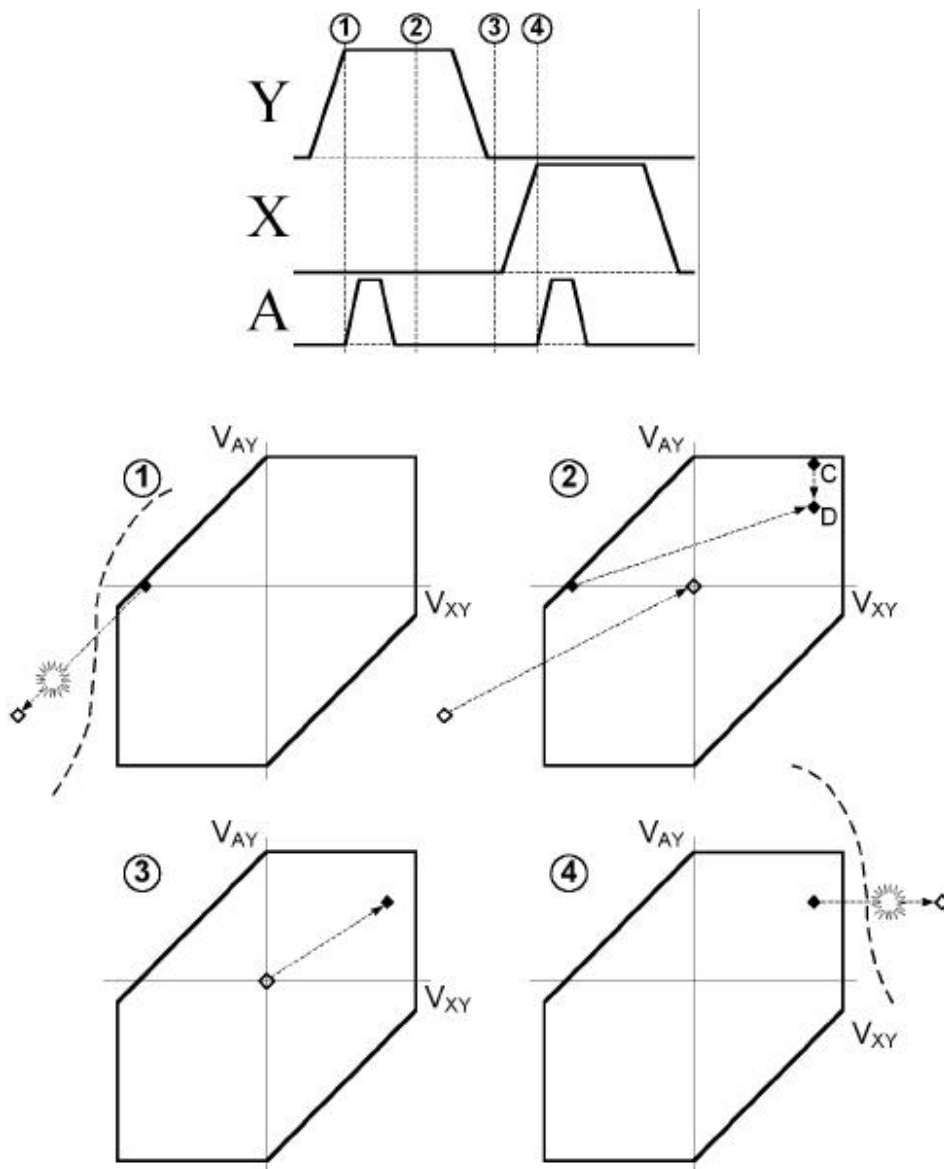
Figure 5-8: Changes of cell and wall voltages during sustain period in case of adopting auxiliary pulse shown in Case 3 of Fig. 5-2.
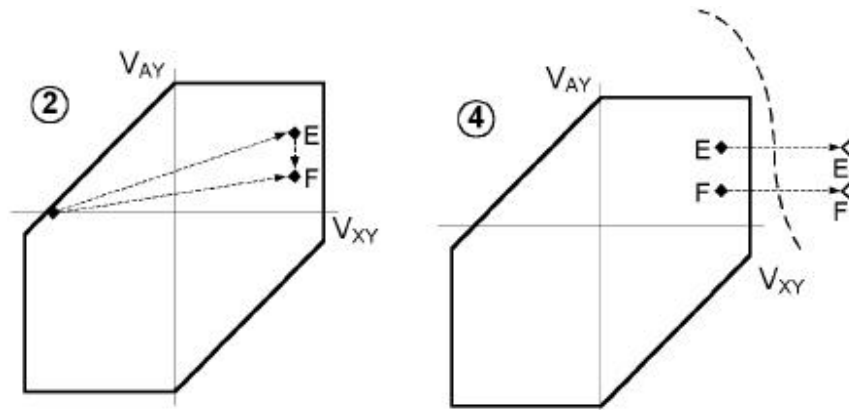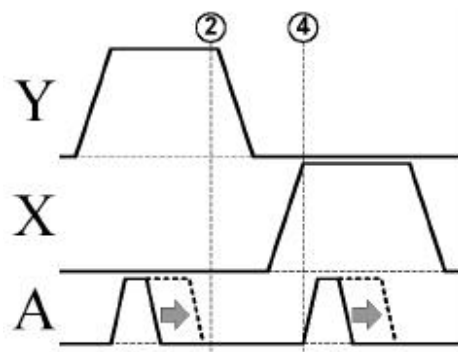
Figure 5-9: Effect of change of auxiliary pulse width in case of adopting auxiliary pulse shown in Case 3 of Fig. 5-2.

5.1.2 Analysis using Discharge Simulation Program

Figure 5-10 shows voltage waveforms applied to simulate operation of auxiliary address pulse. Employed simulation program is SIPDP-3D (Kinema Software - demo version) which is used widely as a PDP simulation tool. Applied waveforms shown in Fig. 5-10, are composed of address step, conventional sustain step, and measuring step. In address step, address discharge is occurred between Y and A electrodes by applying negative pulse to Y electrode and positive pulse to A electrode at same time. Next, positive pulse applied to Y electrode induces sustain discharge between X and Y electrodes in conventional sustain step. In measuring step, two kinds of waveforms are applied to A electrode together with positive pulse applied to X electrode to validate operation of auxiliary address pulse, as shown in Fig. 5-10. Electric potential and electron density are compared in two cases of conventional method and auxiliary address pulse method at time of T marked on Fig. 5-10. Figure 5-11 shows plots of electric potential in cases of conventional method and auxiliary address pulse method. In case of auxiliary address pulse method, electric potential distribution between Y and A electrodes is dense, where that is sparse in case of conventional method, as shown in Figs. 5-11 (a) and (b). Therefore, discharge between Y and A electrodes can be occurred easily by applying auxiliary address pulse. Figure 5-12 shows plots of electron density in cases of conventional method and auxiliary address pulse method. In case of auxiliary address pulse method, electron density is high nearby X and A electrodes, where that is high nearby only X electrode in case of conventional method, as shown in Figs. 5-12 (a) and (b). In other words, only discharge between X and Y electrodes is occurred, and discharge path becomes X-Y in conventional method. And, discharge between X and Y electrodes and discharge between A and Y electrodes by auxiliary address pulse, and discharge path becomes X-A-Y in auxiliary address pulse method, thereby inducing a wider discharge compared

to conventional method.
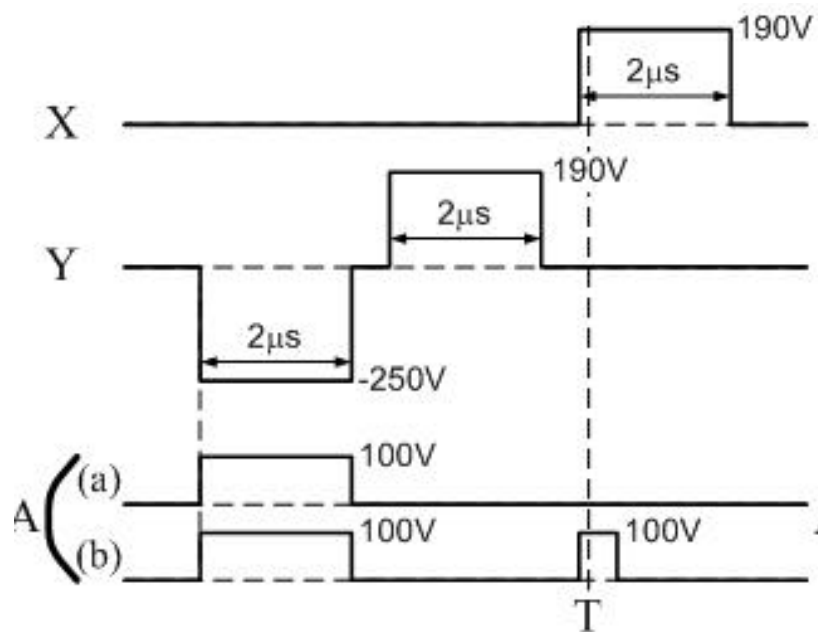
Figure 5-10: Voltage waveforms applied to simulate potential and electron density in cases of conventional method (a), and auxiliary address pulse method (b).
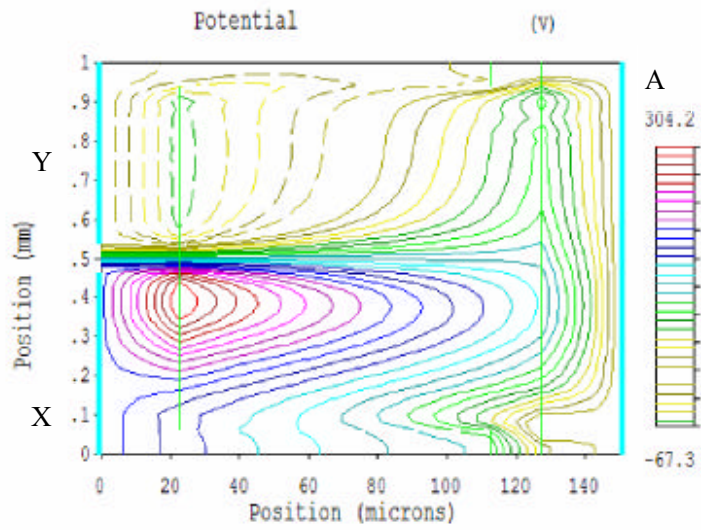
(a)
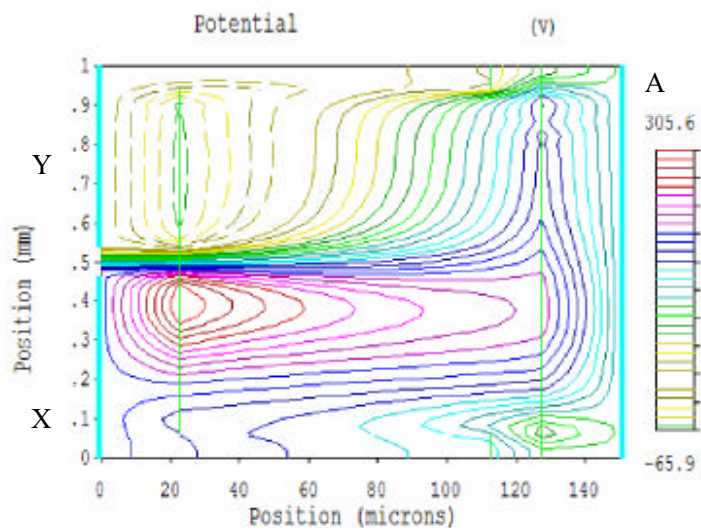
(b)

Figure 5-11: Plots of potential at time of T marked on Fig. 5-10 in cases of conventional method (a), and auxiliary address pulse method (b).
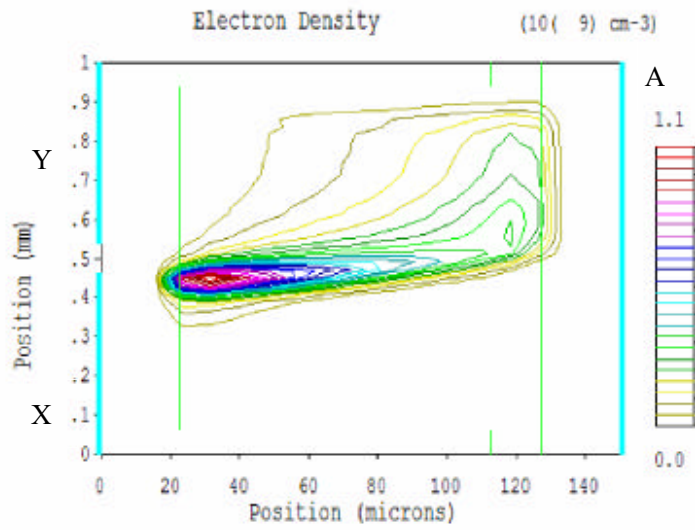
(a)
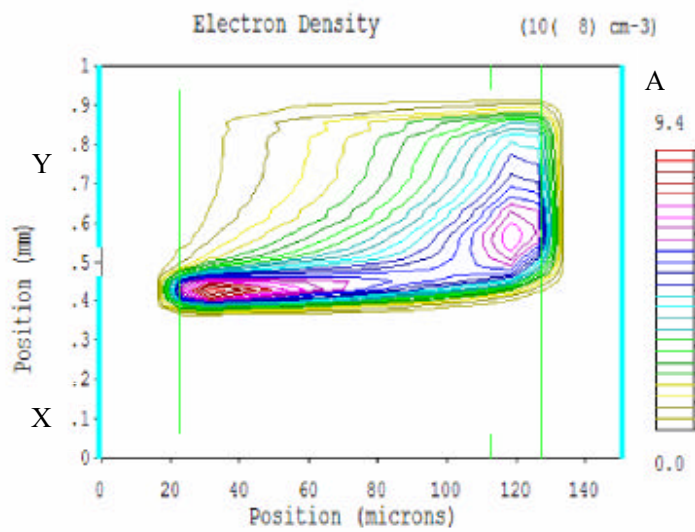
(b)

Figure 5-12: Plots of electron density at time of T marked on Fig. 5-10 in cases of conventional method (a), and auxiliary address pulse method (b).

5.2 IMPROVEMENT IN COLOR TEMPERATURE USING AUXILIARY PULSE

5.2.1 Color Temperature in AC-PDP

The low color temperature of the PDP is inherently attributed to the lower blue luminance than the red or green luminance. Several new methods have been suggested to improve the color temperature of the PDP. Some suggested methods are as follows: an asymmetric barrier rib [40], a color filter [41], and a new protection layer [42]. Nevertheless, these methods cannot solve the low color temperature problem fundamentally. Another conventional problem about the color temperature of the PDP is that the color temperature cannot be varied arbitrarily depending on the preference of the customers once the cell structure and the related driving scheme are fixed. The white color in the PDP is realized by a superposition of the R, G, and B lights emitted from the R, G, and B cells. In general, the white color in a display device such as the PDP can be characterized by the color temperature, or more specifically, the correlated color temperature, which is defined as the temperature of the blackbody radiator whose perceived color most closely resembles that of the given radiator [43]. The low color temperature in the current ac-PDP is fundamentally attributed to the lower blue luminance than the red or green luminance. The physical spectrum intensity in the blue region of 380 nm to 500 nm are quite stronger than those in the green region of 500 nm to 580 nm and the red region of 580 nm to 780 nm, whereas the perceiving efficiency of the human eyes is very low in the blue region. Accordingly, the blue luminance needs to be increased considerably so as to improve the color temperature of the AC-PDP.

In a conventional driving scheme, no auxiliary pulse is applied to the address electrode A during a sustain-period, when the sustain pulses are alternately applied to the sustain electrodes X and Y. Consequently, the

address electrodes are not utilized to produce a plasma during a sustain-period. Thus, the luminance from the R, G, and B cells of the PDP is controlled only by the sustain pulses. Since the sustain pulses are commonly connected to the R, G, and B cells, the luminance levels of the R, G, and B colors are difficult to control separately in the current driving technique of the PDP with three electrodes. However, the address electrodes parallel with the symmetric striped barrier ribs are located individually in each R, G, and B cell. If the address electrodes are used to take part in the discharge by proper applying of the different auxiliary pulses to the address electrodes during a sustain-period, the luminance levels among the R, G, and B cells can be controlled independently [44]-[46].

In this chapter, a new driving scheme using an auxiliary pulse is suggested to improve the color temperature and acquire flexibility of the color temperature in an ac-PDP. The luminance levels of the R, G, and B lights can control arbitrarily by selective applying of the various auxiliary pulses to the R, G, and B cells during a sustain-period. The variations of the luminance levels for the R, G, and B cells are also examined under the various auxiliary pulsing conditions such as changes in the amplitude, width, and delay time of a pulse. In order to improve and control the color temperature, the blue luminance should increase remarkably, whereas the red luminance should decrease slightly with independent control of each color luminance.

5.2.2 Independent Control of Luminance Levels for R, G, and B Cells Using Auxiliary Address Pulse

Figure 5-13 illustrates the changes in the R, G, and B luminance levels of the 4-inch test panel in the case of adopting the two different types of auxiliary pulses, *i.e.*, the luminance-enhancing pulse and the luminance-lessening pulse. All the auxiliary short pulses applied at the same starting
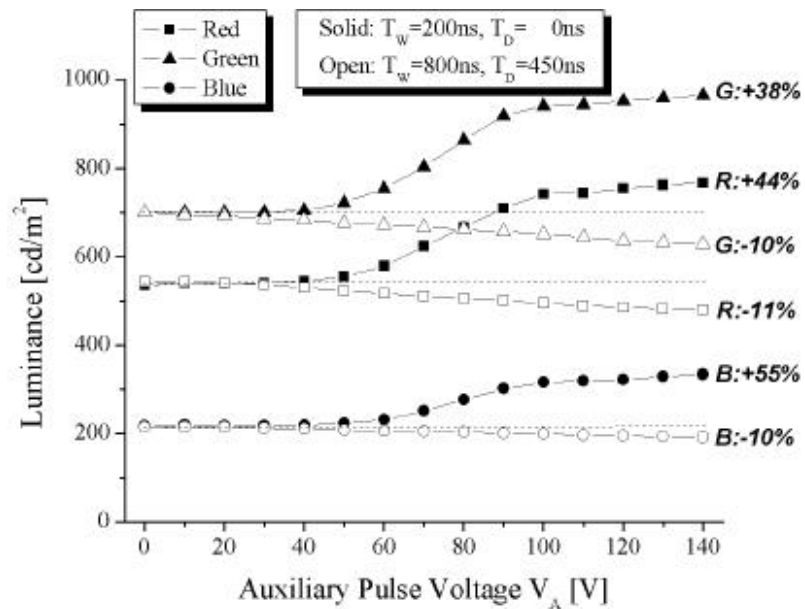
Figure 5-13: Changes in R, G, and B luminance levels of 4-in. test panel by applying two different types of auxiliary pulses: luminance-enhancing auxiliary pulse (solid mark) and luminance-lessening auxiliary pulse (open mark).

time as the two sustain pulses can also act as the luminance-enhancing pulses, which can increase the luminance levels of the R, G, and B lights (not shown here). In particular, the maximum enhancement of the R, G, and B luminance levels is obtained at the pulse width of 200 ns, as shown in the solid marks of Fig. 5-13. As shown in the maximum luminance enhancing pulse condition of Fig. 5-13, the increase rates in the luminance levels for the R, G, and B lights are 44 % (from 535 cd/m^2 to 768 cd/m^2) for a red color, 38 % (from 701 cd/m^2 to 967 cd/m^2) for a green color, and 55 % (from 217 cd/m^2 to 336 cd/m^2) for a blue color, each being compared to the luminance level with no auxiliary pulse. On the other hand, all the auxiliary short pulses with delay times up to 600 ns relative to the two sustain pulses can also reduce the luminance levels of the R, G, and B lights (not shown here). It is observed that the application of the auxiliary short pulse with a width of 800 ns and a delay time of 450 ns achieves the maximum reduction of the luminance levels of the R, G, and B lights, as shown in the open marks of Fig. 5-13. As shown in the minimum luminance-lessening pulse condition of Fig. 5-13, the decrease rates in the luminance levels for the R, G, and B lights are 11 % (from 535 cd/m^2 to 487 cd/m^2) for a red color, 10 % (from 701 cd/m^2 to 632 cd/m^2) for a green color, and 10 % (from 217 cd/m^2 to 195 cd/m^2) for a blue color, each being compared to the luminance level with no auxiliary pulse. The visible spectra emitted from the R, G, and B cells of the 4-inch test panel are also measured when the luminance-enhancing pulses and luminance-lessening pulses are applied to the address electrodes, respectively, as illustrated in Figure 5-14. Under the luminance-enhancing pulse conditions of Fig. 5-14 (a), the R, G, and B spectra are increased. Similarly, under the luminance-lessening pulse conditions of Fig. 5-14 (b), the R, G, and B spectra are decreased.

5.2.3 Improvement of Color Temperature Using Independent Control of Luminance Levels for R, G, and B Cells

Figure 5-15 shows the timing diagram of the voltage waveforms in the new driving scheme to improve the color temperature based on the experimental result. For the independent control of the luminance levels for the R, G, and B colors, three different types of auxiliary pulses are applied to the address electrodes of the R, G, and B cells, respectively. Since the high color temperature in the PDP can be obtained by increasing the blue luminance and simultaneously by decreasing the red luminance, the blue luminance-enhancing pulses, *i.e.*, the auxiliary pulses with V_{AB} (140 V), T_{WB} (200 ns), and T_{DB} (0 ns) are applied to the blue cells so as to increase the blue luminance, whereas the red luminance-lessening pulses, *i.e.*, the auxiliary pulses with V_{AR} (140 V), T_{WR} (800 ns), and T_{DR} (450 ns) are applied to the red cells so as to decrease the red luminance, as illustrated in Fig. 5-15. As for the green cells, no auxiliary pulses are used like the conventional driving method. No misfiring problems are observed in this driving condition.

Figure 5-16 (a) illustrates the visible spectra of the white color emitted from the R, G, and B cells in the case of adopting the new driving scheme of Fig. 5-15 relative to the conventional driving scheme. The new driving scheme increases the intensity of blue light in the range of 400 nm to 500 nm considerably, but decreases the intensity of red light in the range of 580 nm to 640 nm slightly. There is no significant change in other regions. Fig. 5-16 (b) illustrates the changes in the color temperature related to the black body locus on the CIE (1931) (*x, y*)-chromaticity coordinate measured from the 4-in. test panel in the case of employing the new driving scheme relative to the conventional driving scheme. The solid square marks denote the National Television System Committee (NTSC) standard coordinates, and the linked solid circles denote the black body locus with the related color temperatures. As a result of adopting the new driving scheme of Fig. 5-15,

the color temperature is increased from 5,398 K to 10,980 K without reducing the luminance, as denoted in the open triangle mark in the CIE chromaticity coordinates of Fig. 5-16 (b). This transition of the coordinates of the color temperature toward the blue region from (0.3395, 0.3059) to (0.2940, 0.2614) has resulted from the increment of 55 % in the blue luminance and the simultaneous decrement of 11 % in the red luminance. Table 5-1 shows the CIE chromaticity coordinates and their correlated color temperatures in various auxiliary pulse conditions. The color temperature of the PDP can be controlled in wide range by using the new driving scheme with various auxiliary pulse conditions, as shown in Table 5-1.
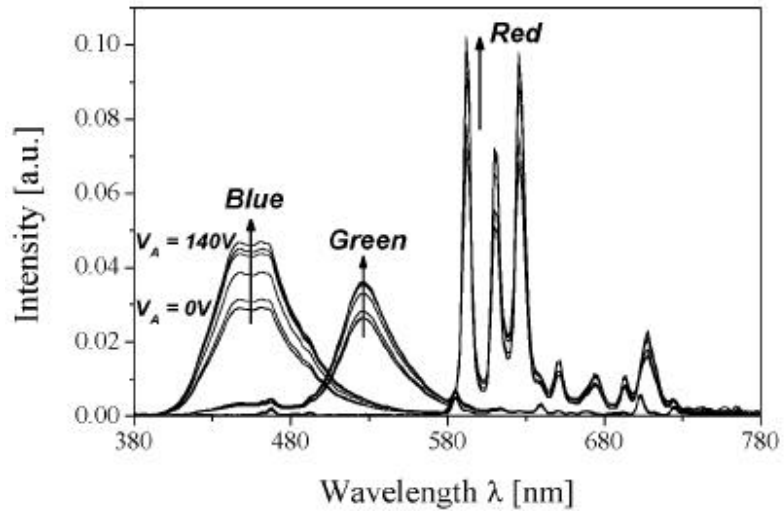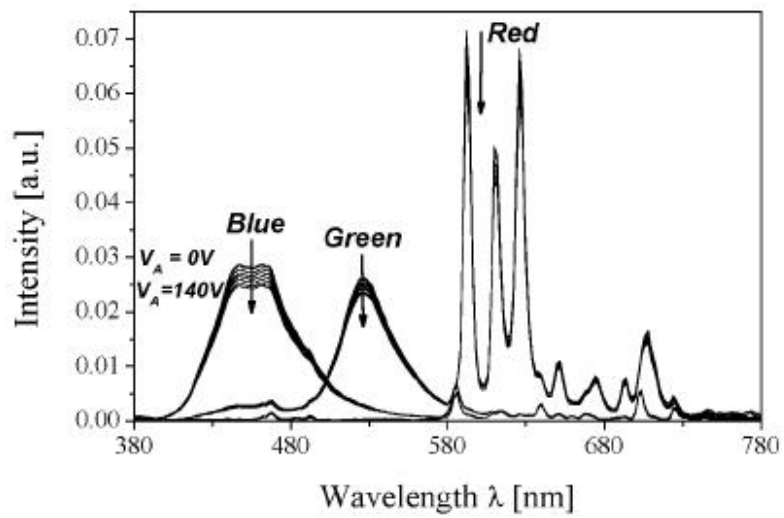
Figure 5-14: Visible spectra from R, G, and B cells of 4-in. test panel when luminance-enhancing auxiliary pulse (a) and luminance-lessening auxiliary pulse (b) are applied to address electrodes, respectively.

81
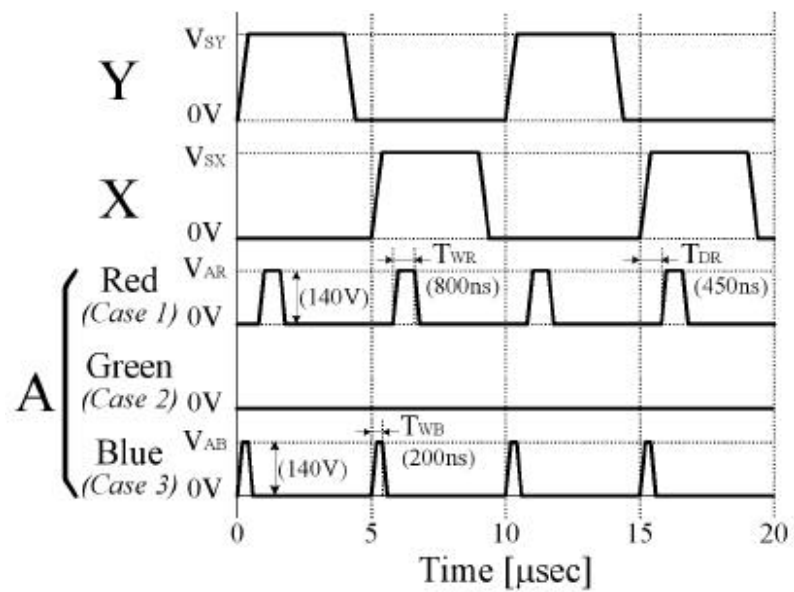
Figure 5-15: Timing diagram of sustain voltage waveforms, V_{SX} and V_{SY}, and three different types of auxiliary pulses V_{AR}, $V_{AG}(=0)$, and V_{AB}, where V_{SX} and V_{SY} are applied to sustain electrodes and V_{AR}, $V_{AG}(=0)$, and V_{AB} are simultaneously applied to address electrodes of R, G, and B cells, respectively for maximally improving color temperature.
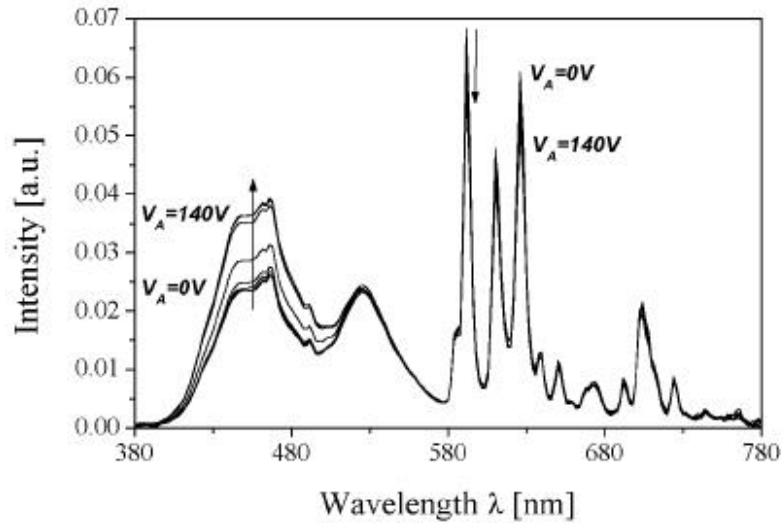
(a)
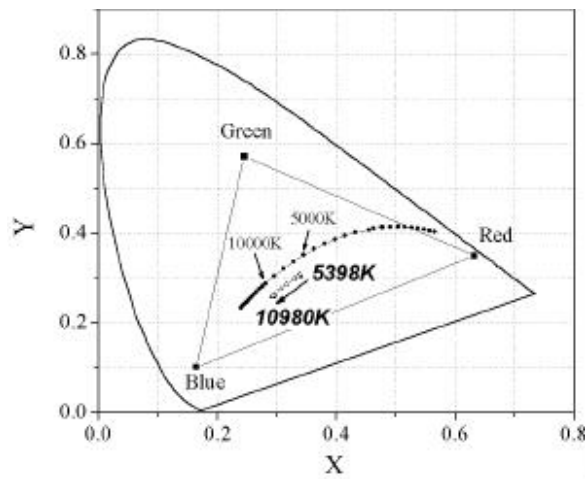
(b)

Figure 5-16: Visible spectra (a) of white color emitted from R, G, and B cells in case of adopting new driving scheme relative to conventional driving scheme, Changes of color temperature (b) related to black body locus on CIE (1931) chromaticity coordinates measured from 4-inch test panel in case of adopting new driving scheme relative to conventional driving scheme.

83

Table 5-1: Color temperature variations using new driving scheme in 4-inch test panel.

Red		Green		Blue		V_A [V]	CIE 1931		Color
T_{WR}	T_{DR}	T_{WG}	T_{DG}	T_{WB}	T_{DB}		x	y	Temperature [K]
800 nsec Width	450 nsec Delay	No Auxiliary Pulse		200 nsec Width	No Delay	0	0.3390	0.3048	5398
						10	0.3395	0.3059	5378
						20	0.3392	0.3059	5391
						30	0.3391	0.3064	5401
						40	0.3392	0.3074	5399
						50	0.3388	0.3084	5421
						60	0.3347	0.3051	5637
						70	0.3285	0.2994	6001
						80	0.3160	0.2861	6916
						90	0.3069	0.2763	8027
						100	0.2964	0.2630	10529
						110	0.2943	0.2603	10425
						120	0.2929	0.2588	10772
						130	0.2921	0.2584	10930
						140	0.2918	0.2582	10980

5.3 IMPROVEMENT IN GRAY SCALE LINEARITY USING AUXILIARY PULSE

5.3.1 Low Gray-Level Contour Problem

The image quality of a PDP including a dynamic false contour and a low gray-level contour is not sufficient for the high-class television. CRTs use the electron beam current control method to express the gray scales, however the optical output corresponding to the linear current increase is not linear. For the compensation of nonlinear electro-optical transfer characteristic in a CRT, the video signals received by a television are the gamma-corrected video signals.

On the other hand, the PDP-TV has a linear electro-optical transfer characteristic in a conventional driving method, and the inverse gamma correction is required to display images correctly with the gamma-corrected video signals for the CRT. Because of inverse gamma correction which is a requisite procedure for displaying images of a PDP-TV, several gray levels are merged into a fixed output luminance level, especially for the low input signals up to 50. This merging effect causes abrupt change in visual gradation patterns leading to the low gray-level contours.

A low gray-level contour problem is unavoidable in a typical ADS (Address Display Separated) driving scheme, because it is basically attributed to the inverse gamma correction which is a requisite procedure for displaying images of PDP-TV. The input and output signals of an inverse gamma correction of PDP are 8 bit digital signal, and have 256 different levels. Because of the inverse gamma correction, several gray levels are merged into a fixed output luminance level, especially for the low input signal level up to 50. This merging effect causes abrupt change in visual gradation patterns leading to the low gray-level contours. The CLEAR (High-Contrast, Low Energy Address and Reduction of False Contour Sequence) driving method

has been suggested to improve a gray-level expression in a low luminance image [47]. It is reported that this method contributes to suppressing the low gray-level contour. However, this method is quire different from the typical ADS driving scheme, in that for gray-scale expression the ADS driving scheme uses the combination of subfields, whereas the CLEAR driving method uses the accumulation of subfields. In addition, in a typical ADS driving method, a signal processing method using error diffusion and dithering has been suggested to improve a gray-level expression in a low gray-level region [48]. However, this method may alleviate the low gray-level contour problem more or less, but can not provide the fundamental solution for the low gray-level contour problem. An alternative method which can increase the subfield number up to 209 and gray level up to 2048 using the Address-while-Display (AwD) driving scheme has been proposed [49]. However, the AwD driving scheme is not adopted in the current commercial PDP products because of instability and complicated driving method. In order to counteract the disappearance of several low gray levels due to the inverse gamma correction in a typical ADS driving scheme, it is the best method to increase the luminance-steps available for the low gray scale. The minimum or maximum luminance level per one sustain-cycle should be altered so as to increase the luminance-steps for the low gray level.

However, it is not possible to produce the multi-luminance levels per sustain-cycle under the conventional PDP driving technology. As shown in the plane view of the conventional AC-PDP of Figure 5-17, the sustain pulses are applied commonly to the red, green, and blue cells through the sustain electrodes X and Y during a sustain-period, whereas no signal is applied to the address electrode A during a sustain-period. Thus, the luminance levels from the PDP cells are determined by only the number of the sustain-cycles, so that the minimum luminance level depends on the luminance that one sustain-cycle can create. In the conventional driving scheme, the minimum luminance level per one sustain-cycle is relatively high and fixed at a constant value, meaning that one sustain-cycle can also
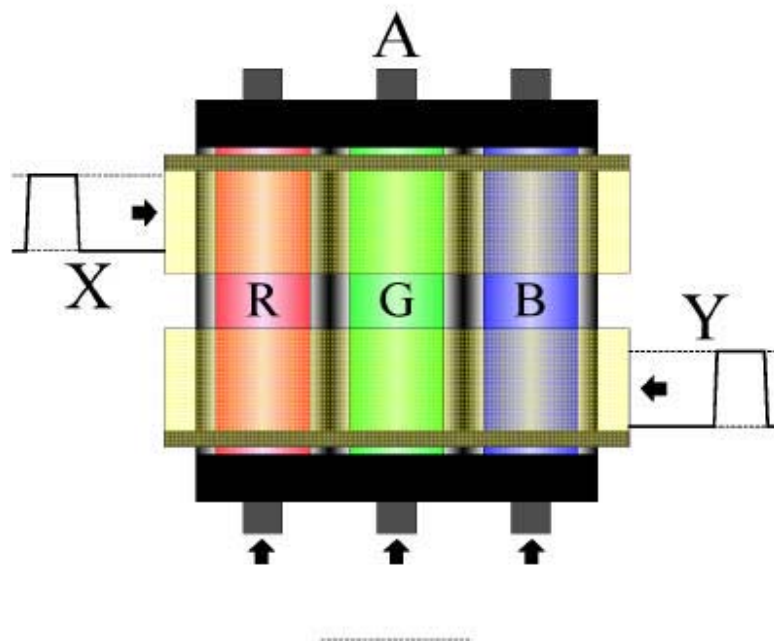
Figure 5-17: Plane view of single pixel comprising red, green, and blue cells and three electrodes X, Y, A of conventional PDP.

produce the only one luminance level; *i.e.* one sustain-cycle can not make the multi-luminance levels under the current PDP cell structure and driving scheme.

In this chapter, a new multi-luminance-level subfield method is proposed to improve the low gray-level color reproducibility. This method can express the various luminance levels in the same one or two sustain-cycle subfield condition by selectively applying the auxiliary address pulses with various amplitudes and delayed times to the address electrodes during a sustain-period [50]-[52].

5.3.2 Improvement of Gray Scale Linearity using Multi-Luminance-Level Subfield Method

In the conventional PDP driving scheme, the 256 gray levels are expressed by a combination of 8 subfields in which each subfield consists of the X-Y sustain pulse pairs. The 1-sustain-cycle subfield is composed of the one X-Y sustain pulse pair, whereas the 2-sustain-cycle subfield consists of the two X-Y sustain pulse pairs, as shown in Figure 5-18. In this work, the new driving scheme, which simultaneously applies the auxiliary short pulses to the address electrodes in addition to application of the sustain pulses, is proposed to subdivide the luminance levels for the 1- and 2-sustain-cycle subfields, as illustrated in Fig. 5-18. The use of the auxiliary short pulse can have a significant influence on the sustain discharge characteristics if the amplitudes and the delayed times of the auxiliary short pulse are varied with respect to the sustain pulse. This means that the variation in the amplitude and delayed time of the auxiliary short pulse can increase or decrease the luminance level per sustain pulse.

In this experiment, the sustain pulses with an amplitude of 180 V and a pulse width of 4 μsec are applied to the sustain electrodes X and Y at 100 KHz condition. For the auxiliary short address pulses applied to the   address
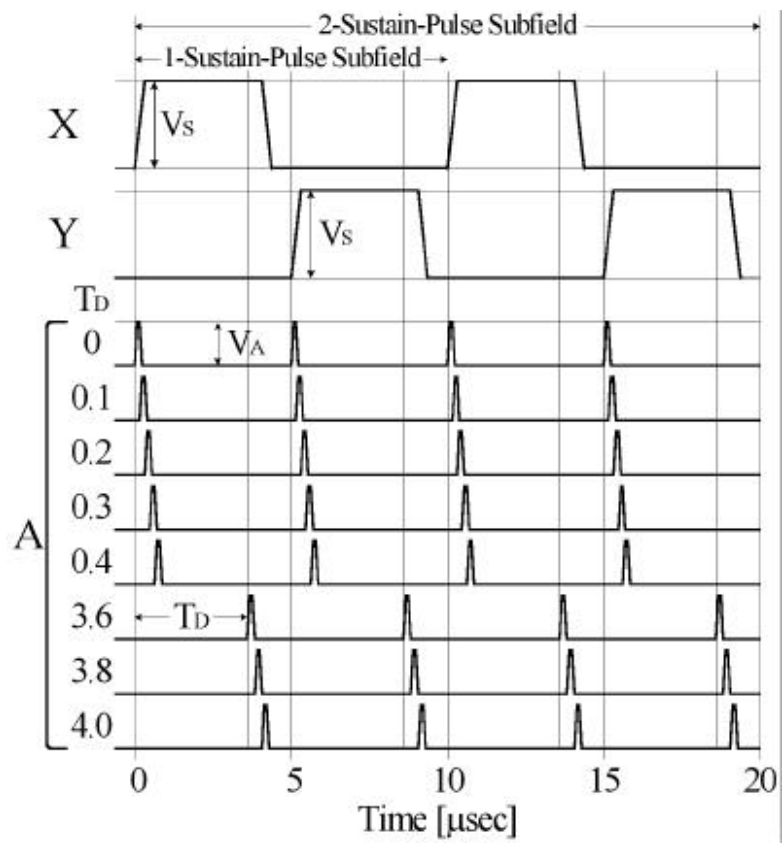
Figure 5-18: New driving scheme for multi-luminance levels in case of 1-sustain-cycle subfield and 2-sustain-cycle subfield.

Table 5-2: Measured luminance data with variation of T_D and V_A of auxiliary short address pulses for 1- and 2-sustain-cycle subfield.

< 1-Sustain-Pulse Subfield >

V_A[V]	30	60	90	120	150
T_D[μsec]	Measured Luminance [cd/m^2]				
0	1.24	1.25	1.25	1.18	0.88
0.1	1.28	1.28	1.29	1.15	1.09
0.2	1.31	1.33	1.38	1.32	1.26
0.3	1.29	1.32	1.34	1.35	1.36
0.4	1.25	1.26	1.27	1.29	1.32
3.6	1.32	1.36	1.37	1.37	1.40
3.8	1.33	1.39	1.40	1.38	1.43
4.0	1.31	1.33	1.38	1.38	1.35
No Aux. Pulse	1.25				

< 2-Sustain-Pulse Subfield >

V_A[V]	30	60	90	120	150
T_D[μsec]	Measured Luminance [cd/m^2]				
0	2.81	2.87	2.05	0.84	1.20
0.1	2.92	2.97	2.72	1.83	1.83
0.2	2.88	2.94	3.07	2.82	2.51
0.3	2.90	2.93	2.99	2.95	2.89
0.4	2.80	2.81	2.80	2.78	2.79
3.6	2.72	2.77	2.79	2.75	2.79
3.8	2.65	2.67	2.65	2.66	2.72
4.0	2.58	2.55	2.57	2.51	2.52
No Aux. Pulse	2.73				
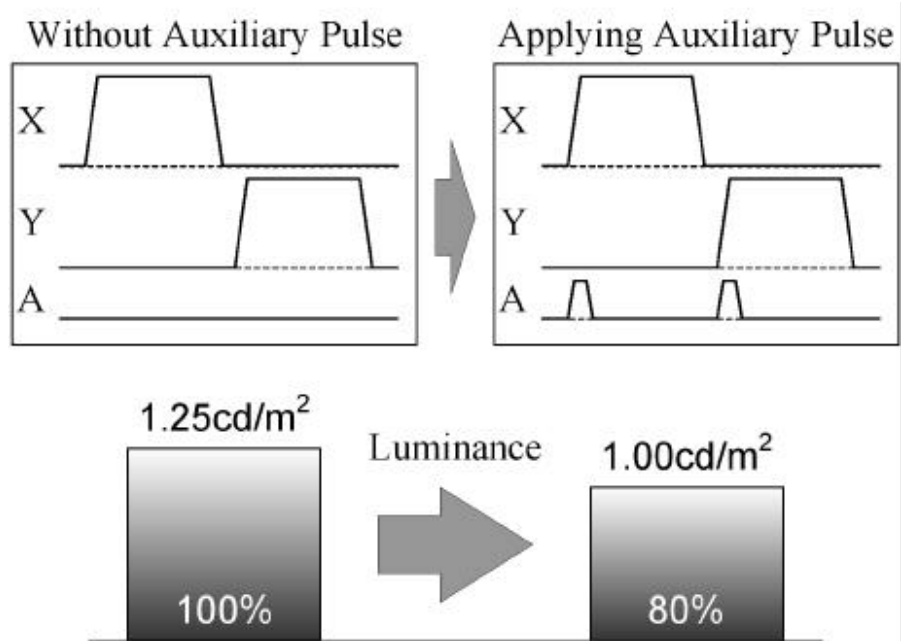
Figure 5-19: Example of multi-luminance-level subfield method by applying auxiliary pulses in sustain period.

electrode A, the amplitudes and the delayed times vary from 30 V to 150 V, and from 0 μsec to 4 μsec, respectively, while the width keeps a constant value of 400 nsec. As shown in Table. 5-2, the various luminance levels are obtained by varying the T_D (delayed time) and V_A (amplitude) of the auxiliary pulses for the 1- and 2-sustain-cycle subfields. The luminance varied from 70 % to 114 % is obtained for the 1-sustain-cycle subfield, whereas the luminance varied from 31 % to 112 % is obtained for the 2-sustain-cycle subfield, indicating that the 1- and 2-sustain-cycle subfields can represent the multi-luminance levels. One example for controlling the luminance by using the multi- luminance-level subfield method is given in Fig. 5-18. As a result of adopting the new driving scheme, it is observed that the diverse luminance levels can be made even in the one or two sustain pulse pairs.

The multi-luminance-level subfield set is selected within the 1- and 2-sustain-cycle subfields according to the following procedure. First, the output luminance level for the conventional 2-sustain-cycle case is assumed to be 2, and this luminance level is chosen as a reference output luminance level. Then, the measured luminance data shown in Table 5-2 are rescaled into the relative luminance data based on the reference luminance level. However, all the various relative luminance levels can not be used in the multi-luminance-level subfields. Of the relative luminance data, only the luminance levels which can satisfy the following multi-luminance selection criteria are selected as multi-luminance-level subfields:

(i) The minimum luminance level can not be given arbitrarily.

(ii) The ith subfield SF_i is not included in the multi-luminance-level subfield set, provided that $L(SF_i) = L(SF_j) + L(SF_k)$ where j, $k < i$ and $j \neq k$. Here, $L(SF_i)$ reperesents the ith output luminance level of the subfield SF_i after the various possible subfields have been sorted and numbered from the minimum luminance level.

(iii) The error produced in the low gray level should not be diffused into the higher gray levels. In other words, an element or the sum of some elements in the multi-luminance-level subfield set must be an integer or at least very close to it:

$$\sum_i L(SF_i) = 1.0 \text{ or } 2.0 \qquad [3]$$

where i is included in the multi-luminance-level subfield set.

(iv) The total subfield number including the multi-luminance-level subfield should be within the 12 subfields because the total subfield must be employed within the limited time of a sustain-period.

As a result of adopting the multi-luminance-level subfield selection criteria, five subfields having the relative output luminance levels of {0.8, 1.0, 1.2, 1.4, 1.6} are chosen as the multi-luminance-level subfield set and finally renumbered from SF_1 to SF_5. The selected luminance levels for the 1- and 2-sustain-cycle subfield are illustrated in Figure 5-20. For the 1-sustain-cycle subfield, SF_1 has a relative luminance level of 0.8, and SF_2 has a relative luminance level of 1.0. For the 2-sustain-cycle subfield, SF_3, SF_4, and SF_5 have the relative luminance levels of 1.2, 1.4, and 1.6, respectively. The new method changes the total subfield number from 8 into 11 by selecting the 2 luminance-steps in the 1-sustain-cycle subfield and the 3 luminance-steps in the 2-sustain-cycle subfield, respectively, whereas other subfields are not modified in this case, as illustrated in Figure 5-21. However, the output luminance levels overlapped by a combination of the multi-luminance-level subfields should be excluded, even though the possible output luminance levels are 32 ($=2^5$) levels by a theoretical combination of the subfields from SF_1 to SF_5. The output luminance levels that matter in this work are limited up to 4, because a severe degradation of image quality is mainly caused in these levels due to the inverse gamma correction procedure in the conventional subfield method. Consequently, the multi-luminance-level subfield
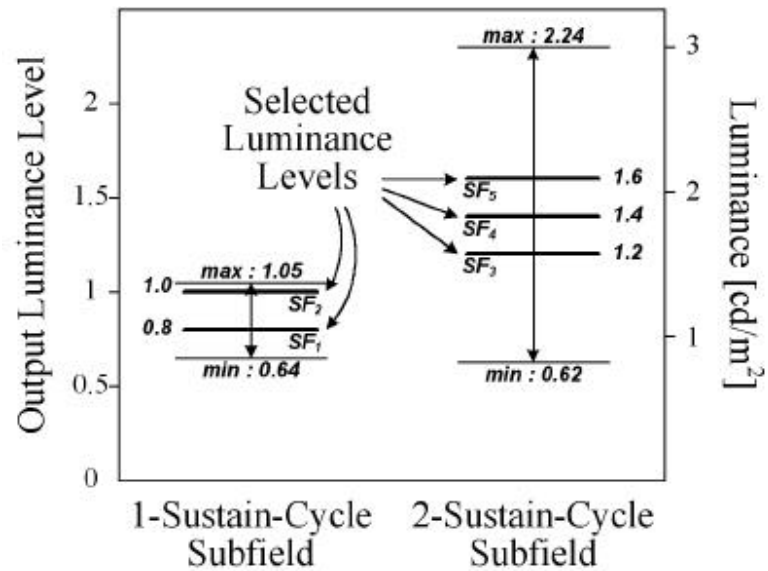
Figure 5-20: Selected luminance levels for 1- and 2-sustain-cycle subfield.
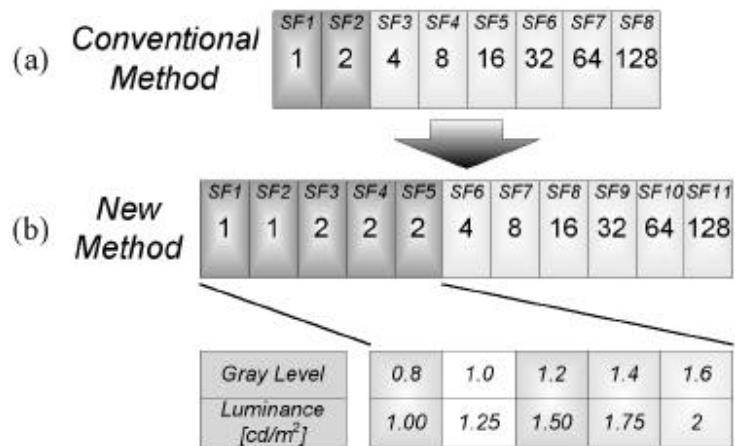
Figure 5-21: Subfield formations and corresponding gray levels of each subfield in conventional method (a) and new multi-luminance-level subfield method (b).

set from SF$_1$ to SF$_5$ is used only to express the low gray levels up to 4, and the specific subfields, for example, SF$_2$ for the output luminance level of 1, and a combination of SF$_1$ and SF$_3$ for the output luminance level of 2, are determined in advance to express the output luminance levels 1 and 2 necessary for the higher gray levels. Therefore, for the output luminance levels up to 4, the 18 luminance levels can be expressed in the new multi-luminance-level subfield method, whereas only the 5 luminance levels can be expressed in the conventional subfield method. It is expected that the resultant 18 luminance levels in the 1- and 2-sustain-cycle subfields can improve the expression capability in the low gray level up to 4, thereby resulting in reducing the low gray level contour in AC-PDP.

Figure 5-22 illustrates the subfield selection algorithms for expressing the gray levels between 0 and 4 in the case of adopting the conventional method and new multi-luminance- level subfield method, respectively. The gray level differences between two successive gray levels are also 0.2 by using this subfield selection algorithm except between the zero gray level and the first gray level of 0.8, for the gray levels up to 4. After the inverse gamma correction adopting the new multi- luminance-level subfield method, the twelve luminance-steps are obtained instead of the conventional three luminance-steps, and the gray scale expression capability is expanded four times for input signals up to 30, as illustrated in the inverse gamma correction tables of Figure 5-23.

Fig. 5-24 shows the luminance levels available after the inverse gamma correction in the cases of adopting the conventional and new multi-luminance-level subfield methods for the gray-levels between 0 and 50, respectively. In Fig. 5-24, the square marks indicates the out luminance level relative to the input signal level in the case of the conventional inverse gamma correction method, whereas the triangle marks shows the out luminance level relative to the input luminance level in the case of the inverse gamma correction using the new multi- luminance-level subfield method. The output luminance levels after the inverse gamma correction in

the new method show almost the same tendency with an analog method represented by the straight line, whereas the out luminance levels after the inverse gamma correction in the conventional method shows the several discontinuous luminance steps.

5.3.3 Simulation Results

Figures 5-25 and 5-26 show the inverse gamma correction simulation results of the gamma-corrected red, green, blue gradation images and the yellow rose images that contain the gray-levels up to 50, when the analog method (a), the conventional digital method (b), and the new multi-luminance-level subfield method (c) are used.

The gray-levels in the simulation results of Figs. 5-25 and 5-26 are stretched up to 250 for a displaying purpose. As illustrated in the simulation results of the inverse gamma correction for the images of Figs. 5-25 and 5-26, the multi-luminance-level subfield method suppresses the low gray-level contours that appear in the conventional digital method, and thus improves the color reproducibility to almost the same level compared with the analog method.

Gray Level \ SF	SF1	SF2	SF3
0			
1	■		
2		■	
3	■	■	
4			■

■ : ON
□ : OFF

Gray Level \ SF	SF1	SF2	SF3	SF4	SF5	SF6
0						
0.8	■					
1.0		■				
1.2			■			
1.4				■		
1.6					■	
1.8	■					
2.0	■		■			
2.2	■			■		
2.4	■				■	
2.6		■			■	
2.8			■		■	
3.0	■	■				
3.2	■	■		■		
3.4	■	■			■	
3.6	■	■			■	
3.8		■	■		■	
4.0						■

■ : ON
□ : OFF
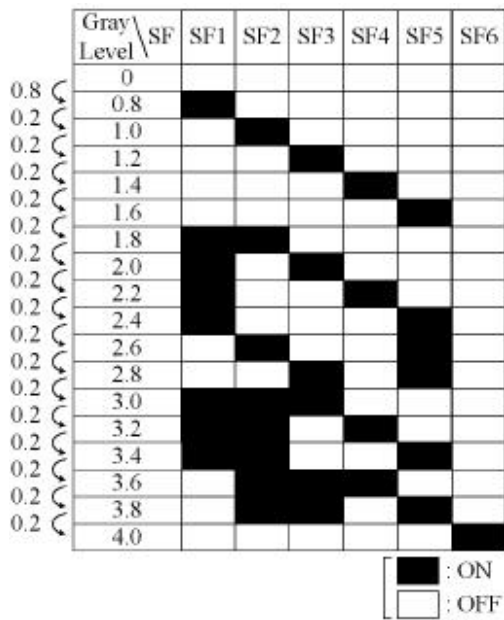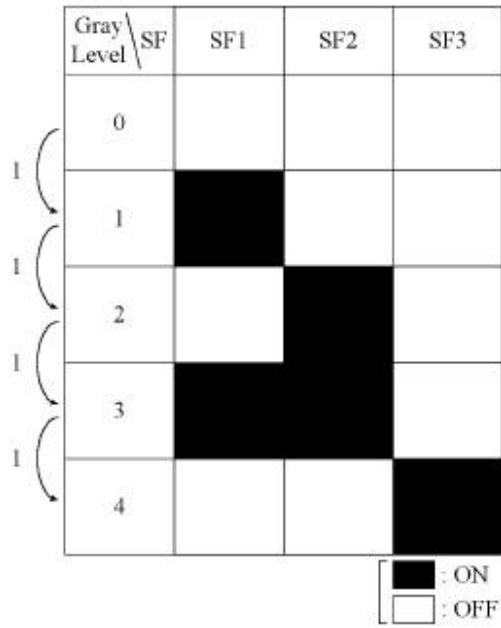
(a)

(b)

Figure 5-22: Subfield selection algorithms for expressing gray-levels between

0 and 4, in conventional method (a) and new multi-luminance-level subfield method (b).
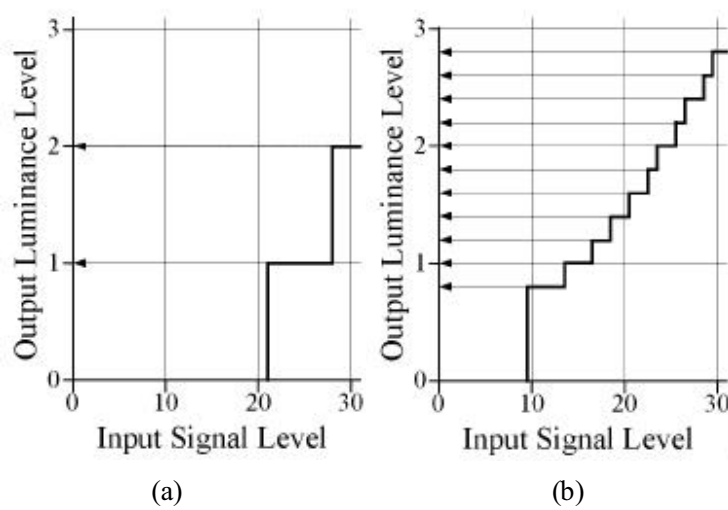
Figure 5-23: Inverse gamma correction tables of conventional method (a) and new multi-luminance-level subfield method (b) for input signal level between 0 and 30.
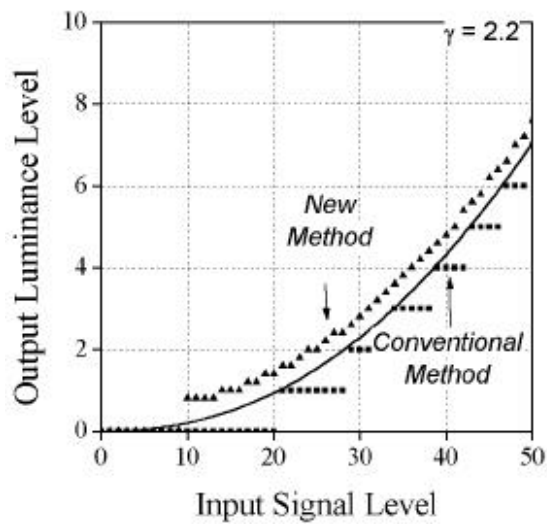
Figure 5-24: Luminance levels available after inverse gamma correction in case of adopting conventional method (square mark) and new multi-luminance-level subfield method (triangle mark) for input signal levels between 0 and 50.

      (a)   (b)

         (c)
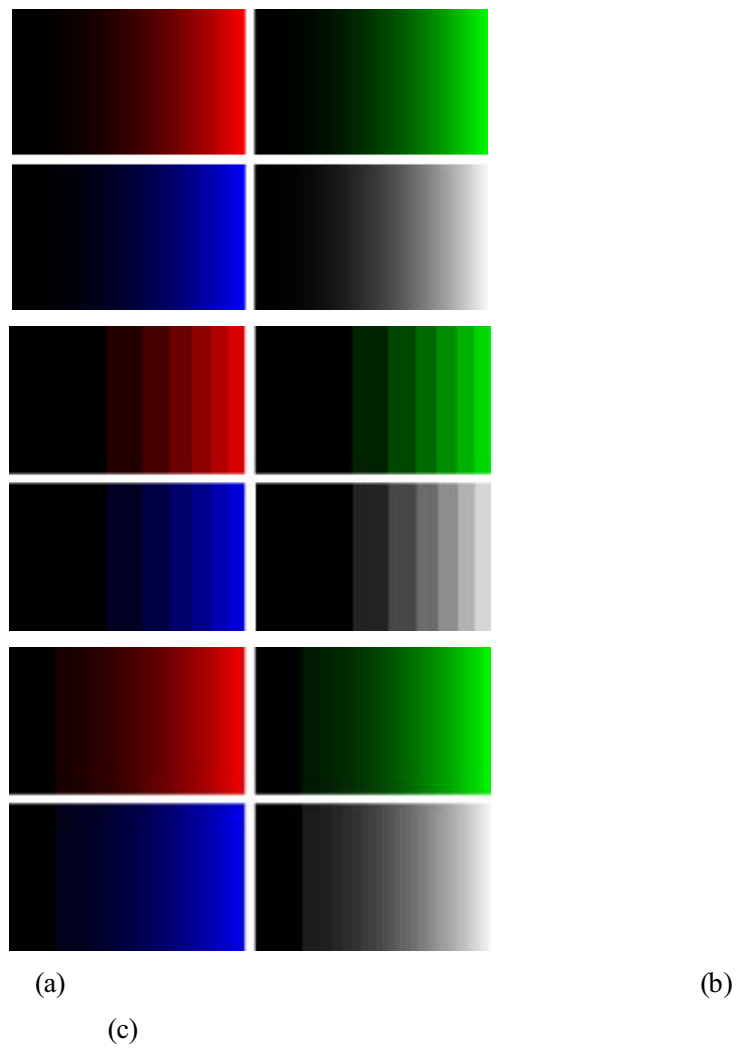
Figure 5-25: Simulation results of inverse gamma correction for red, green, blue, and white gradation images using analog method (a), conventional digital method (b), and new multi- luminance-level subfield method (c).

Figure 5-26: Simulation results of inverse gamma correction for yellow rose image using analog method (a), conventional method (b), and new multi-luminance-level subfield method (c).

6. BIPOLAR SCAN WAVEFORM

6.1 ADDRESSING SPEED IN AN AC-PDP

The ADS (Address Display Separated) driving scheme, even if used most commonly, has the low light emission duty factor problem due to the long total address time [53]. As the resolution of PDP gets higher, this problem gets more serious. Although the well-known visual problems of PDP can be lessened by using more several subfields [54], this solution also makes the light emission duty factor smaller. Therefore, the fast address technique is the most important issue for the realization of a high resolution PDP with high-class image quality. There have been many efforts to increase the light emission duty factor by reducing an address time using the various methods, such as the AwD (Address while Display) driving scheme [55], the MAoD II driving scheme [56], the partial line doubling method [53], and the plural screens method [57]. However, these methods have several weak points such as the instability in driving, the requirement of additional driving circuits, and the image quality degradation, so that more improvement is still needed.

In this chapter, a new address waveform using the bipolar scan waveform is proposed to increase the light emission duty factor without any side effects mentioned above. The bipolar scan waveform uses the two-step scan pulse with two voltage polarities, which can separate the conventional address discharge into two different discharge modes: a space charge generation mode and a wall charge accumulation mode [59]-[61].

In general, an address discharge in PDP means that the cells to display images are selected out prior to displaying images by accumulating the wall charges after firing the cells according to the image data from the address driver. As shown in the conventional address waveform and the related IR waveform of Figure 6-1 (a), the address discharge was produced between the scan (Y) and address (A) electrodes by simultaneous application of a falling
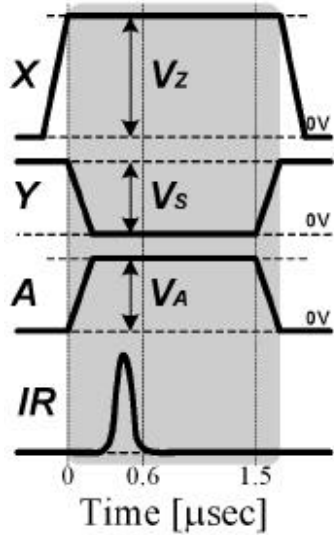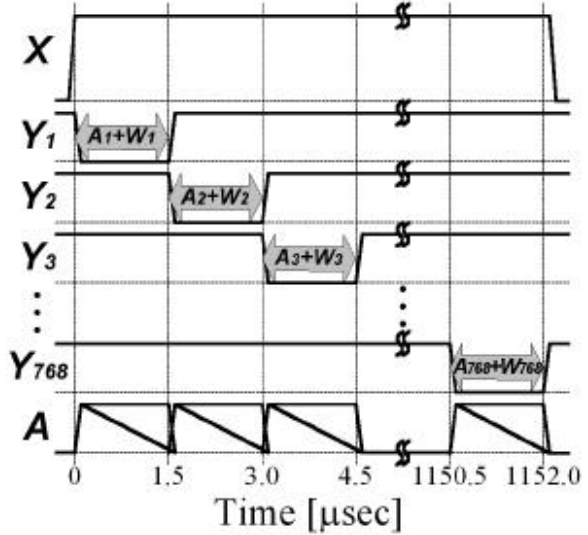
Figure 6-1: Voltage and IR waveforms during single line scanning (a) and address sequence during address-period (b) in case of adopting conventional address scheme in XGA grade PDP.

scan pulse with a voltage drop of V_s and a rising address pulse with a voltage rise of V_A. For the successful address procedure, the address discharge should play two roles as follows: one is to generate the space charges for wall charges in the selected cell by simultaneous application of the scan (Y) and address (A) pulses, and the other is to accumulate the wall charges under the scan (Y) and sustain (X) electrodes by using the space charges produced from the address discharge for the ensuing sustain discharge. In the conventional address scheme, it is thought that the space charge generation for wall charges is inseparable from the wall charge accumulation during an address discharge. Accordingly, it is often thought that the scan and address pulses should have the same pulse width.

As shown in the IR waveform Fig. 6-1 (a), the address discharge was started at 0.3 µs and extinguished at 0.6 µs after the starting point of the scan and address pulses. However, the sufficient wall charge accumulation from the space charges by the gap voltage (V_z) between the sustain (X) and scan (Y) electrodes takes over 1.5 µs, which means that the wall charge accumulation needs a longer time than the space charge generation. Fig. 6-1 (b) shows the address sequence during an address-period in XGA grade (1024 × 768 pixels) PDP according to the conventional address scheme. The address sequence was executed line by line from the first (Y_1) to the last (Y_{768}) scan line. Each scan line must be scanned independently to avoid the misfiring problem, as shown in Fig. 6-1 (b). The total address time depends on how long the address pulses stay on the address electrode per scan line. Thus, the total address time is determined by the address pulse width multiplied by the number of horizontal resolution of PDP. If we assume a XGA grade PDP using 8 subfields and 300 µs setup period per one subfield, the total address time per one subfield is 1152 µs and the light-emission duty factor is just 30 % for a TV-field.

6.2 IMPROVEMENT IN ADDRESSING SPEED USING BIPOLAR SCAN PULSE

Based on a new concept that the space charge generation can be separated from the wall charge accumulation during an address discharge, the bipolar scan waveform employed in the current research is introduced in Figure 6-2 (a). The new scan waveform in Fig. 6-2 (a) has two-step scan pulse with two voltage polarities: a negative voltage polarity for producing an address discharge and a positive voltage polarity for accumulating wall charges. In the new address scheme using the bipolar scan waveform, the voltage and IR (infrared: 828 nm) waveforms applied to the three electrodes (X, Y, and A) during a single line scanning are shown in Fig. 6-2 (a). The first address discharge, hereafter called 'primary address discharge,' was produced within 0.6 μs between the scan (Y) and address (A) electrodes by simultaneous application of a falling scan pulse with a negative voltage of V_S and a rising address pulse with a positive voltage of V_A at the time of T_2. After applying the negative scan and the positive address pulses for 0.6 μs, a reverse scan pulse with a positive voltage of V_R was applied to produce the additional address discharge, hereafter called 'secondary address discharge,' at the time of T_4. The secondary address discharge was produced between the scan (Y) and sustain (X) electrodes due to a gap voltage of V_{YX} (=V_R+V_Z). Note that this secondary address can be produced even at low gap voltage due to the presence of the space charges remaining still after the primary address discharge. Accordingly, the secondary address discharge was produced only in the cells where the primary address discharge had been produced. The reverse scan pulse width greater than 1.5 μs can accumulate the sufficient wall charges for the subsequent sustain discharges.

Fig. 6-2 (b) shows the address procedure during an address-period in XGA grade PDP in the case of adopting the new address scheme. For the bipolar scan waveform, the negative pulse part was not overlapped with any other
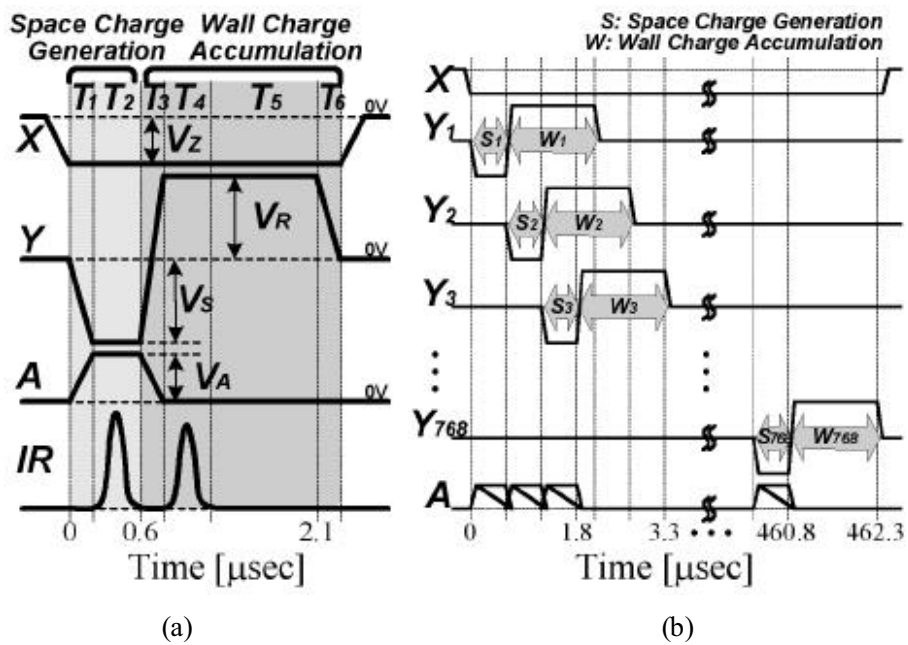
Figure 6-2: Voltage and IR waveforms during single line scanning (a) and address sequence during address-period (b) in case of adopting new address scheme in XGA grade PDP.

address pulse, whereas the reverse pulse part was overlapped with another address pulse. However, since the voltage polarity of the reverse pulse part was the same as that of the address pulse, no misfiring discharge was observed at the overlapping situation on condition that the voltage increase slope in the transition from the negative pulse into the reverse pulse was properly controlled. The other stable operating conditions are as follows: V_S = -150 ~ -170 V at V_A = 80 V and V_R = 140 V or V_R = 80 V ~ 140 V at V_A = 80 V and V_S = -160 V. As a result, the address time for a single scan line can be reduced to just 0.6 μs without any undesired address discharge, as shown in Fig. 6-2 (b). If we assume a XGA grade PDP using 8 subfields and 300 μs setup period per one subfield, the total address time per one subfield is 462.3 μs and the light-emission duty factor is increased to 63 % for a TV-field.

The 4-in. test panel with a gas mixture of Ne + Xe (4 %) and a pressure of 400 Torr was employed to measure the address discharge characteristics in the case of adopting the bipolar scan waveform, and its structure and dimensions were the same as the conventional 42-in. wide VGA grade PDP with a cell pitch of 360 μm. The size of the active area was 75.60 mm × 47.52 mm. The total number of the displaying cells was 70 × 44 pixels. In this experiment, in order to examine the validity of the proposed bipolar scan waveform, the special reset waveforms, which consisted of a pair of narrow pulses and another pair of ramp-pulses with a voltage of 180 V, were used to erase only the accumulated wall charges within the cells prior to the address discharge for the purpose of minimizing the effects of wall and space charges generated from the reset discharge. As a result of adopting the special reset waveform prior to an address discharge, the minimized priming effect led to a fast primary address discharge (< 0.6 μs) simply by raising the amplitude of the address pulse. As for the bipolar scan waveform, its voltage levels were determined based on the firing threshold voltage characteristics. In the case of 4-inch test panel employed in the current study, the firing threshold voltages between the three electrodes were observed to be
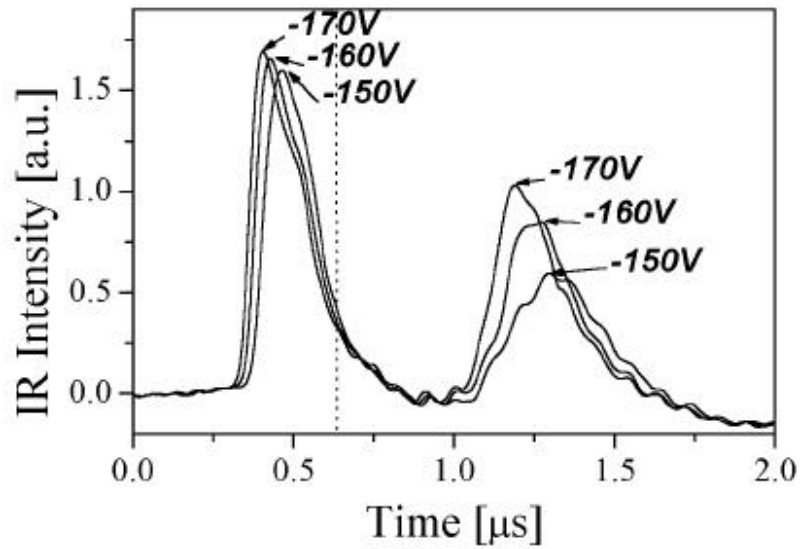
Figure 6-3: Dependence of primary and secondary address discharges on negative scan pulse voltage (V_s).
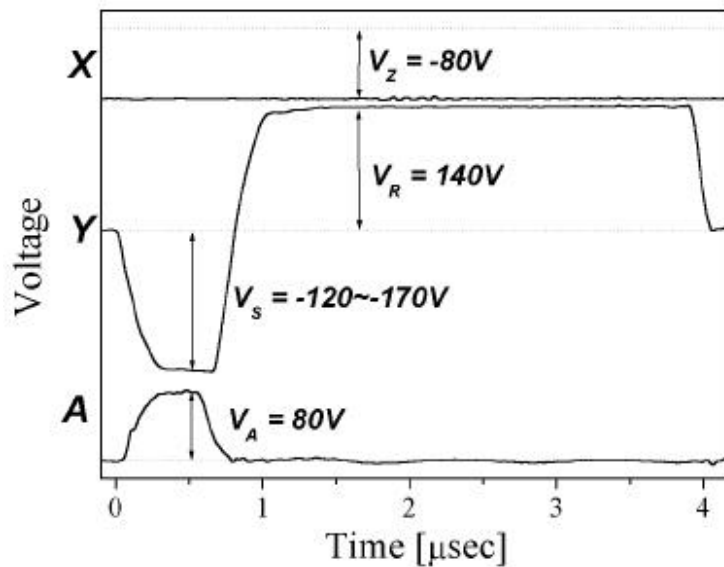
Figure 6-4: New fast addressing voltage waveforms applied to three electrodes X, Y, and A during address period.

230 V for V_{XY} and V_{YX} (between two sustain electrodes), 170 V for V_{AX} and V_{AY} (A: anode, X or Y: cathode), and 250 V for V_{XA} and V_{YA} (X or Y: anode, A: cathode). From these data, the voltages were determined to be -160 V for V_S, 140 V for V_R, 80 V for V_A, and -80 V for V_Z, respectively, as shown in Figure 6-4. The width of the address pulse was the same as that of the negative scan pulse, and their values were 0.6 μs, whereas the width of the reverse scan pulse was 1.5 μs. These bipolar scan pulse conditions satisfy that the on-off state of the cells is exactly decided by the application of address pulse without a misfiring discharge. The address discharge characteristics were measured according to the changes in the negative scan voltage (V_S) and reverse scan voltage (V_R). Figure 6-3 shows the dependence of the primary and secondary address discharges on the negative scan voltage (V_S). Other conditions of the bipolar scan waveform are the same as those listed above. If the negative scan voltage (V_S) was below -150 V, the primary address discharge was not strong enough to induce a stable secondary address discharge. On the other hands, the negative scan pulse voltage (V_S) greater than -170 V could produce a weak primary address discharge without any application of address pulse, implying that undesired sustain discharges would be induced. Accordingly, the stable operation range of the negative scan voltage (V_S) was determined from -150 V to -170 V. As shown in Fig. 6-3, in proportion as the negative scan pulse voltage (V_S) increased from -150 V to -170 V, both the primary and second address discharges were initiated fast and their discharge intensities became stronger. The IR intensity of Fig. 6-3 shows that the stable and strong secondary address discharge can be obtained provided the primary address discharge can generate the larger amount of space charges.

Figure 6-5 illustrates the dependence of secondary address and ensuing sustain discharges on the reverse scan voltage (V_R) where the negative scan voltage (V_S) is fixed at -160 V. Although the space charges were generated sufficiently during a primary address discharge, the reverse scan voltage (V_R) less than 80 V could not produce a strong secondary address discharge, so
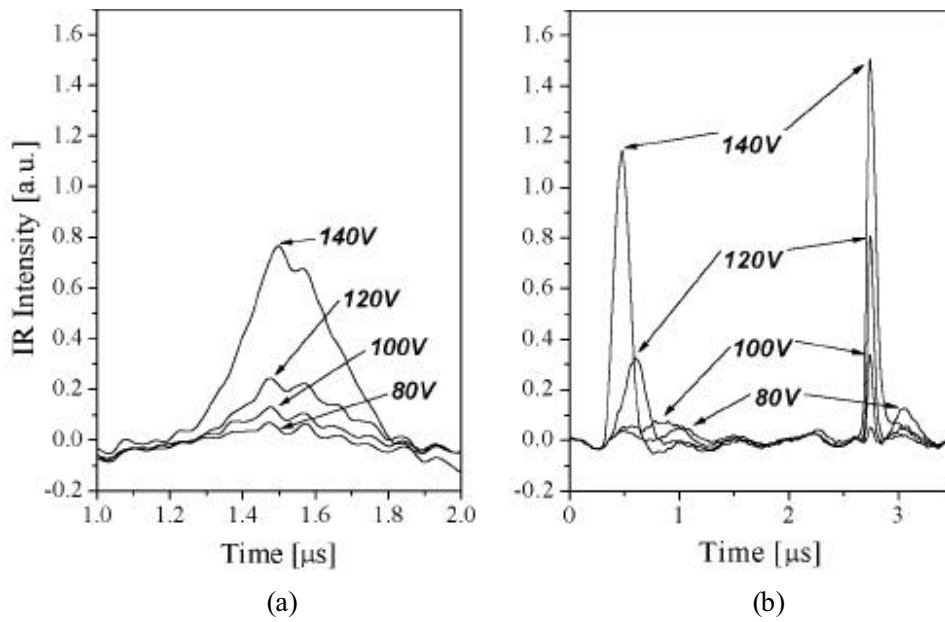
Figure 6-5: Dependence of secondary address (a) and ensuing sustain (b) discharges on reverse scan pulse voltage (V_R).

that the wall charges could not be accumulated sufficiently for the stable sustain discharges. On the other hand, the reverse scan voltage (V_R) greater than 140 V could induce a secondary address discharge regardless of the existence of a primary address discharge. Thus, the stable operation range of the reverse scan voltage (V_R) was determined from 80 V to 140 V. As shown in Fig. 6-5 (a), the higher reverse scan voltage (V_R) produced the stronger secondary address discharge, thereby resulting in accumulating more wall charges below the sustain (X) and scan (Y) electrodes. Consequently, the subsequent sustain discharges also got more stable at the reverse scan voltage of 140 V.

By adopting the new bipolar scan waveform during an address-period, the scanning time for a single scan line was reduced from 1.5 µs to 0.6 µs, so that the address time for single subfield at XGA grade PDP was reduced from 1152 µs to 462.3 µs, as shown in Figs. 6-1 (b) and 6-2 (b). As a result, the light emission duty factor was improved up to 63 % if the subfields of the XGA grade PDP were 8, and the reset period was 300 µs per single subfield. This considerable improvement of a light emission duty factor can contribute to the accomplishment of high luminance, high resolution, and high-class image quality in the PDP. However, an undesired writing discharge problem is occurred by the triggering effect of data pulses of adjacent scan line in the new addressing waveform. In following chapter, its solution is suggested and other problems related with this solution are discussed.

6.3 UNDESIRED WRITING DISCHARGE PROBLEM AND COUNTER MEASURES

Figure 6-6 illustrates the timing diagram of new addressing waveform for the successive two scan lines, nth and n+1th. After the addressing process of nth scan line Y_n denoted by the dotted lines at the times of T_1 and T_2, n+1th

Figure 6-6: Timing diagram of new addressing waveform for successive two scan lines during addressing sequence.

Figure 6-7: Solution of undesired writing problem by means of increasing transition time T_{TR} from scan voltage V_S to reverse voltage V_R.
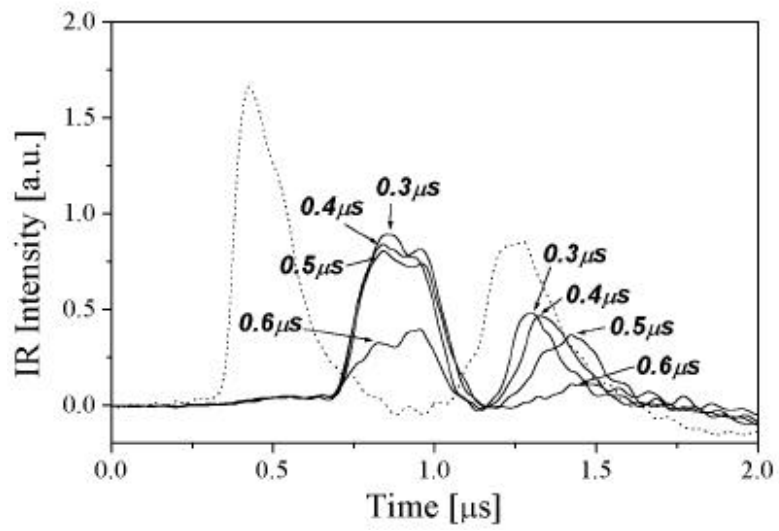
Figure 6-8: Change of IR waveforms emitted from undesired writing discharge with increase of transition time T_{TR} at addressing process.

scan pulse and data pulse D_{n+1} are applied for the addressing process of n+1th scan line Y_{n+1} at the time of $T_3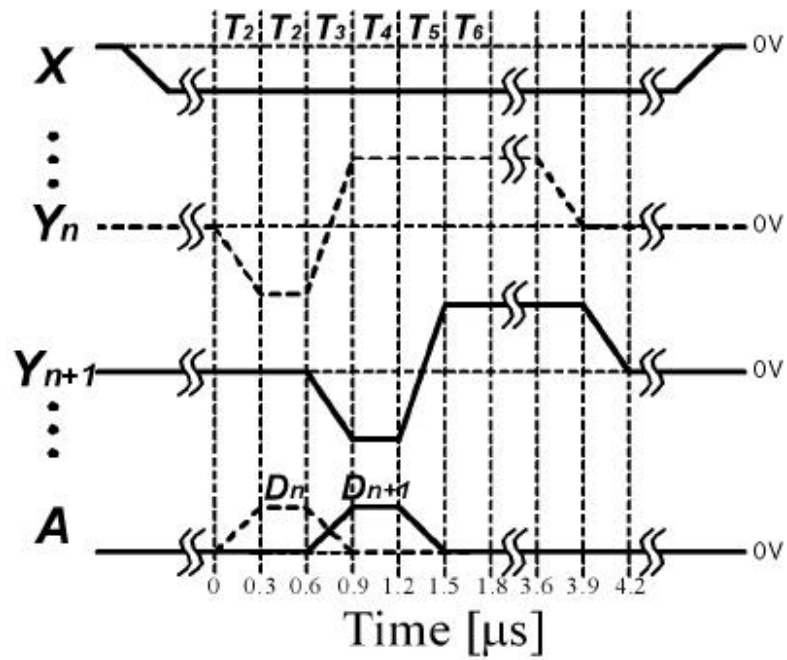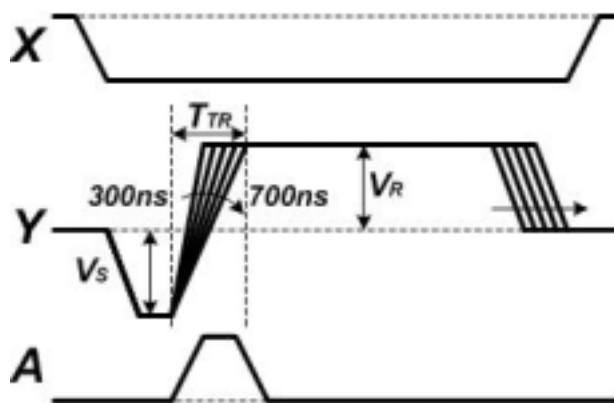$. At this time, the voltage of nth scan line Y_n is changed from the scan voltage V_S to the reverse scan voltage V_R, and this considerable voltage change causes the strong electric fields in all cells. If there is no appliance of $n+1^{th}$ data pulse D_{n+1}, the undesired writing discharge problem is not occurred, however the data pulse D_{n+1} can trigger the undesired writing discharge at the cells of nth scan line Y_n which must not be selected. These undesired writing discharges get stronger under the conditions of higher voltage change rate of scan pulses and higher data pulse voltage.

In this manner, the undesired writing discharge problem can be solved by two methods. First method is to reduce the voltage of data pulses which trigger the undesired writing discharge in previous scan line. However, if the voltage of data pulses is reduced, the voltage of scan pulse must be raised for the successful writing discharge between the scan and data pulses, thereby inducing a higher voltage changing rate of scan electrodes. The other method is to lower the voltage changing rate of scan electrodes by increasing the transition time T_{TR} from the scan voltage V_S to the reverse voltage V_R, as shown in Figure 6-7. This solution does not require any other changes except the transition time and the lag of reverse pulse, thus the undesired writing problem can be solved without any other additional problems.

Figure 6-8 shows the measured IR waveforms emitted from the cells which must not be selected. The dotted line represents the IR waveforms emitted from the addressed cells in the previous scan line. In the case of transition time T_{TR} of 0.3 μs, a undesired writing discharge is produced by the triggering effect of data pulses, and an additional discharge is also produced, thus the undesired cells are turned-on during a sustain- period. However, the increase in the transition time T_{TR} can lower the electric field induced by an abrupt change of scan pulse from the scan voltage V_S to the reverse scan voltage V_R, thereby enabling to suppress the undesired writing discharge problem, as shown in Fig. 6-8. With the increase in the transition time T_{TR}

from 0.3 μs to 0.6 μs, the undesired writing discharge is weakened, and the additional discharge is also weakened at the same rate. In the case of transition time T_{TR} of over 0.7 μs, the undesired writing problem is solved clearly. Meanwhile, the increase in the transition time T_{TR} must not affect a desired writing discharge, and weaken the subsequent sustain discharges. Figure 6-9 shows the measured IR waveforms emitted from the cells which must be addressed with various transition times T_{TR}. In longer transition time T_{TR} conditions, even though the additional discharge is delayed, the peaks and the widths of IR waveforms at additional discharge are almost the same. This phenomenon shows that the amount of space charges remaining in the discharge space after the writing discharge is almost the same in the significant time duration.

From this result, it is guaranteed that the addressing process in a desired cell is executed successfully. Moreover, there is no change in the sustain discharge characteristics as a result of the successful addressing process, as shown in Figure 6-10. As a result, the undesired writing discharge problem of the new addressing waveform is solved by means of increasing the transition time for lowering the voltage changing rate of scan electrode at addressing process. This solution does not affect the desired writing discharge and the sustain discharge characteristics with the increases of addressing time of a subfield by just 0.4 ms from 463.8 ms to 464.2 ms in WXGA grade AC-PDP.

Figure 6-11 shows the dynamic votage margin (b) between the address and sustain voltages measured from the checkered pattern (a) of the 4-in. test panel. The checkered pattern of Fig. 6-11 (a) consisted of 5 × 5 squares to display the white and black images alternately. In the checkered pattern, the white square means the on-cells that are composed of 42 × 8 cells, whereas the black square means the off-cells that are composed of 42 × 8 cells. To check a misfiring discharge between adjacent cells, the white square was surrounded by the black square and vice versa. As a result of measuring the dynamic voltage margin under the checkered pattern displayed by the stable

bipolar scan pulse conditions such as the negative scan voltage, $-V_S$ of -165 V, the reverse scan voltage, V_R of 140 V for 3 µs, and the address pulse width of 0.7 µs, the stable margin for the address voltage, V_A was obtained over 65 V, whereas the address discharge was not produced below the V_A of 65 V. Figure 6-12 shows the experimental result of gray scale expression test. In this test, two subfields with different luminance weight are used to express 4 gray level. From this result, it is verified that the bipolar scan waveform is operated stably in gray level expression.
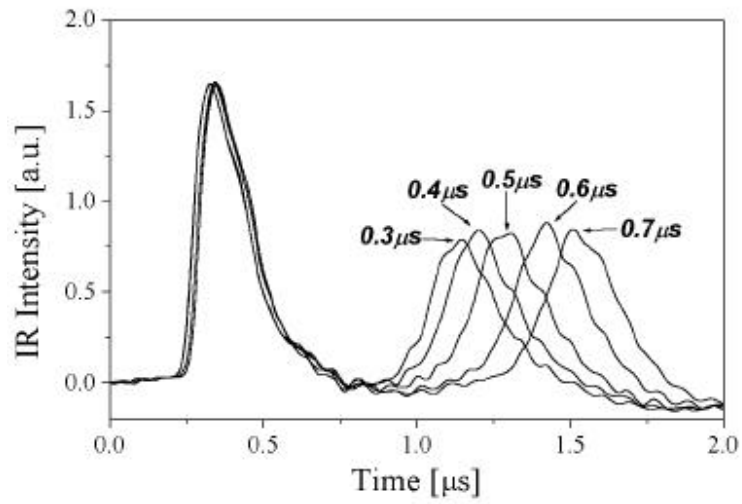
Figure 6-9: Changes of IR waveforms emitted from addressed cells with increase of transition time T_{TR} at addressing process.
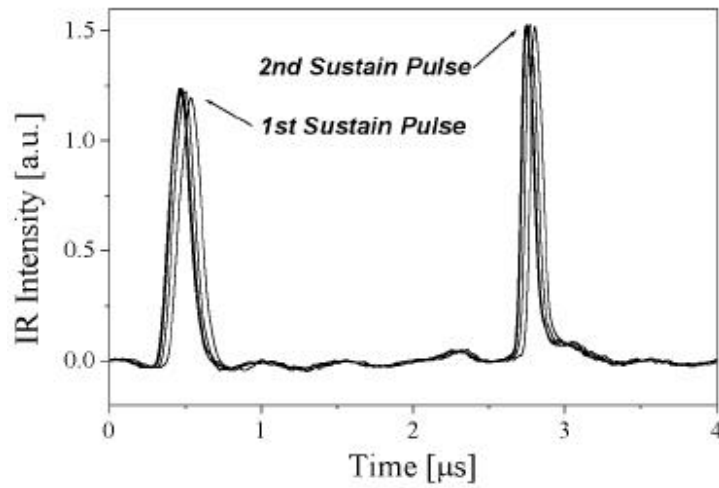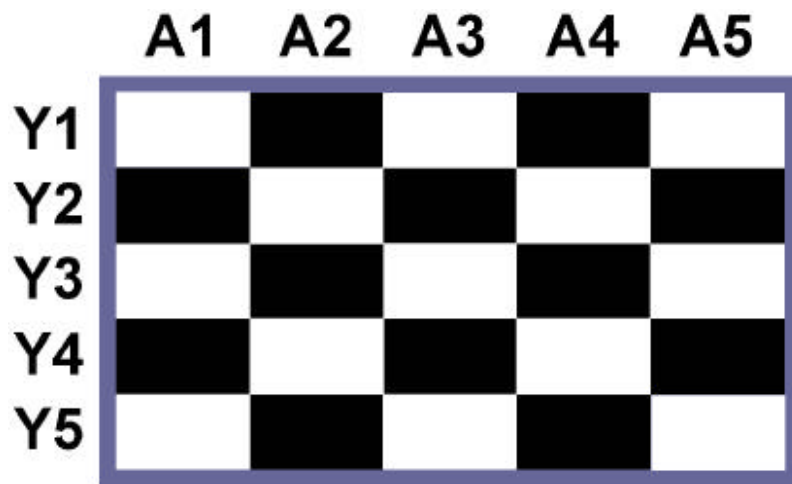

Figure 6-10: Effects of transition time T_{TR} on sustain discharges.

(a)
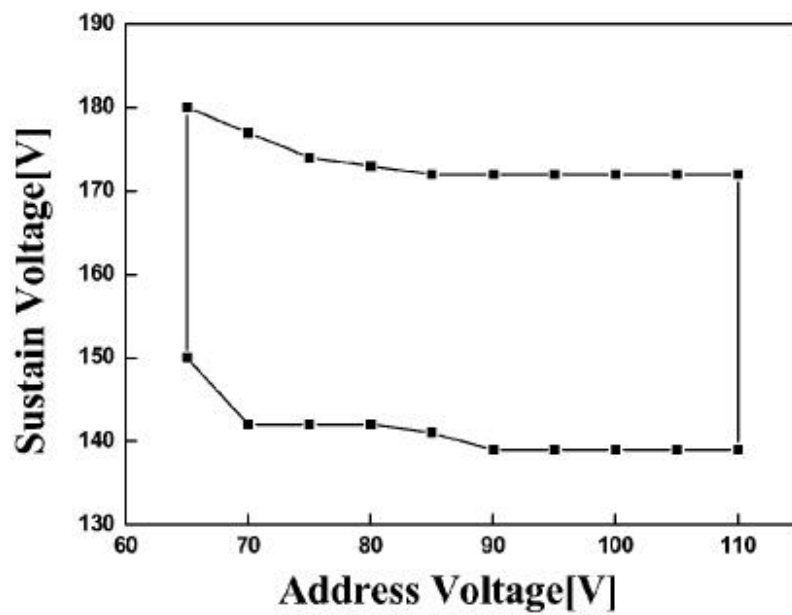
(b)

Figure 6-11: Dynamic voltage margin (b) measured from checkered pattern (a) of 4-inch test panel.
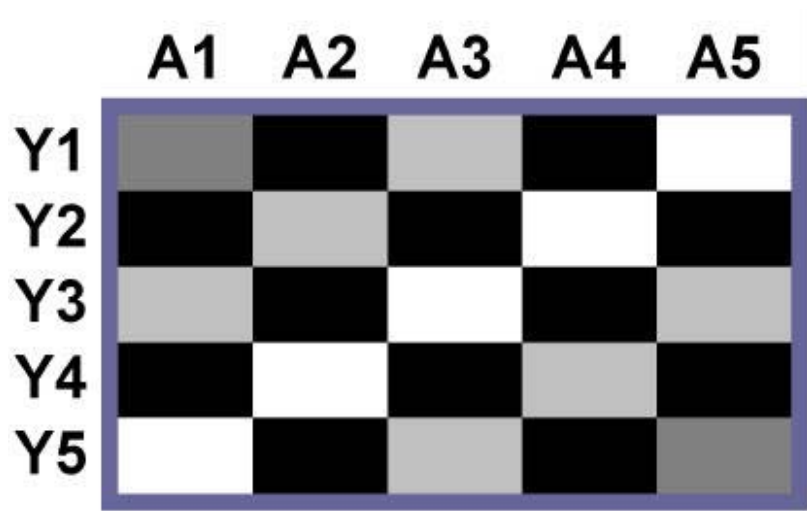
(a)
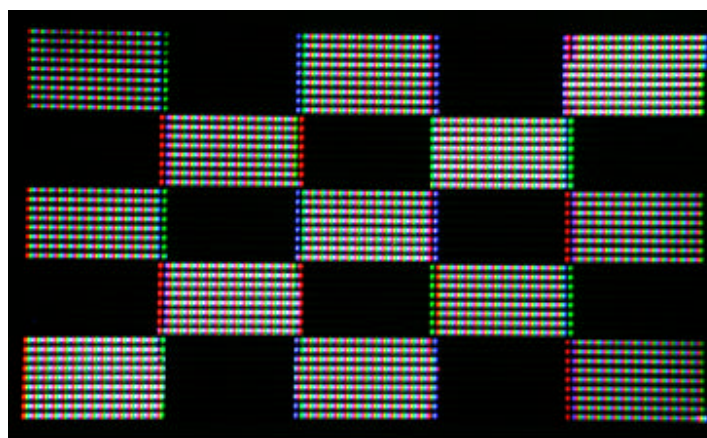
(b)

Figure 6-12: Test pattern for gray scan expression (a) and captured image of 4-inch test panel (b).

CONCLUSIONS

This paper suggested new driving methods to improve the driving characteristics of a three-electrode-type AC-PDP, including the luminance, luminous efficiency, color temperature, gray level expression, and addressing speed. The proposed driving methods are also evaluated using a 4-inch AC-PDP test panel, and the experimental results summarized and discussed. A Vt closed curve, a powerful method for analyzing driving waveforms is introduced and utilized to verify the operation of the suggested driving methods.

A new ramped-square sustain waveform is proposed to improve the luminous efficiency of an AC-PDP. The new sustain waveform is a superimposed waveform that adds a ramp-waveform to a square-waveform and has an increasing voltage slope between the rising and falling edge. This waveform can induce a longer sustained discharge at the rising edge plus a self-erasing discharge at the falling edge, thereby improving the luminous efficiency. When measuring the luminous characteristics, such as the luminance and luminous efficiency, based on the square-voltage and ramp-voltage (or voltage slope) of the proposed sustain pulse, it was found that the luminance and luminous efficiency strongly depend on the characteristics of the discharge relation between the main discharge at the rising edge and the self-erasing discharge at the falling edge of the ramped-square sustain waveform. With an increase in the square-voltage of the ramped-square sustain waveform, the luminance increases, yet the luminous efficiency decreases. Conversely, with an increase in the ramp-voltage of the ramped-square sustain waveform, both the luminance and the luminous efficiency increase. When compared with the conventional square sustain waveform, the proposed sustain waveform with a 9.3 V/μsec voltage slope achieved a maximal 65 % higher luminous efficiency in a

4-inch AC-PDP test panel, even at a low frequency (62 KHz). Plus, a 22 % improvement in the luminance and 36 % improvement in the luminous efficiency were simultaneously obtained based on the proper adjustment of the square-voltage and ramp-voltage of the ramped-square sustain waveform.

A new driving scheme is presented to improve and increase the flexibility of the color temperature in an AC-PDP without decreasing the gain of the G and R signals or employing asymmetric cell structures. As such, independent control of the R, G, and B emissions is achieved by the selective application of various narrow auxiliary pulses to the R, G, and B address electrodes during a sustain-period. Consequently, the auxiliary pulses can control the luminance levels independently from the R, G, and B cells based on the fast and efficient formation of plasma or slightly disturbing the wall-charge accumulation. The application of various auxiliary pulses leading to the simultaneous control of each color's luminance allowed the new driving scheme to improve the color temperature from 5,396 K to 10,980 K in a 4-in. test panel with almost the same peak white luminance as that for the conventional driving scheme.

A new multi-luminance-level subfield method is proposed to improve the low gray-level color reproducibility based on reducing the low gray-level contour of an AC-PDP. The luminance levels in 1-pulse and 2-pulse subfields are fine-tuned into 5 luminance-steps by applying various auxiliary pulses to the address electrode in the same sustain-pulse subfields. As a result, the 28 luminance levels produced in the low gray level up to 6 by the new multi-luminance-level subfield method were confirmed to help suppress the low gray-level contour in the inverse gamma corrected images of an AC-PDP. Therefore, if this method is combined with error diffusion and dithering methods, a low gray-level contour could be more efficiently suppressed.

A new bipolar scan waveform is proposed to considerably reduce the addressing time during an address period in an AC-PDP. The new bipolar scan waveform reduces the scanning time per single scan line from 1.5 μs to 0.6 μs by separating the address discharge mode into two different discharge modes: a space-charge generation mode and wall-charge accumulation mode. When compared with the conventional addressing waveform in the single scan ADS driving scheme for an XGA grade PDP, the bipolar scan waveform reduced the total address time per single subfield by about 50 %, thereby achieving an almost two-fold improvement in the light emission time for one TV field. However, the new addressing waveform also incurs an undesired writing discharge problem related to the triggering effect of data pulses for an adjacent scan line. In this paper, the undesired writing discharge problem is solved by increasing the scan pulse transition time T_{TR} from 0.3 μs to 0.7 μs, without causing any change in the desired writing discharge and sustain discharge characteristics.

REFERENCES

[1] Larry F. Weber, "Status and Trends of Plasma Display Device Research", *Eurodisplay '99 Digest*, pp.1-6, 1999.

[2] Larry F. Weber, "Plasma Display Devices Challenges", *Asia Display '98 Digest*, pp.15-27, 1998.

[3] J. Ryeom, K. H. Kang, S. C. Lee and C. B. Park, "High-Luminance and High-Contrast HDTV PDP with Overlapping Driving Scheme," *IDW '99 Digest,* pp.743-746, 1999.

[4] T. Komaki, H. Taniguchi, K. Amemiya, "High luminance AC-PDPs with Waffle-structured Barrier Ribs," *IDW '99 Digest*, pp.587-590, 1999.

[5] T. Nishio, K. Amemiya, "High Luminance and High Definition 50-in. Diagonal co-planar Color PDPs with T-Shaped Electrodes," *SID '99 Digest*, 1999.

[6] M. Klein, R. Snijkers, and G. Hagelaar, "Energy Loss Mechanisms in AC-PDP Discharges," *IDW '99 Digest*, pp.695-698, 1999.

[7] Jeong Hyun Seo, Woo Joon Chung, Cha Keun Yoon, Joong Kyun Kim, and Ki-Woong Whang, "Discharge Efficiency Analysis of an AC PDP by Numerical Simulation," *IDW '99 Digest*, pp.667-669, 1999.

[8] G. Oversluizen, M. Klein, S. de Zwart, S. van Heusden, and T. Dekker, "Improvement of the discharge efficiency in plasma displays," *J. Appl. Phys.*, vol.91, no.4, pp.2403-2408, 2002.

[9] G. J. M. Hagelaar, M. H. Klein, R. J. M. M. Snijkers, and G. M. W. Kroesen, "Energy loss mechanisms in the microdischarges in plasma display panels," *J. Appl. Phys.*, vol.89, no.4, pp.2033-2039, 2001.

[10] Markus H. Klein, Rob J. M. M. Snijkers, and Gerjan J. M. Hagelaar, "Energy Loss Mechanisms in AC-PDP Discharges," *IEICE Trans.*

Electron., vol.E83-C, no.10, pp.1602-1607, 2000.

[11] T. Okamura, S. Fukuda, K. Koike, H. Saigou, T. Kitagawa, M. Yochikai, M. Koyama, T. Misawa, and Y. Matsuzaki, "PDP Optical Filter with Sputtered Multilayer Coatings and Organic Dyes," *IDW '00 Digest*, pp.783-786, 2000.

[12] Koichi Wani, "A Novel Driving Scheme and Panel Design for Realization of a Picture Quality Equivalent to CRTs," *IDW '99 Digest*, pp.775-778, 1999

[13] Yoichi Sata, Kimio Amemiya, Masataka Uchidoi, "Recent Progresses of Device Performance and Picture Quality in Color Plasma Displays," *IDW '00 Digest*, pp.695-698, 2000

[14] J. Hoppenbrouwers, R. van Dijk, T. Holtslag, "A Comparison of Motion Artifact Reduction Method in PDPs," *IDW '99 Digest*, pp.779-782, 1999.

[15] I. Kawahara and K. Sekimoto, "Dynamic Gray-Scale Control to Reduce Motion Picture Disturbance for High-Resolution PDP," *SID '99 Digest*, 1999.

[16] M. Yamada, K. Sawa, T. Shiga, S. Mikoshiba, T. Ohe, K. Toda, Ueda, and K. Kariya, "Doubling of PDP resolution for Moving Pictures by Use of a Virtual Pixel Technique," *IDW '00 Digest*, pp.703-706, 2000.

[17] S. Weitbruch, R. Zwing, and C. Correa, "PDP Picture Quality Enhancement Based on Human Visual System Relevant Features," *IDW '00 Digest*, 699-702, 2000

[18] M. Ishii, T. Shiga, K. Igarashi, and S. Mikoshiba, "Driving of PDPs with 208 Sub-Fields Using a Grouped Address-While-Display Scheme," *SID '01 Digest*, pp.1134-1137, 2001.

[19] Larry F. Weber, ``The Promise of Plasma Displays for HDTV," *SID '00 Digest*, pp.402-409, 2000.

[20] K. Sakita, K. Takayama, K. Awamoto, and Y. Hashimoto, "High-speed Address Driving Waveform Analysis Using Wall Voltage Transfer Function for Three Terminals and Vt Close Curve in Three-Electrode Surface-Discharge AC-PDPs," *SID '01 Digest*, pp.1022-1025, 2001.

[21] K. Sakita, K. Takayama, K. Awamoto, and Y. Hashimoto, "Analysis of Cell Operation at Address Period Using Wall Voltage Transfer Function in Three-electrode Surface-Discharge AC-PDPs," *IDW '01 Digest*, pp.841-844, 2001.

[22] Koich Sakita, Kunio Takayama, Kenji Awamoto, and Yasunobu Hashimoto, "Ramp Setup Design Technique in Three-electrode Surface-discharge AC-PDPs," *SID '02 Digest*, pp.948-951, 2002.

[23] T. Kishi, T. Sakamoto, S. Tomio, K. Kariya, and T. Hirose, "A New Driving Technology for PDPs with Cost Effective Sustain Circuit," *SID '01 Digest*, pp.1236-1239, 2001.

[24] M. S. Kim, Y. J. Lee, S. K. Lee, W. J. Kim, Y. D. Kim, S. J. Moon, Y. H. Kwon, S. J. Yoo, and J. D. Kim, "Correlation Between Operating Margin and Vt Close Curve in AC PDP," *Eurodisplay '02 Digest*, pp.727-730, 2002.

[25] H. Inoue, Y. Seo, K. Sakita, and Y. Hashimoto, "Numerical Analysis of Vt Close Curve for Non-Uniform Wall Charge Distribution in Three-Electrode AC-PDP," *Eurodisplay '02 Digest*, pp.931-934, 2002.

[26] N. Uemura, Y. Yajima, Y. Kawanami, S. Ho, H. Nakahara, Y. Hatano, N. Kouchi, and K. Suzuki, "Rib Height Dependence of Vacuum Ultraviolet Emission Efficiency in Surface-Discharge AC PDPs," *IDW '99 Digest*, pp.595-598, 1999.

[27] L. C. Pitchford, J. Kang, C. Punset and J. P. Boeuf, "Calculated characteristics of radio-frequency plasma display panel cells including the

influence of xenon metastables," *J. Appl. Phys.*, vol.92, no.12, pp.6990-6997, 2002.

[28] G.Veronis and U.S.Inan, "Cell geometry designs for efficient plasma display panels," *J. Appl. Phys.*, vol.92, no.9, pp.4897-4905, 2002.

[29] G.Veronis and U.S.Inan, "Simulation studies of the complanar electrode and other plasma display panel cell designs," *J. Appl. Phys.*, vol.91, no.12, pp.9502-9512, 2002.

[30] Cha Keun Yoon, Jin Ho Yang, Woo Jun Cheong, Kyung Cheol Choi, and Ki-Woong Whang, "High Luminance and Efficacy AC-PDP with Segmented Electrode in Delta Color Arrayed Rectangular Subpixels," *IDW '00 Digest*, pp.627-630, 2000.

[31] T. Hashimoto, A. Iwata, "Improvement of Luminance Efficiency in an ACPDP by Self-Erase Discharge Waveform," *SID '99 Digest*, 1999.

[32] Shin-Tai Lo, Chern-Lin Chen, Kun-Ming Lee, and Jih-Fon Huang, "Improvement of Luminous Efficiency by a Novel Sustaining Waveform for Plasma Display Panels," *SID '00 Digest*, pp.702-705, 2000.

[33] Heung-Sik Tae, Ki-Duck Cho, Sang-Hun Jang, and Kyung Cheol Choi, "Improvement of the Luminous Efficiency Using Ramped-Square Sustain Waveform in an AC Surface Discharge Plasma Display Panel," *IEEE Trans. Electron Devices*, vol.48, no.7, pp.1469-1472, 2001.

[34] Heung-Sik Tae, Ki-Duck Cho, Sang-Hun Jang, and Jeong-Hae Lee, "New Ramped-Square Sustain Waveform for Improving Luminance and Luminous Efficiency of an AC Surface-Discharge Plasma Display Panel," *IEICE Trans. Electron.*, vol.84-C, no.11, pp.1653-1658, 2001.

[35] Ki-Duck Cho, Sang-Hun Jang, Heung-Sik Tae, Beong-Ha Lim, Dongho Lee, and Kyung Cheol Choi, "Improvement of Luminous Efficiency Using Ramped- Square Sustain Waveform in a Surface-Discharge

AC-PDP," *IDW '00 Digest*, pp.655-658, 2000.

[36] C. Punset, J.-P. Boeuf, and L. C. Pitchford, ``Two-dimensional simulation of an alternating current matrix plasma display cell: Cross-talk and other geometric effects'', *J. Appl. Phys.*, vol. 83, no. 4, pp. 1884-1897, 1998.

[37] Y. Ikeda, J. P. Verboncoeur, P. J. Christenson, and C. K. Birdsall. ``Global modeling of a dielectric barrier discharge in Ne-Xe mixtures for an alternating current plasma display panel'', *J. Appl. Phys.*, vol. 86, no. 5, pp. 2431-2441, 1999.

[38] C. Punset, S. Cany, and J.-P Boeuf, ``Addressing and sustaining in alternating current coplanar plasma display panel'', J. Appl. Phys., vol. 86, no. 1, pp. 124-133, 1999.

[39] Sang-Hun Jang, Ki-Duck Cho, Heung-Sik Tae, Kyung Cheol Choi, and Seok-Hyun Lee, "Improvement of Luminance and Luminous Efficiency Using Address Voltage Pulse During Sustain-Period of AC-PDP," *IEEE Trans. Electron Devices*, vol. 48, no. 9, pp. 1903-1910, 2001.

[40] H. Tachibana, A. Matsuda, S. Haruki, N. Kosugi, K. Wani, L. F. Weber, " Improvement of Ramp-Discharge Characteristics by Using New Green Phosphor," *IDW '00 Digest*, pp.651-654, 2000.

[41] T. Okamura, S. Fukuda, K. Koike, H. Saigou, T. Kitagawa, M. Yoshikai, M. Koyama, T. Misawa, and Y. Matsuzaki, "PDP Optical Filter with Sputtered Multilayer Coatings and Organic Dyes," *IDW '00 Digest*, pp.783-786, 2000.

[42] Takao Sawada, Ko Sano, and Manabu Akiba, "Improvement of Color Temperature for PDP by Using Gd Doped MgO Protecting Film," *IDW '01 Digest*, pp.829-832, 2001.

[43] Gnter Wyszecki and W. S. Stiles, *Color Science - Concepts and*

Methods, Quantitative Data and Formulae, 2nd ed., A Wiley-Interscience Publication: John Wiley & Sons, Inc., 1982, pp.1-82.

[44] Ki-Duck Cho, Sang-Hun Jang, Heung-Sik Tae, Beong-Ha Lim, Dongho Lee, and Kyung Cheol Choi, "Improvement of Luminous Efficiency Using Ramped-Square Sustain Waveform in a Surface-Discharge AC-PDP," *IDW '00 Digest*, pp.655-658, 2000.

[45] Ki-Duck Cho, Heung-Sik Tae, and Sung-Il Chien, "Improvement of Color Temperature using independent control of red, green, blue luminance in AC Plasma Display Panel," *IEEE Trans. Electron Devices*, vol.50, no.2, pp.359-365, 2003.

[46] Ki-Duck Cho, Heung-Sik Tae, and Sung-Il Chien, "Improvement of Color Temperature Using Address Voltage Pulse During Sustain Period of AC-PDP," *SID '01 Digest*, pp.794-797, 2001

[47] T. Tokunaga, H. Nakamura, M. Suzuki, and N. Saegusa, ``Development of New Driving Method for AC-PDPs," *IDW '99 Digest*, pp.787-790, 1999.

[48] Larry F. Weber, ``The Promise of Plasma Displays for HDTV," *SID '00 Digest*, pp.402-409, 2000.

[49] S. Seki, M. Ishii, T. Shiga, K. Igarashi, and S. Mikoshiba, "A 16-Bit Drive of 1080p PDPs for High Quality Image Expression," *SID '00 Digest*, pp.714-717, 2000.

[50] Ki-Duck Cho, Heung-Sik Tae, and Sung-Il Chien, "Improvement of Low Gray Scale Linearity using Multi-Luminance-Level Subfield Method in Plasma Display Panel," *IEEE Trans. Consumer Electronics*, vol.48, no.3, pp.377-381, 2002.

[51] Ki-Duck Cho, Heung-Sik Tae, and Sung-Il Chien, "New Multi-Luminance-Level Subfield Method for Reducing Low Gray-Level

Contour in AC Plasma Display Panel," *IEICE Trans. Electron.*, vol.E86-C, no.4, pp.682-685, 2003.

[52] Ki-Duck Cho, Heung-Sik Tae, and Sung-Il Chien, "Improvement of Low Gray Scale Linearity using Multi-Luminance-Level Subfield Method in Plasma Display Panel," *ICCE '02 Digest*, pp.1-4, 2002.

[53] J. Hoppenbrouwers, R. van Dijk, T. Hostslag, and F. Laffargue, "Address Time Reduction in PDPs by means of Partial Line Doubling," *SID '01 Digest*, pp.1142-1145, 2001.

[54] Shigeo Mikoshiba, "Visual Artifacts Generated in Frame-Sequential Display Devices," *SID '00 Digest*, pp.384-387, 2000.

[55] S. Seki, M. Ishii, T. Shiga, K. Igarashi, and S. Mikoshiba, "A 16-Bit Drive of 1080p PDPs for High Quality Image Expression," *SID '00 Digest*, pp.714-717, 2000.

[56] Kyoungho Kang, Jooyul Lee, Seongchan Lee, Heehwan Kim, Namsung Jung, Kiwoong Whang, and Changbae Park, "A New 42-in. AC PDP Using MAoD II Driving Scheme," *SID '01 Digest*, pp.1130-1133, 2001.

[58] Eun-Cheol Lee, Young-Bok Song, Bong-Koo Kang, and Young-Hwan Kim, "Plasma Display Panel with Plural Screens," U.S. Patent 5914563, 1999.

[59] Ki-Duck Cho, Heung-Sik Tae, Sung-Il Chien, "Bipolar Scan Waveform for Fast Address in AC Plasma Display Panel," *IEICE Trans. Electron.*, vol.E87-C, no.1, pp.116-119, 2004.

[60] Ki-Duck Cho, Heung-Sik Tae, Sung-Il Chien, "New Fast Addressing Waveform for XGA Grade AC Plasma Display Panel," *Eurodisplay '02 Digest*, pp.333-336, 2002.

[61] Ki-Duck Cho, Heung-Sik Tae, Sung-Il Chien, Jeung-Hae Lee, "New Addressing Technique for Reduction of Addressing Time in AC PDP,"

IDW '02 Digest, pp.885-888, 2002.

교류형 Plasma Display Panel를 위한 새로운 어드레스 및 서스테인 파형

조 기 덕

경북대학교 대학원 전자공학과 전파공학전공
(지도교수 태흥식)

(초 록)

플라즈마 디스플레이 패널(PDP)은 CRT를 대체할 수 있는 강력한 후보로 주목받고 있으나, 구동 특성상의 여러 심각한 문제점들을 안고 있다. 본 논문에서는 최근 PDP의 문제점으로 대두되고 있는 휘도, 발광효율, 색온도, 저계조 표현력, 기입 속도 등을 포함하는 구동 특성들을 향상시킬 수 있는 여러 가지 새로운 구동 방법들을 제안하였다. 각각의 제안된 구동 방법들은 4인치 AC-PDP 테스트 패널을 이용하여 실험을 하였으며, 그 실험결과를 정리하고 분석하였다. 또한, 구동파형을 분석할 수 있는 강력한 방법 중 하나인 Vt closed curve를 소개하고, 제안된 방법들을 검증하는데 응용되었다.

먼저, PDP의 휘도와 발광효율을 동시에 향상시키기 위하여 ramped-square sustain 파형을 제안하였다. 실험을 통해 휘도와 발광효율은 ramped-square sustain 파형의 상승 부분에서의 주 방전과 하강 부분에서의 자기 소거방전 간의 방전 특성 관계에 크게 영향을 받는 것으로 분석되었다. 4인치 AC-PDP 테스트 패널을 62KHz로 ramped-square sustain 파형으로 구동한 경우, 최적의 square 전압과 ramp 전압 조건에서 22%의 휘도 향상과 36% 발광효율 향상을 동시에 얻을 수 있었다.

sustain 구간 동안 address 전극에 펄스를 인가하는 auxiliary address 펄스를 이용하여 AC-PDP의 red, green, blue 휘도를 독립적으로 가변함으로써,

white 휘도의 감소없이 색온도를 향상시킬 수 있고 가변시킬 수 있는 방법을 제안하였다. 각 색상의 휘도를 동시에 가변시킬 수 있는 다양한 조건의 auxiliary address pulse를 인가함으로써, 4인치 테스트 패널에서 일반적인 구동파형과 비교하여 동일한 white 휘도를 유지하면서 색온도를 5,396K에서 10,980K로 향상시킬 수 있었다.

저계조 표현력을 향상을 통해 저계조에서 발생되는 윤곽선을 감소시키기 위해서는 multi-luminance-level subfield 방법을 제안하였다. 1 sustain 주기와 2 sustain 주기를 가지는 subfield에서 address 전극에 auxiliary pulse를 다양한 조건으로 인가함으로써 동일한 sustain 주기를 가지면서도 휘도를 5단계까지 나눌 수 있었다. 결과적으로, 제안된 multi-luminance-level subfield 방법을 이용하여 계조 6까지의 저계조 구간에서 28개의 휘도 단계를 구현하여 AC-PDP 의 저계조 윤곽선을 저감시킬 수 있음을 확인하였다.

마지막으로, 기입 속도를 크게 향상시키기 위해 bipolar scan 파형을 제안하였다. bipolar scan 파형은 두 단계로 이루어져 있으며, address 구간동안 기존 파형에서는 하나로 발생되는 방전 모드를 벽전압 발생 모드와 벽전압 축적 모드의 두가지 모드로 나눌 수 있다. single scan ADS 구동법에 적용한 경우, bipolar scan 파형은 기존 scan 파형과 비교하여 기입에 소요되는 시간을 약 50% 정도로 줄일 수 있었으며, 1 TV-field동안 발광시간을 약 2배 정도 향상시킬 수 있었다.